Valorisation of Pyrolytic Tyre Char as Filler in Polypropylene

by

Cleopatra Saul

Thesis presented in partial fulfilment
of the requirements for the Degree

of

MASTER OF ENGINEERING

(Chemical Engineering)

in the Faculty of Engineering

at Stellenbosch University

The financial assistance of the National Research Foundation (NRF) towards this research is hereby acknowledged. Opinions expressed and conclusions arrived at, are those of the author and are not necessarily to be attributed to the NRF.

Supervisor

Mr Petrie van Wyk

Co-Supervisor

Dr Itziar Iraola-Arregui

December 2019

DECLARATION

By submitting this thesis electronically, I declare that the entirety of the work contained therein is my own, original work, that I am the sole author thereof (save to the extent explicitly otherwise stated), that reproduction and publication thereof by Stellenbosch University will not infringe any third party rights and that I have not previously in its entirety or in part submitted it for obtaining any qualification.

Date: December 2019

PLAGIARISM DECLARATION

1. Plagiarism is the use of ideas, material and other intellectual property of another's work and to present it as my own.
2. I agree that plagiarism is a punishable offence because it constitutes theft.
3. I also understand that direct translations are plagiarism.
4. Accordingly all quotations and contributions from any source whatsoever (including the internet) have been cited fully. I understand that the reproduction of text without quotation marks (even when the source is cited) is plagiarism.
5. I declare that the work contained in this assignment, except where otherwise stated, is my original work and that I have not previously (in its entirety or in part) submitted it for grading in this module/assignment or another module/assignment.

Student number:

Initials and surname: C.L. Saul

Signature:

Date: December 2019

ABSTRACT

Pyrolytic tyre char (PT-char) produced during waste tyre pyrolysis is conventionally perceived as a waste stream due to its high amounts of impurities. The aim of this research study is to investigate and analyse the feasibility of PT-char as filler in order to enhance the mechanical properties and degradation stability of polypropyelen (PP) composites.

In the present study, the untreated PT-char was first demineralised with acid-base lixiviants (nitric acid and sodium hydroxide) to remove impurities. The impurity removal step was followed by surface modification using 3-methacryloxypropyletrimethoxysilane (3-MPTS) and titanium IV 2,2 (bis-2-propenolatomethyl) butanolato, tris (dioctyl) pyrophosphato-O (LICA 12) coupling agents and maleic anhydride-grafted polypropylene (MAgPP) compatibiliser to improve the filler reactivity towards the polymer. PP composites filled with various amounts of unmodified and modified PT-char were produced and tested for mechanical properties and degradation stability.

The untreated PT-char and the demineralised PT-char were characterised in terms of their particle size, surface area, proximate and ultimate analysis and surface functional groups. Demineralisation reduced the ash content from 16.5 wt.% to 2.70 wt.%, average particle size decreased significantly from 89.9 µm to 11.0 µm and the surface area increased slightly from 73.9 m^2/g to 76.7 m^2/g. Functional groups such as carbonyl, carboxylic and hydroxyl groups were present on the surface of the untreated PT-char before any treatment. Silanol group which belong to the silane was present on the modified PT-char. However, phosphate group which belong to titanate could not be verified on the modified PT-char since it appear on the unmodified PT-char.

Incorporation of PT-char increased the mixing torque of PP composites melt due to rigid particles of PT-char, which limit the movement of PP chains. The mixing torque of PP composites increased with an increase in PP-char loading. Surface modification enhanced the interface between PT-char and the PP matrix by reducing the mixing torque.

Incorporation of unmodified PT-char did result in some improvements in some mechanical properties such as tensile strength and elongation at break of PP composites, due to its

heterogeneous spherical particle shape which gave uniform distribution of stress. On the other hand, demineralisation of PT-char reduced the mechanical properties. This was due to reduction in minerals compounds contained within PT-char which are beneficial for mechanical properties of PP composites. PT-char loading higher than 1.94 wt.% reduced the mechanical properties of PP composites, particularly with demineralised PT-char. This was due to the aggregation tendency of small particle sizes which caused defects in the composites system. Surface modification with silane and titanate coupling agents improved the mechanical properties of PP composites due to the enhancement of the interface between PT-char and the PP matrix. However, the performance of MAgPP compatibiliser was very poor due to an insufficient esterification process between the anhydride groups of the MAgPP and the hydroxyl groups of the PT-char.

Thermal and photo-oxidative degradation studies revealed that demineralised PT-char is less pro-degradant than untreated PT-char due to lower transition metal content in its surface. Higher PT-char loadings (0.77 wt.% and 1.94 wt.) accelerated thermal and photo-oxidative degradation, particularly with demineralised PT-char regardless of surface modification. This was due to aggregation tendency of PT-char particles which caused defects in the composites system. Surface modification with 3-MPTS and LICA 12 leads to significant improvements in the thermal and photo-oxidative degradation stability of PP composites particularly at lower PT-char loading (0.38 wt.%), due to an enhanced interface between PP and the PT-char. However, MAgPP compatibiliser accelerated the thermal-oxidative degradation of PP composites due to thermo-responsive groups, such as carboxylic acids, which originate from partial hydrolysis of maleic anhydride.

Keywords: Waste tyre, PT-char, composites, surface modification

OPSOMMING

Pirolitiese bandverkoolsel (PT-char) geproduseer tydens pirolise van afvalbande word konvensioneel beskou as ’n afvalstroom as gevolg van die hoë hoeveelhede onsuiwerhede. Die doel van hierdie navorsingstudie is om die lewensvatbaarheid van PT-char as vuller te ondersoek en analiseer om die meganiese eienskappe en degradasie stabiliteit van polipropileen samestellings te verhoog.

In die huidige studie is onbehandelde PT-char eers gedemineraliseer met suurbasis loogmiddels (salpetersuur en natriumhidroksied) om onsuiwerhede te verwyder. Die stap om onsuiwerhede te verwyder is gevolg deur oppervlak modifikasie deur 3-metakrieloksiepropieletrimetoksiesilaan (3-MPTS) en titanium IV 2,2 (bis-2-propenolatometiel) butanolato, tris(dioktiel)pirofosfaato-O (LICA 12) koppelingsagente te gebruik, en maleïensuuranhidried-geënte polipropileen (MAgPP) verbinder om die vuller reaktiwiteit na die polimeer te verbeter. PP-samestellings gevul met verskeie hoeveelhede ongemodifiseerde en gemodifiseerde PT-char is geproduseer en getoets vir meganiese eienskappe en degradasie stabiliteit.

Die onbehandelde en gedemineraliseerde PT-char is gekarakteriseer in terme van hul partikelgrootte, oppervlakarea, naaste- en eindanalise en oppervlak funksionele groepe. Demineralisering verminder die asinhoud van 16.5 gew.% Tot 2.70 gew.%, Gemiddelde deeltjiegrootte het aansienlik afgeneem van 89.9 µm tot 11.0 µm en die oppervlakte het effens toegeneem van 73.9 m^2/g tot 76.7 m^2/g. Funksionele groepe soos karboniel-, karboksiel- en hidroksielgroepe was teenwoordig op die oppervlak van die onbehandelde PT-char voor enige behandeling. Silanol-groep wat aan die silaan behoort, was teenwoordig op die gewysigde PT-char. Fosfaatgroepe wat aan titanaat behoort, kon egter nie op die gewysigde PT-char geverifieer word nie, aangesien dit op die ongemodifiseerde PT-char verskyn.

Inkorporasie van PT-char het die menging wringkrag van PP-samestellingsmeltsel verhoog as gevolg van rigiede partikels van PT-char, wat die beweging van PP-kettings beperk. Die menging wringkrag van PP-samestellings verhoog met ’n verhoging in PT-char-lading.

Oppervlak modifikasie versterk die tussenvlak tussen PT-char en die PP-matriks deur die menging wringkrag te verminder.

Inkorporasie van ongemodifiseerde PT-char het tot sommige verbeteringe in sommige meganiese eienskappe gelei soos treksterkte en verlenging van die breek as gevolg van sy heterogene sferiese partikel vorm wat tot uniforme verspreiding van spanning lei. Aan die ander kant het die demineralisering van PT-char die meganiese eienskappe verminder. Dit was te danke aan die vermindering in minerale verbindings wat in PT-char bevat is, wat voordelig is vir meganiese eienskappe. PT-char lading hoër as 1,94 gew.% het die meganiese eienskappe van PP-samestellings verminder, veral met gedemineraliseerde PT-char. Dit was as gevolg van die aggregasie geneigdheid van klein partikelgroottes wat defekte in die samestellingsisteem veroorsaak het. Oppervlak modifikasie met silaan- en titanietkoppelingsagente het die meganiese eienskappe verbeter as gevolg van die verterking van die tussenvlak tussen PT-char en die PP-matriks. Die doeltreffendheid van MAgPP-verbinder was egter baie swak as gevolg van ’n onvoldoende esterifikasieproses tussen die anhidriedgroepe van die MAgPP en die hidroksielgroepe van die PT-char.

Termiese en foto-oksidatiewe degradasiestudies het bekend gemaak dat gedemineraliseerde PT-char minder pro-degradent as onbehandelde PT-char is as gevolg van laer oorgangmetaalinhoud in sy oppervlakte. Hoër PT-char-lading (0.77 gew.% and 1.94 gew.%) het termiese en foto-oksidatiewe degradasie versnel, veral met demineralisasie ongeag van oppervlak modifikasie. Dit was te danke aan die versamelingstendens van PT-char deeltjies wat defekte in die samestellingsstelsel veroorsaak het. Oppervlak modifikasie met 3-MPTS en LICA 12 lei tot beduidende verbeteringe in die termiese en foto-oksidatiewe degradasie stabiliteit van PP-samestelling, veral by laer PT-char-lading (0,38 gew.%), as gevolg van ’n versterkte tussenvlak tussen PP en die PT-char. MAgPP-verbinder het die termiese-oksidatiewe degradasie van PP-samestelling egter versnel as gevolg van termo-responsiewe groepe, soos karboksielsure, wat ontstaan uit gedeeltelike hidrolise van maleïensuuranhidried.

Sleutelwoorde: Afvalbande, PT-char, samestellings, oppervlak modifikasie

ACKNOWLEDGEMENTS

I express gratitude toward God for giving me strength and persistence to finish my research project. A special thanks to my supervisors, Mr Petrie van Wyk and Dr Itziar Iraola-Arregui for your positive inputs and comments. A special thanks to REDISA for financial support.

I would also like to appreciate the following individuals:

1. Professor Percy Van Der Gryp, Professor Johann Ferdinand Görgens and Professor Guven Akdogan for your guidance.
2. Technical and analytical staff of Stellenbosch University, Department of Process Engineering.
3. REDISA Research Group.
4. Mrs. Francis Layman for her wonderful assistance with ordering of chemical required to complete my experiments.
5. Department of Polymer Chemistry of Stellenbosch University for allowing me to use the Injection Molder, FTIR and Impact test instruments.
6. Roediger Agencies for your UV instrument and tensile test.
7. Nelson Mandela University, Department of Polymers for allowing me to use your melt-blending instrument.
8. My colleagues, Dr Malusi Mkhize, Dr Anthony Ndiripo and Miss Nthabiseng Seleme for your continued support

TABLE OF CONTENTS

DECLARATION i

PLAGIARISM DECLARATION ii

ABSTRACT iii

OPSOMMING v

ACKNOWLEDGEMENTS vii

LIST OF FIGURES xii

LIST OF TABLES xv

NOMENCLATURE xvii

CHAPTER 1: INTRODUCTION 1

1.1. Background 1

1.1.1 Waste tyre 1

1.1.2 PP composites 2

1.2. Problem statement 2

1.3. Aim 3

1.4. Significance of research study 3

1.5. Project scope and limitations 3

1.6. Thesis overview 6

CHAPTER 2: LITERATURE REVIEW 7

2.1. Pyrolysis and demineralisation 7

2.1.1 Tyre overview 7

2.1.2 Waste tyre pyrolysis 8

2.1.3 PT-char physical properties 9

2.1.4 PT-char composition 12

2.1.5 Possible applications of PT-char 17

2.1.6 Demineralisation 17

2.1.7 Concluding remarks 22

2.2. PP composite properties 23
2.2.1 PP composites and fillers properties 23
2.2.2 Surface modification 27
2.2.3 Mechanical properties 35
2.2.4 Degradation stability 40
2.2.5 Concluding remarks 43
CHAPTER 3: HYPOTHESIS AND OBJECTIVES OF THE STUDY 44
3.1. Research questions 44
3.2. Hypothesis 44
3.3. Objectives 45
CHAPTER 4: EXPERIMENTAL METHODS AND PROCEDURE 46
4.1. Materials 46
4.2. PT-char characterisation 48
4.2.1 Particle size distribution of PT-char 48
4.2.2 Proximate, ultimate analysis and chemical composition of ash 48
4.2.3 Surface morphology of PT-char 48
4.2.4 Surface area of PT-char 49
4.2.5 Surface chemistry of PT-char 49
4.3. Demineralisation of PT-char 49
4.4. Surface modification of PT-char 50
4.4.1 3-MPTS treatment 50
4.4.2 LICA 12 treatment 50
4.4.3 MAgPP treatment 51
4.5. Production of PP composites 51
4.5.1 Melt blending (Internal mixer) 51
4.5.2 Injection moulding 52
4.6. Determination of PP composites properties 52

4.6.1 Mechanical properties of PP composites 52
4.6.2 Degradation stability of PP composites 53
4.7. Experimental design 55
4.7.1 Statistical experimental design 55
4.7.2 Statistical analysis 58
CHAPTER 5: EXPERIMENTAL RESULTS AND DISCUSSIONS 59
5.1. PT-char particle characterisation 59
5.1.1 Particle size distribution of PT-char 59
5.1.2 Surface morphology of PT-char 61
5.1.3 Proximate, ultimate analysis and chemical composition of ash 62
5.1.4 Surface area of PT-char 67
5.1.5 Surface chemistry of PT-char 68
5.1.6 Concluding remarks 71
5.2. Melt blending characteristics 71
5.2.1 Concluding remarks 75
5.3. PP composites impact strength and surface fracture 76
5.3.1 PP composites impact strength 76
5.3.2 PP composites surface fracture 79
5.3.3 Concluding remarks 83
5.4. Thermal-oxidative degradation 83
5.4.1 Concluding remarks 90
5.5. PP composites tensile properties 91
5.5.1 PP composites tensile strength 91
5.5.2 PP composites young modulus 93
5.5.3 PP composites elongation at break 95
5.5.4 Concluding remarks 96
5.6. Photo-oxidative degradation 97

5.6.1 Concluding remarks 101
CHAPTER 6: CONCLUSIONS 102
6.1. Summary 102
6.2. PT-char characterisation 102
6.3. Mechanical properties 102
6.4. Degradation 103
CHAPTER 7: RECOMMENDATIONS 105
CHAPTER 8: REFERENCES 107
CHAPTER 9: APPENDICES 125
Appendix A: Types of silane coupling agents 125
Appendix B: Types of titanate coupling agents 126
Appendix C: Heating temperature ramp used for proximate analysis 127
Appendix D: PP composites formulations 127
Appendix E: Full factorial design for the analysis of mechanical properties and degradation studies 129
Appendix F: Proximate analysis 132
Appendix G: Ultimate analysis 132
Appendix H: Chemical composition of the ash 133
Appendix I: Adsorption-isotherms of PT-UC and PT-DC 136
Appendix J: FTIR spectra of coupling agents and compatibiliser 136
Appendix K: PP composites torque graphs 138
Appendix L: PP composites main effects and interaction plots: Impact Strength 140
Appendix M: PP composites surface fractured images 143
Appendix N: PP composites main effects and interactions plots: Tensile properties 144
Appendix O: PP composites main effects and interactions plots: Degradation 151

LIST OF FIGURES

Figure 1.1: Research project scope. 5
Figure 2.1: Tyre components 7
Figure 2.2: Chemical structure of 3-methacryloxypropyltrimethoxysilane. 29
Figure 2.3: Reaction of silane with inorganic substrate (filler). 30
Figure 2.4: Chemical structure of titanium 2,2(bis-2-propenolatomethyl)butanolato,tris (dioctyl)phosphato-O 32
Figure 2.5: Diagrammatic representation of LICA 12 monomolecular formation. 33
Figure 2.6: Chemical structure of Maleic-anhydride grafted Polypropylene. 34
Figure 2.7: A reaction scheme between the filler surface and MAgPP. 35
Figure 4.1: Typical sample of an impact bar. 52
Figure 4.2: Typical image sample of a tensile bar. 53
Figure 4.3: Experimental flow diagram. 57
Figure 5.1: Particle size distribution of a) PT-UC and b) PT-DC. 60
Figure 5.2: Surface morphology of PT-UC and PT-DC particles at different magnifications: a) and c) at 50X magnification and b) and d) at 500X magnification. 62
Figure 5.3: FTIR spectra of PT-UC and PT-DC. 68
Figure 5.4: FTIR spectra of PT-UC and PT-DC coupled with 3-MPTS or LICA 12 69
Figure 5.5: FTIR spectra of PT-UC and PT-DC with 3-MPTS and LICA 12. 70
Figure 5.6: Mixing torques vs time for (a) pure PP, (b) unmodified PP composites filled with UC and (c) unmodified PP composites filled with DC. 72
Figure 5.7: Mixing torques for 3-MPTS modified PP composites. 73
Figure 5.8: Mixing torques for LICA 12 modified PP composites 74
Figure 5.9: Mixing torques for PP composites modified with MAgPP at various PT-char loadings. 75
Figure 5.10: Impact strength of pure PP and the unmodified PP composites 76
Figure 5.11: Impact strength of pure PP and the modified PP composites filled with UC. 77
Figure 5.12: Impact strength of pure PP and the modified PP composites filled with DC. 78
Figure 5.13: Fracture surface images of pure PP, PP+UC and PP+DC composites at different PT-char loadings (0.38 and 7.91 wt.%). 80
Figure 5.14: Fracture surface image of PP+UC and PP+DC composites, modified with 3-MPTS and LICA 12 at 0.38 wt.%. 81

Figure 5.15: Fracture surface images of PP+DC+MAgPP composites at 0.38 and 7.91 wt.%. 82
Figure 5.16: FTIR spectrum of thermally degraded pure PP under different time intervals: a) hydroxyl region and b) carbonyl region.....84
Figure 5.17: CI versus time plots of thermally degraded pure PP and unmodified PP composites.....85
Figure 5.18: CI versus time plots of thermally degraded pure PP and 3-MPTS modified PP composites.....86
Figure 5.19: CI versus time plots of thermally degraded pure PP and LICA 12 modified PP composites.....88
Figure 5.20: CI versus time plots of thermally degraded pure PP and MAgPP modified PP composites.....89
Figure 5.21: Tensile strength of PP composites at different PT-char loadings. 92
Figure 5.22: Young modulus of PP composites at different PT-char loadings. 93
Figure 5.23: Elongation at break of PP composites at different PT-char loadings.....95
Figure 5.24: CI versus time plot of photo-degraded pure PP and unmodified PP composites. 97
Figure 5.25: CI versus time plots of photo-degraded pure PP and 3-MPTS modified PP composites.....98
Figure 5.26: CI versus time plots of photo-degraded pure PP and LICA 12 modified PP composites.....100
Figure 9.1: Proximate analysis heating temperature ramp.....127
Figure 9.2: Adsorption-Desorption Isotherms of a) PT-UC and b) PT-DC. 136
Figure 9.3: FTIR spectrum of 3-MPTS.....137
Figure 9.4: FTIR spectrum of LICA 12. 137
Figure 9.5: FTIR spectrum of MAgPP. 137
Figure 9.6: Temperature vs. time plots of pure PP and unmodified PP composites.....138
Figure 9.7: Temperature vs. time plots for modified PP composites.....139
Figure 9.8: Main effects of impact strength of PP composites. 141
Figure 9.9: Interactions plots of impact strength of the PP composites.....142
Figure 9.10: Surface fractured images of PP composites at 1.94 wt.%. 143
Figure 9.11: Main effect plots of tensile strength of PP composites. 145
Figure 9.12: Interactions plots of tensile strength of the PP composites. 146
Figure 9.13: Main effects plots of young modulus of PP composites. 147

Figure 9.14: Interactions plots of young modulus of PP composites. 148
Figure 9.15: Main effects of elongation at break of PP composites. 149
Figure 9.16: Interactions plots of elongation at break of PP composites.....150
Figure 9.17: Main effects plots of thermal-oxidative degradation of PP composites.....152
Figure 9.18: Interactions plots of thermal-oxidative degradation of PP composites.....153
Figure 9.19: Main effects plots of photo-oxidative degradation of PP composites.....154
Figure 9.20: Interactions plots of photo-oxidative degradation of PP composites.....155

LIST OF TABLES

Table 2.1:Typical tyre composition. 8
Table 2.2: Typical surface area and particle sizes of PT-char reported from the literature. 10
Table 2.3: Surface areas of commercial CB used in tyres. 10
Table 2.4: Proximate analysis of PT-char obtained at different pyrolysis temperature. 12
Table 2.5: Ultimate analysis of PT-char obtained at different pyrolysis temperature. 14
Table 2.6: The mineral content of PT-char reported from the literature. 16
Table 2.7: Acid-base demineralisation conditions of PT-char found in the literature. 19
Table 2.8: Typical applications of PP composites. 24
Table 2.9: Various particle sizes and surface areas of fillers used in PP composites. 25
Table 2.10: Typical mechanical properties of homopolymer PP filled with various unmodified particulate fillers. 36
Table 4.1: Acid-base lixiviants used in the study. 47
Table 4.2: Coupling agents used in the study. 47
Table 4.3: Factors and their levels. 55
Table 5.1: Average particle size of PT-UC and PT-DC (µm). 59
Table 5.2: Particle size, cumulative distribution of PT-UC and PT-DC. 60
Table 5.3: Proximate Analysis of PT-UC and PT-DC (wt.%). 62
Table 5.4: Ultimate analysis of PT-UC and PT-DC (wt.%). 63
Table 5.5: Chemical composition of the ash within PT-UC and PT-DC 64
Table 5.6: The surface area analysis of PT-UC and PT-DC (m^2/g) 67
Table 5.7: The pore size analysis of PT-UC and PT-DC. 67
Table 5.8: Analysis of variance of the impact strength of the PP composites. 76
Table 5.9: CI of thermally degraded pure PP and unmodified PP composites. 85
Table 5.10: CI of thermally degraded pure PP and 3-MPTS modified PP composites. 87
Table 5.11: CI of thermally degraded pure PP and LICA 12 modified PP composites. 88
Table 5.12: CI of thermally degraded pure PP and MAgPP modified PP composites. 89
Table 5.13: Analysis of variance of the tensile strength of the PP composites. 92
Table 5.14: Analysis of variance of the young modulus of the PP composites. 94
Table 5.15: Analysis of variance of the elongation at break of the PP composites. 95
Table 5.16: CI of photo-degraded pure PP and unmodified PP composites. 97
Table 5.17: CI of phot-degraded pure PP and 3-MPTS modified PP composites. 99

Table 5.18: CI of photo-degraded pure PP and LICA 12 modified PP composites. 100
Table 9.1: Types of silane coupling agents.....125
Table 9.2. Types of titanate coupling agents. 126
Table 9.3: Composites formulations for PP and UC/DC.....128
Table 9.4: Full factorial design ($2^1 4^1 5^1$) for analysis of impact strength.....129
Table 9.5: Full factorial design ($2^1 4^1 3^1$) for thermal-oxidative degradation studies. 130
Table 9.6: Full factorial design ($2^1 3^1 3^1$) for analysis of tensile properties and photo-oxidative degradation studies.....131
Table 9.7: Proximate analysis results (wt.%).....132
Table 9.8: Ultimate analysis results (wt.%). 132
Table 9.9: Chemical composition of the ash in PT-UC (wt.%). 134
Table 9.10: Chemical composition of the ash in PT-DC (wt.%). 135
Table 9.11: Analysis of variance for the impact strength of PP composites. 140
Table 9.12: Analysis of variance for the tensile properties of PP composites.....144
Table 9.13: Analysis of variance for degradation studies of PP composites. 151

NOMENCLATURE

Abbreviation	Definition
3-MPTS	3-Methacryloxypropyl trimethoxy Silane
BET	Brunauer Emmett Teller
BJH	Barrett-Joyner-Halenda
CB	Carbon Black
Conc.	Concentration
CA	Coupling Agent
Dem	Demineralisation
DC	Demineralised Char
EDX	Electron dispersive X-ray analysis
EB	Elongation at Break
FTIR	Fourier Transform Infrared Spectroscopy
HPP	Homopolymer Polypropylene
IS	Impact Strength
MAgPP	Maleic anhydride grafted polypropylene
MFR	Melt Flow Rate
Mn	Number-average molecular weight
PP	Polypropylene
PT-char	Pyrolytic Tyre Char
PT-UC	Pyrolytic-Tyre Untreated Char
PT-DC	Pyrolytic-Tyre Demineralised Char
SEM	Scanning Electron Microscope
Temp	Temperature
TS	Tensile Strength
TGA	Thermal Gravimetric Analysis
UV	Ultraviolet
UC	Untreated Char
Mw	Weight-average molecular weight
YM	Young Modulus

Symbol	Definition	Unit
$A_{3\text{-MPTS}}$	Amount of 3-MPTS	ml
A_F	Amount of the filler	g
$A_{C=O}$	Area of the carbonyl peak	m^2
$A_{C\text{-}H}$	Area of the reference peak	m^2
CI	Carbonyl Index	
Ash_c	Ash content	wt.%
$MCA_{3\text{-MPTS}}$	Minimum coating area of 3-MPTS	m^2/g
$Mass_a$	Weight percent of the element within the ash content	wt.%
$Mass_b$	Actual weight percent of the element within the carbon matrix	wt.%
SA_F	Surface area of the filler	m^2/g
wt.%	Weight percentage	

CHAPTER 1: INTRODUCTION

1.1. Background

1.1.1 Waste tyre

Worldwide, the number of vehicles is increasing and the global market for tyres is anticipated to reach 2.5 billion units by 2022 [1]. This results in an increase of end of life tyres [1]. Due to their complex structure and varied composition, tyres do not degrade easily on landfill and need large landfill space. Waste tyre disposal causes severe environmental and human health problems as they can possibly be a breeding ground for insects causing serious illnesses, such as West Nile Virus [2, 3]. In addition, tyres are often burned in an open environment in order to extract steel and this results in major environmental problems such as air, water and soil pollution [4, 5].

Several methods are used to manage waste tyres, including re-treading, product recycling, energy recovery and material recycling [6]. The challenge with these conventional methods is that the production of the waste tyres is increasing and therefore surpasses the consumption capacity of these methods [7, 8]. Pyrolysis is a well-known technique that is able to solve the waste tyre disposal problems due to its ability to produce valuable products such as tyre derived oil (TDO), pyrolytic tyre gas (PT-gas) and pyrolytic tyre char (PT-char) [9].

Currently, TDO and PT-gas already have a market. TDO can be used as a fuel or it can be added as one of the constituents of petroleum refinery feedstock and PT-gas has a high calorific value and therefore it can be utilised to supply energy during pyrolysis [7, 10]. During pyrolysis, PT-char yields about 30 wt.% to 40 wt.% and for this reason, the process economy relies upon its application and market value [11]. PT-char can be used in different applications; such as low grade fuel due to its high calorific value [12, 13], low grade carbon black (CB) since it contains CB used during tyre manufacturing [14–16] or it can be upgraded into activated carbon (AC) [11, 17]. Nonetheless, due to its high concentration of inorganic impurities (zinc, silica, calcium, etc.) [17, 18], this becomes a challenge. However, demineralisation of PT-char is an effective technique for reducing the inorganics present within PT-char [17–22].

1.1.2 PP composites

Synthetic polymer composites are one of the most popular composites today compared to any other material [12]. This is due to the fact that they are inexpensive, light weight, and durable materials [12]. In polymer composites, the polymer matrix holds the reinforcement while the reinforcement improves the polymeric properties such as mechanical properties and degradation stability. Polypropylene (PP) is a linear hydrocarbon polymer which falls under the family of polyolefin including polyethylene and polybutene. PP composites are widely used in numerous applications such as automotive, household appliances, packaging, consumer products, building and construction [14, 15, 23, 24].

PP has a low tensile modulus and poor impact resistance, especially at lower temperatures [25]. In addition, it is susceptible to oxidation, ultraviolet (UV) radiation degradation and it has relatively low thermal resistance [26, 27]. Therefore, various reinforcing fillers such as fibre, talc, calcium carbonate, mica, silica and CB, are introduced into PP composites in order to extend its properties and reduce the cost [23]. The performance of PP composites depends mostly on the nature of the reinforcing filler. Consequently, it is critical to carefully select the type of additive depending on the properties that are desired.

The majority of industrially used fillers are naturally inorganic and polar. Therefore, problems arise from poor compatibility with hydrocarbon polymer matrices. This incompatibility, results in poor mechanical properties. To develop greater compatibility, surface modifiers are generally utilised to alter the surface characteristics of the filler [28]. This increases the interactions between the filler and the polymer matrix and consequently improves the dispersion of the filler in the polymer matrix [16, 29].

1.2. Problem statement

The disposal of waste tyres can become harmful to the environment if not managed properly. As mentioned previously, pyrolysis is a popular method of managing waste tyre due to the generation of valuable products such as: TDO, PT-gas and PT-char. Currently, the produced PT-char is highly contaminated with inorganic impurities and it is often disposed in landfill

[17, 19, 20]. The market value of PT-char is therefore very low, reducing waste tyre pyrolysis sustainability. Therefore, an additional, value adding alternative use for PT-char is desired.

1.3. Aim

The aim of this research study is to investigate and analyse the feasibility of PT-char as filler in order to enhance the mechanical properties and degradation stability of PP composites.

1.4. Significance of research study

This study will seek to find a potential use of PT-char in PP composites. The use of PT-char, produced by pyrolysis, as alternative filler can potentially reduce the cost of PP composites and extend PP properties. It could also lead to increased interest in the recycling of waste tyres; thereby alleviating environmental problems associated with waste tyres. Furthermore, re-using CB contained within PT-char will decrease the manufacture of new CB and thus decreasing emission of fossil-based CO_2. In addition, it could potentially increase the economic feasibility of waste tyre pyrolysis since it produces a large supply of PT-char.

1.5. Project scope and limitations

Previously, a study was done to determine the best pyrolysis conditions to optimise the extraction of valuable products such as limonene [30]. In the present work, the objective is not to modify the pyrolysis conditions but rather to focus on the use of the solid residue (PT-char), which is formed during the same reaction. The main aim was to conduct a preliminary study using the PT-char to investigate its potential use as filler in PP composite. The results obtained with the PT-char have not been compared with other commercial fillers due to the disadvantages presented by the PT-char in comparison to others fillers: broader particle size range, higher organic and inorganic pollutant content, heterogeneity depending on the material which is pyrolysed, etc.

The study covered the demineralisation of PT-char (with nitric and sodium hydroxide), which is performed in order to reduce impurities, since transition metal impurities in fillers have been known to accelerate degradation of PP [31]. The characteristics of the untreated PT-char

were compared to the demineralised PT-char in order to understand the influence of demineralisation. This was followed by utilisation and evaluation of the influence of surface modifiers (silane, titanate and maleic anhydride grafted polypropylene (MAgPP)) on the rheological properties of PP. The aim with the use of the surface modifiers was to increase the strength of the composites by increasing the strength of interactions between the matrix and the filler surface. The study did not investigate the demineralisation and surface modification conditions. Therefore no optimisation processes were carried out.

Since the study is of a preliminary nature, only short term mechanical properties (impact strength, tensile properties) of PP composite were investigated. The study was limited to accelerated weathering and does not extend to natural weathering testing. The accelerated weathering test was chosen in order to give an indication as to how the performance of PP composites containing the waste material compares with that of PP on its own, before doing an in-depth study of natural weathering. Furthermore, the analysis of degradation was limited to thermal and photo-oxidative degradation and no natural weathering was performed. The influence of MAgPP compatibiliser was not investigated for tensile properties and photo-oxidative degradation studies due to its poor performance on impact strength and thermal-oxidative degradation studies and because of the big amount of composites samples to test. Finally, all experiments were limited to laboratory scale. The research scope is graphically represented in **Figure 1.1**.

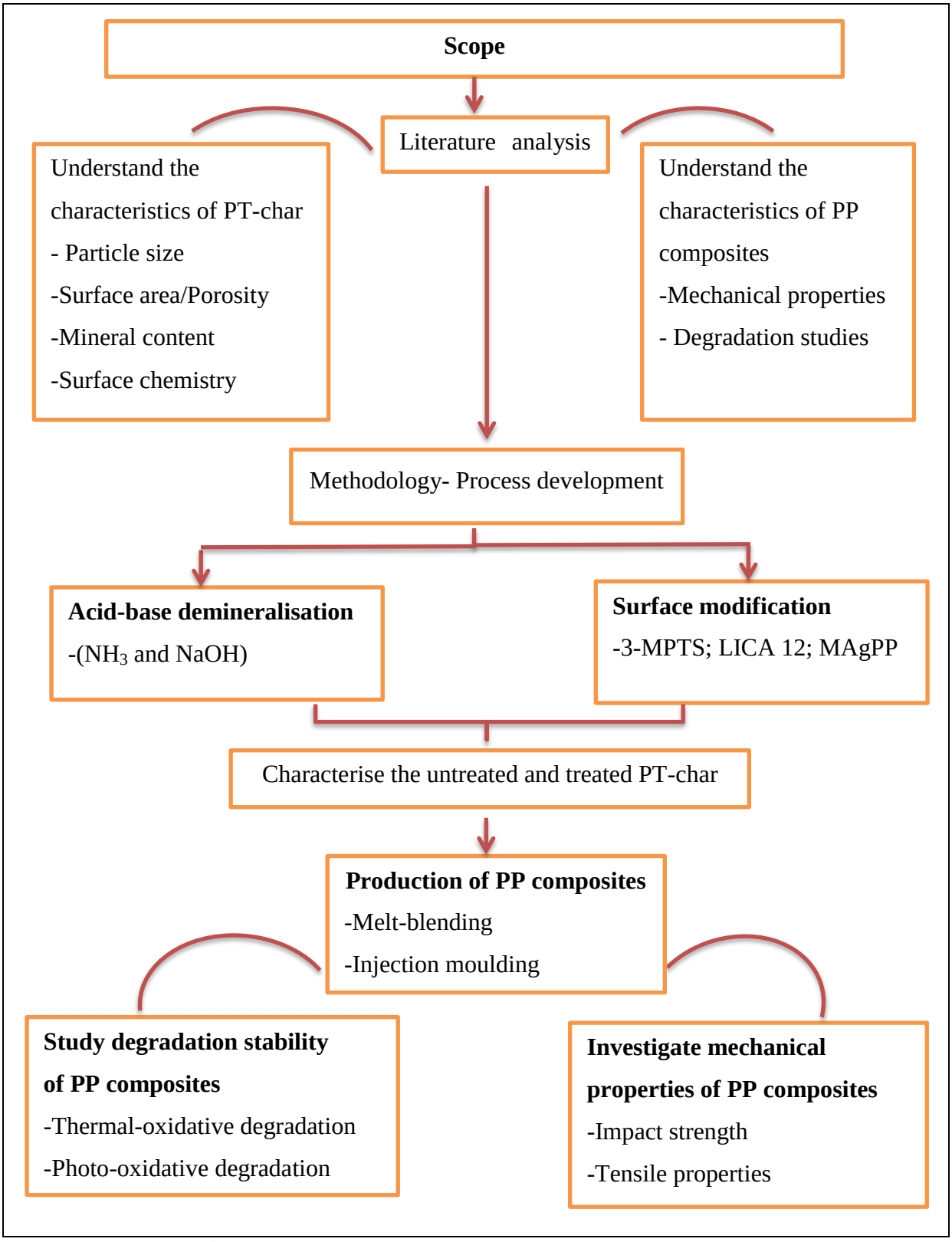

Figure 1.1: Research project scope.

1.6. Thesis overview

The thesis is split into the following chapters:

- **Chapter 1**

The background and problem statement of the study are introduced. The aim of the study and its significance are also identified. The thesis is also presented.

- **Chapter 2**

An overview of pyrolysis is presented in order to understand the properties of PT-char and how to improve them using acid-base demineralisation. Relevant information pertaining to PP composites and their properties are further discussed as well as different surface modifiers and their mode of action.

- **Chapter 3**

The research questions and objectives are described in this section. The scope of the project and the project limitations are also defined.

- **Chapter 4**

The materials that were used, and the experimental design that was selected are described. Furthermore, an overview is given of the analysis techniques and methods that were used.

- **Chapter 5**

Experimental results are described with further discussions supported by the literature.

- **Chapter 6**

The conclusions that were reached in this investigation are explained in detail.

- **Chapter 7**

Recommendations for future work based on these findings from this investigative study are discussed.

CHAPTER 2: LITERATURE REVIEW

2.1. Pyrolysis and demineralisation

2.1.1 Tyre overview

A tyre (**Figure 2.1**) [32] is a polymeric composite, consisting of various layers of natural and synthetic rubber, textile material, steel belt and cord [33]. It is circular in shape so as to be able to rotate as it moves. Tyres are made up of different parts, including body plies, sidewall, tread, bead filler, blocks, carcass, heels and bead bundle, and they all have different functions [32, 34]. For instance, the functions of the body plies are to provide strength to the tyre and resistance to road damage [32]. The belt assists the tread to stay afloat and in contact with road. The tread comes in contact with the road and it is usually hard [32]. The sidewall protects the body plies and beads hold the tyre to the wheel [34]. The inner layer prevents air from penetrating the tyre and the carcass shields the inner coating and supports the vehicle load [32, 34].

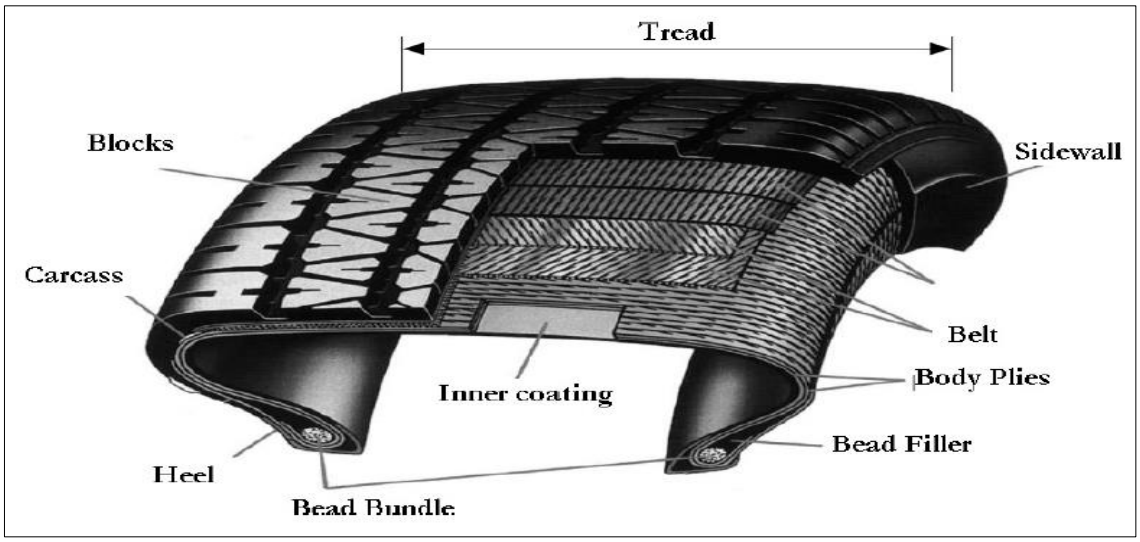

Figure 2.1: Tyre components [32].

Tyres comprise of a range of compounds that assist in making the tyre strong so as to be able to withstand the impact of heat, air and rough conditions (see **Table 2.1**) [33, 35]. The rubber constituents of a tyre consist of different elastomers that include the natural rubber (polyisoprene) and synthetic rubber (polybutadiene and styrene-butadiene) [8, 35, 36]. Tyre

also contain CB filler, which is added to reinforce the rubber and extender oil, which is a blend of aromatic hydrocarbons that helps to soften the rubber [10, 33]. Some tyre manufacturers may replace CB with silicon dioxide to reduce the costs or use their combination to strengthen the rubber chains [37]. Tyre also contains compounds such as zinc oxide, stearic acid, accelerators, anti-degradants and non-metal such as sulphur. The sulphur is added as a vulcanising agent to crosslink the polymer chains of the rubber [35]. Zinc oxide and stearic acid are added to control the vulcanisation process as well as to boost the physical properties of the tyre [35, 36]. Tyre industries use an extensive variety of tyre compositions so as to meet explicit tyre performance requirements. Subsequently, the chemical compositions of tyre vary significantly depending upon the kind of sample used.

Table 2.1:Typical tyre composition [35].

Component	Content (wt.%)
Rubber (elastomers)	62.1
CB	31.0
Extender oil	1.9
Zinc oxide	1.9
Stearic acid	1.2
Sulphur	1.1
Accelerators	0.7

2.1.2 Waste tyre pyrolysis

Pyrolysis is a thermochemical process that is used to break apart solid organic material at high temperatures in the presence of an inert gas to yield oil, gas and char [9, 10, 33, 38, 39]. During waste tyre pyrolysis, the sulphide bonds are firstly broken down followed by carbon bonds [40, 41]. As mentioned, the decomposition of the waste tyre produces three products: solid fraction [PT-char (30 wt.% to 40 wt.%)] [11, 13, 42, 43] and a volatile fraction [PT-gas (5 wt.% to 20 wt.%) [42] and TDO (40 wt.% to 60 wt.%)] [9, 33, 42]. These variations in the percentage yield of the various waste tyre pyrolysis products depend on the tyre composition and the pyrolysis conditions [13]. In this study, the focus is on PT-char.

There are many types of pyrolysis and they can be classified based on the pyrolysis environment, i.e. hydro, steam, oxidative and vacuum [9]. In a vacuum reactor, as the name

indicates, pyrolysis happens in a vacuum system and thus the volatiles formed have little residence time inside the reactor and they are removed as soon as they are created [38]. If the pyrolysis is carried out at atmospheric pressure, normally nitrogen gas is used as carrier gas as it is inexpensive and inert. It also avoids the presence of oxygen that could lead to oxidation [9, 33]. Pyrolysis can also be categorised depending on the temperature, heating rate and volatile residence time [9]. Consequently, pyrolysis is classified as either slow or fast [9, 44]. In slow pyrolysis, a low heating rate is required and the pyrolytic decomposition is usually slow, enhancing the formation of the solid phase [9, 44]. Fast pyrolysis is associated with rapid thermal decomposition at high temperature with a high heating rate and short vapour residence time; thus promoting high liquid yield [9, 44]. Pyrolysis can also be categorised depending on the reactor used, i.e. fixed bed (batch), fluidised bed, rotary kiln, rotating cone, entrained bed and vacuum [9, 33, 35]. The fluidised bed, entrained bed and rotating cone reactors are associated with fast pyrolysis [9], while fixed bed and rotary kiln reactors are associated with slow pyrolysis [9, 38].

Waste tyre pyrolysis has been examined by several scientists which have found that the operating conditions have a major influence on the pyrolysis products [35, 43, 45–48]. Pyrolysis conditions such as residence time, temperature, heating rate, the catalyst used, pressure and type of feedstock (type of tyre) can be altered in order to maximise or minimise the different products [43]. Since pyrolysis is not part of the scope of this investigation, this study will not elaborate on the typical operating conditions.

2.1.3 PT-char physical properties

PT-char is visible as a soot-like powder with different particle sizes, depending on the size of the pyrolysis feedstock and the processing conditions [49]. PT-char is composed of heterogeneous structure while CB has a graphite-like structure with primary particles that have spherical shapes [20, 37]. The particle size of the PT-char is normally larger than those of commercial CB due to the ash content and the organic depositions [20]. The particle size of commercial CB ranges from 10 nm to 500 nm [50, 51] while those of PT-char have been found to range from 23 nm to 210 µm [10, 20, 52]. Due to the finer particle size of CB, its particles often aggregate in grape-like clusters [51], while those of the PT-char aggregate in spherical particle shape [52]. The aggregates fuse together by attractive Van der Waals forces to create agglomerates [50]. **Table 2.2** and **Table 2.3** present the particle size and surface

area of PT-char and commercial CB used in tyre production, as reported by different previous studies.

Table 2.2: Typical surface area and particle sizes of PT-char reported from the literature.

Pyrolysis temperature (°C)	BET surface area (m^2/g)	Particle size	Details	Reference
400	71.9			[21]
425	46.5			[53]
450 to 650	47.5			[11]
450	93.0			[39]
750	91.0			
1000	139			
500	69.5	≤ 210 µm		[10]
500	84.2			[54]
550	72.0			[55]
550	72.4	52 nm		[51]
550	51.0	23 nm	42 µm aggregate size	[52]
550	69.2	96 nm		[20]
600 to 700	73.0			[56]
450	61.0			[57]
475	65.0			
500	64.0			
525	68.0			
560	67.0			
600	65.0			

Table 2.3: Surface areas of commercial CB used in tyres.

CB grade	BET surface area (m^2/g)	Reference
N351	73.0	[35]
N650	38.0	
N110	138	[19]
N330	83.0	
N660	36.0	

N550	43.0	[58]
N774	28.0	
N326	60.0 to 90.0	[51]
N339		
N347		
N234	120.4	
N375	89.6	
N775	26.8	

The surface area of PT-char is generally low. It ranges from 30 m^2/g to 90 m^2/g depending on the composition of the waste tyre and the pyrolysis conditions [10, 22]. Some studies have also reported surface area of up to 139 m^2/g [39]. PT-char surface area is usually low because of its high ash content and some carbonaceous deposits which may be present on the surface of PT-char [20]. Previously reported studies describe PT-char with diverse porosity structure [17, 22, 54, 59]. Several researchers [54, 59–62], have analysed the pore structure of PT-chars and found them to be mainly mesoporous. According to Zhu *et al*. [54], the presence of mesopores in the PT-char mostly originates from the inter-aggregate holes due to the gasification removal of the carbon that remains reserved in the holes. The nature of the pores present in the PT-char is influenced by the initial feedstock employed and also the pyrolysis conditions [63–67]. For instance, the feedstock with high volatile matter content tends to produce PT-char with high pore volumes and lower proportions of micropores [67, 68] while PT-chars produced at lower temperature exhibit a higher degree of mesopores and micropores [64, 65]. A high heating rate has been found to generate PT-char with lower micropores volume and greater proportions of larger pores than otherwise identical PT-chars made at lower heating rates [64–66].

The PT-char's particle size and surface area are essential attributes of a filler since the level of reinforcement mainly depends on them [17]. Usually, small particle size is preferred in the reinforcement industry due to its efficient reinforcement ability [50, 69]. Furthermore, the degree of interaction of the filler with the matrix is determined by the surface area of the filler [17]. A detailed explanation on the influence of particle size and surface area on the level of reinforcement and degradation stability of PP composites will be discussed in section 2.2.1.

2.1.4 PT-char composition

The composition of PT-char relies mainly on the waste tyre feedstock and the pyrolysis parameters used [9]. **Table 2.4**, **Table 2.5** and **Table 2.6** present some of the literature reported results of proximate and ultimate analysis as well as chemical composition analysis of the ash content. Once waste tyre pyrolysis is complete, most of the rubber and the extender oil is changed into TDO and PT-gas while some become part of the PT-char composition [37]. The inorganic compounds of the tyre become constituents of the impurities or ash in the PT-char and some may volatise and end up in the TDO or the PT-gas product [37]. As shown in **Table 2.4**, PT-char contains fixed carbon which ranges between 68.7 wt.% and 91.3 wt.% and some extra carbonaceous deposits [37]. The carbon mainly originates from the commercial CB filler that was added during tyre manufacture since the rubber constituents of the tyre only produce about ~ 4 wt.% of the carbon [33]. The carbonaceous deposits originate from incomplete pyrolysis of tyre rubber during pyrolysis [33, 37]. The moisture has been reported to be ≤ 5 wt.% [13] and the volatiles (which corresponds to the rubber and the extender oil) content range from 0.4 wt.% to 47.4 wt.% [5, 37, 45, 55, 70, 71].

Several researchers [5, 39, 45, 46, 48, 55, 70], reported an ash content which ranges between 5.6 wt.% and 20.5 wt.%. According to Buekens [72], the variations in ash content of PT-char results from the differences in the type of the tyre used for pyrolysis feedstock. These differences include the variety of inorganic minerals used during tyre manufacture [9, 33]. **Table 2.4** further shows that an increase in temperature reduces the volatile residue content while the fixed carbon is increased [39, 48, 70]. It is also evident that an increase in temperature reduces the amount of moisture and ash [48].

Table 2.4: Proximate analysis of PT-char obtained at different pyrolysis temperature.

Pyrolysis temperature (°C)	Solid residence time (min)	Moisture (wt.%)	Volatile matter (wt.%)	Fixed carbon (wt.%)	Ash (wt.%)	References
350	30		47.4	45.7	6.9	[45]
400			25.9	64.9	9.2	
450			6.7	77.6	15.7	
500			6.0	78.2	15.8	

550			5.5	78.4	16.1	
575			5.5	78.2	16.3	
600			5.2	78.5	16.3	
700			5.0	78.9	16.1	
450		3.4	16.1	67.5	12.5	[46]
500		2.4	16.1	69.2	12.3	
550		1.3	7.0	77.2	14.6	
600		2.0	5.9	77.9	14.3	
650		1.5	6.3	78.3	13.9	
450	45	0.9	14.2	76.3	8.6	[70]
500		0.5	3.5	86.1	9.9	
450	120	0.4	7.8		8.3	[39]
750		0.4	5.6		8.3	
1000		0.2	1.1		5.6	
500		0.4	3.2	82.2	14.6	[17]
550	60	0.5	0.4	90.5	8.6	[55]
550		0.4	1.8	91.3	12.5	[58]
550	240	0.7	3.5	82.1	13.8	[73]
550	40	3.6	12.8	71.9	15.3	[48]
600		3.0	10.8	76.1	13.2	
680		1.4	5.2	83.0	11.8	
600	60	1.2	9.7	68.7	20.5	[5]

The ultimate analysis (**Table 2.5**) shows that the hydrogen and nitrogen content decreases with an increase in temperature [39, 48, 74]. The decrease in the hydrogen content indicates reduced formation of solid hydrocarbons due to short solid residence time. The reduction in volatile matter content with increased temperature and short residence time supports this supposition. The hydrogen content varies from 0.2 wt.% to 2.3 wt.% as shown in **Table 2.5**. Hydrogen content that is greater than 1 wt.% can be considered a sign of a not-fully pyrolysed residue [75] since hydrogen originates from the rubber and some carbonaceous deposits [13]. Nitrogen originates from accelerators used during rubber vulcanisation and from antioxidants [37]. Furthermore, sulphur is mostly retained in the ash content of the PT-char. The amount of oxygen is slightly higher. The oxygen was derived from the oxygen

surface intermediate formed during the making of CB filler by partial combustion of hydrocarbons [76].

Table 2.5: Ultimate analysis of PT-char obtained at different pyrolysis temperature.

Pyrolysis temperature (°C)	Solid residence time (min)	C (wt.%)	H (wt.%)	N (wt.%)	S (wt.%)	O (wt.%)	References
450		82.1	2.1	0.5	2.3		[46]
500		82.2	2.3	2.3	2.3		
550		80.8	1.5	2.4	2.4		
600		81.0	1.4	2.5	2.5		
650		81.0	2.0	2.4	2.4		
450	120	88.2	0.6	0.1	1.9		[39]
750		88.6	0.3	0.3	2.0		
1000		92.1	0.2	0	1.2		
500		80.4	0.4	0.7	3.6	0.3	[17]
500	60	82.7	0.4	≤ 0.1	2.2		[10]
500	720	84.8	1.0	0.1	1.0	0.4	[54]
500	300	78.8	1.1	0.3	2.0	7.0	[77]
500		85.2	1.2	0.6	2.0		[78]
550		86.3	0.3	0.3	2.8		[58]
550	240	81.5	1.00	0.5	3.3	13.7	[73]
550	60	83.0	1.4	0.4	1.7	13.5	[74]
800		78.5	0.5	0.3	2.40	18.3	
550	40	85.3	1.8	0.3	2.1		[48]
600		85.6	1.3	0.3	2.3		
680		85.2	0.9	0.2	2.6		
600	60	83.2		0.7	2.4	8.7	[5]

As seen from **Table 2.6,** the ash content of the PT-char has a diverse chemical composition with zinc and silicon being the only major inorganic constituents, followed by calcium and magnesium. Calcium is derived from calcium carbonate which also used to replace CB filler and magnesium is derived from small steel wire fragments which were not detached from the

tyre before pyrolysis [79]. PT-char may contain some traces of elements, such as phosphorus, iron, copper, titanium, potassium, cadmium, barium, cobalt, chromium, manganese and nickel [18, 20, 37, 50, 68, 79]. The chemical composition of the tyres differs depending on the nature of the tyre (truck or car) and the brand that produces them [79]. The metals present within the PT-char can be in their elemental form or in their corresponding oxide, sulphide or chloride form [33]. PT-char is not suitable for use as a CB filler due to its high mineral content, which substantially decreases the CB reinforcing ability [20, 80, 81], unlike commercial CB that presents a maximum ash percentages between 0.1 wt.% and 2 wt.% [19, 71]. As mentioned earlier, the composition of PT-char is determined by the process parameters such as temperature, heating rate, pressure, residence time, type of pyrolysis reactor and the waste tyre feedstock (compositions of the tyre) [9, 48]. Therefore, results from different studies may vary due to the differences in pyrolysis conditions.

Table 2.6: The mineral content of PT-char reported from the literature.

References	[68]						[39]			[55]	[48]		
Pyrolysis temperature (°C)	450	475	500	525	560	600	450	750	1000	550	550	600	680
Residence time (min)	90						120			60	40		
Unit	wt.%	wt.%	wt.%	wt.%	wt.%	wt.%	wt.%	wt.%	wt.%	wt.%	ppm	ppm	ppm
Mg	0.60	0.60	0.90	0.60	0.40	0.60	0.15	0.15	0.25	0.09			
Al	0.30	0.20	0.30	0.40	0.20	0.30				0.13	11000	14400	12500
Si	1.00	0.90	0.90	1.10	0.50	1.40	1.69	1.64	3.66	2.66			
P	0.06	0.06	0.05	0.06	0.06	0.05							
Cl	0.06	0.06	0.08	0.06	0.09	0.05							
K	0.10	0.20	0.10	0.10	0.10	0.10	0.10	0.09	0.23	0.14			
Ca	0.60	0.60	1.20	1.00	1.80	0.80	0.13	0.15	0.29	0.37			
Ti	0.02	0.03	0.02	0.04	0.02	0.04	0.02	0.02	0.04				
Cr											45.0	53.0	30.0
Fe	0.30	0.30	0.30	0.30	0.20	0.30	0.04	0.06	0.12	0.09	5480	5830	6310
Cu										0.01	205	150	430
Zn	3.60	3.30	4.10	3.70	4.00	3.50	6.68	6.33	0.940	2.53	40600	25000	42700
Pb							0.01	0	0		581	575	446
Cd											9.60	7.80	8.60
Ni											50.0	93.0	50.0
Hg											2.20	1.50	2.20

2.1.5 Possible applications of PT-char

The application of PT-char depends on its chemical composition and surface chemistry. PT-char can be utilised as a fuel due to its high energy content (30 MJ/kg). However, the high ash content (mainly sulphur) hinders its use as a fuel [42, 75]. PT-char can replace CB in different applications including: reinforcement in the rubber industry, due to its similar characteristics (physical and textural) [20, 43, 80, 82]; in the plastic industry, due to its stabilising effect in thermal [83, 84] and photodegradation [84, 85] or as a pigment in ink, due to its conductivity properties [86]. PT-char can also be upgraded to AC for wastewater treatment [11, 18, 22, 43, 59, 87–89]. There are more studies carried out on AC [11, 18, 22, 43, 59, 87–89] than CB [20, 43, 80, 82], probably because it is easier to produce AC than CB due to its aggregation tendency [45].

2.1.6 Demineralisation

As mentioned, PT-char has a diverse chemical composition with zinc and silicon being the major inorganic constituents, followed by calcium and magnesium. PT-char contains some traces of elements such as phosphorus, iron, copper, titanium, potassium, cadmium, barium, cobalt, chromium, manganese, nickel, lead and antimony [18, 20, 37, 50, 68, 79]. As mentioned, metals contained within PT-char may appear in their elemental form or in the form of their corresponding oxide or sulphide. For instance, inorganic minerals such as zinc oxide and silicon dioxide are generally present within a tyre. However, zinc oxide can also be changed into zinc in the presence of hydrogen [39], or it can react with sulphur and form zinc sulphide above pyrolysis temperature of 700 °C [7, 90, 91]. Metals such as titanium, aluminium and magnesium, tend to form oxide in the presence of air and therefore, they will partially be in their oxide form [49].

Iron and magnesium have been reported to derive from residue of metal wires within the tyre which were not removed by a magnet before the pyrolysis process [75, 79]. Even though sulphur has a low boiling point of 444.7 °C, a substantial amount of sulphur still remains within the PT-char due to the presence of carbon sulphur complexes which are quite stable, even at high temperature of around 1000 °C [11, 92]. Since, silicon has a high boiling point, it is unable to leave the sample with the volatiles during pyrolysis and consequently it remains in the PT-char [79]. Therefore, most metals contained in the PT-char are unable to

evaporate during pyrolysis since they require high temperature and therefore they reside within the PT-char after pyrolysis. All these inorganic elements make up the ash content found in PT-char and subsequently results in a low surface area (30 m^2/g to 90 m^2/g) [10, 22].

An effective way of reducing the ash content in the surface of PT-char is by a demineralisation process. Demineralisation is a leaching process that involves liquid-solid extraction. During demineralisation, the soluble fraction is separated from an insoluble solid [93, 94]. The demineralisation process can be performed using numerous acids and bases which aid in reducing the content of the inorganic compounds and some tarry products inside the surface of the PT-char [18, 20, 37, 68]. By removing the inorganic impurities inside the PT-char, the surface area; as well as the mesopore and micropore volume can be improved [17, 21, 22, 54, 57, 88, 89, 95–97], and the particle size of PT-char further reduced [20].

Acid-base lixiviants have been utilised previously by several researchers [17–21, 88]. Some even performed sequential extraction using two different acids or an acid and a base [17, 88]. They have noticed that their combinations reduced the high amount of ash since their combinations creates salts that are soluble in water-based solutions [17, 88]. Iraola-Arregui *et al*. [79], concluded from their review that acid-base demineralisation should be performed after waste tyre pyrolysis due to the cross-linked chemical structure of the tyre rubber which is extremely resistant to chemicals. Several researchers carried out demineralisation of PT-char and their results are presented in **Table 2.7**.

Table 2.7: Acid-base demineralisation conditions of PT-char found in the literature.

Dem. agent	Conc. of dem. agent (M or N)	Dem.agent to sample ratio	Extraction temp. (°C)	Extraction time (min or h)	Initial ash wt.%	Removed ash (wt.%)	Details	Reference
H_2SO_4	1 N	10 ml/g	60	30 min	14.6	6.8	Optimal found to be 1 N for H_2SO_4 and 5 N for NaOH. Dem. increased the surface area of PT-char from 43.1 m^2/g in the untreated PT-char to 53.0 m^2/g in the case of 1 N H_2SO_4 and 64.8 m^2/g in the case of 1 N H_2SO_4 and 5 N NaOH.	[17]
H_2SO_4 + NaOH	1 N:1 N					5.8		
	1 N:2 N					4.8		
	1 N:3 N					4.4		
	1 N:4 N					4.1		
	1 N:5 N					3.1		
	1 N:10 N					3.0		
HNO_3	10 M	30 % Vol.	Room temp.	48 h	5.7		Dem. increased the surface area from 71.9 m^2/g in the untreated PT-char to 78.8 m^2/g in the case of HCl, 77.0 m^2/g in the case of HCOOH and slightly decreased to 52.1 m^2/g in the case of HNO_3 and 59.2 m^2/g in the case of H_2O_2 The pore size increased from 14.2 nm to 21.3 nm and the pore volume from 0.3 cm^3/g to 0.4 cm^3/g	[21]
HCl								
HCOOH								
H_2O_2								

HNO_3		20 wt.%	80	60 min	16.2	7.5	Dem. increased the surface area from 69.2 m^2/g in the untreated PT-char to 88.6 m^2/g.	[20]
NaOH	3 N				12.2	9.1	Optimal found to be 6 N NaOH because it gives maximum percentage of metal oxide removal	[18]
HNO_3						9.9		
H_2SO_4						10.3		
HCl						9.5		
H_2SO_4	1 N		Room temp	24 h			Dem. PT-char was crushed and sieved through 45.0 µm particle size prior to analysis. Dem. increased surface area of PT-char from 85.0 m^2/g to 870 m^2/g in the case of HCl and 800 m^2/g in the case of H_2SO_4	[88]
HCl								
HCl		10 wt.%	100	2 h	14.3		PT-char pyrolysed at different temp. (550 °C, 650 °C, 800 °C) was used as feed.	[96]
					14.8			
					13.5			

Mostly, the use of hydrochloric acid, sulphuric acid and nitric acids for demineralisation is reported in the literature [17, 18, 22, 57, 68, 88, 96, 98]. Hydrochloric acid, sulphuric acid and nitric acid have proven to be effective in the removal of substantial amounts of metals from PT-char [21, 88, 95]. Nitric acid has previously been used to reduce ash content by more than 90 % [95] and the use of hydrochloric acid and nitric acid has resulted in the highest reduction in the sulphur content of the PT-char, at 65 % and 68 % reduction respectively [21]. Since nitric acid is an oxidising agent [79], it is used to oxidise the surface of PT-char by forming oxygenated functional groups (carbonyl, carboxylic, phenolic and lactonic) so as to increase its reactivity [21].

Several researchers [17, 18, 87], have also discussed the influence of two alkalis, sodium hydroxide [17, 18] and potassium hydroxide [87]. Both alkalis are known to react and dissolve silicon, aluminium and zinc [17]. However, sodium hydroxide has been shown to be more effective, as it is a stronger alkali than potassium hydroxide. To some extent, sodium hydroxide has also been proven to be more efficient even than acid, reaching an efficiency of about 25.2 % against the 22.2 % of hydrochloric acid [18]. Furthermore, sodium hydroxide is generally used in composites production in order to activate the surface of the fillers by introducing –OH groups which are essential for the adherence of the coupling agent to the surface of the filler [99, 100].

Oxides can be acidic, basic or amphoteric. Amphoteric compounds have the ability to react both as an acid or a base [101]. Compounds such as zinc oxide, aluminium oxide, titanium oxide, chromium oxide and iron oxide are amphoteric, while magnesium oxide is not [17, 18]. Silicon dioxide is not amphoteric due to its slightly acidic nature and therefore it can only react with basic substances [49]. During demineralisation, dissolution of metal oxides takes place. For instance, by adding hydrochloric acid, sulphuric acid, nitric acid or sodium hydroxide as an acid-base lixiviant, zinc and iron can be dissolved into zinc chloride, zinc sulphate, zinc nitrate, sodium zincate, iron chloride or iron sulphate [18]. The difference in ash removal by the various acids and bases can be explained as a result of the removal of different inorganic compounds by the different acids and bases.

Several parameters such as temperature, concentration of acid-base lixiviants, contact time, contact method (agitation or mixing) have a major influence on demineralisation [102]. Usually, when the concentration of the acid-base is increased, demineralisation efficiency

increases [17, 18]. An increase in reaction temperature and contact time also increases efficiency of demineralisation [17, 102]. When impurities are removed from the PT-char surface, the density and the particle size decreases while the surface area increases [18, 20].

Demineralisation is the most common method to dissolve metals. However, care must be taken when conducting an experiment since reaction of acid lixiviants such as hydrochloric acid, nitric acid and sulphuric acid with the PT-char results in the formation of hazardous fumes, such as chlorine, nitrogen dioxide and sulphur dioxide, respectively [18]. During demineralisation, the performance of the different acids and bases varies as a result of their ability to remove different inorganic components [18]. Due to the high ash content, the use of both an acid and a base is important in order to extract the various ash components. Therefore, both nitric acid and sodium hydroxides will proceed further in this study since they both show potential. In addition to removing the ash, nitric acid was also chosen for its oxidising ability which is necessary in order to increase the reactivity of the surface chemistry of the PT-char. Sodium hydroxide also makes significant contribution to the surface modification by adding hydroxyl groups to the surface.

2.1.7 Concluding remarks

Pyrolysis is a potential process for converting waste tyre into high value products. PT-char in particular, is a heterogeneous waste material due to a variety of compounds that are used during the manufacture of waste tyres and the complexity of the pyrolysis process. Furthermore, it is also highly contaminated by inorganic impurities which may reduce its reinforcement potential.

Therefore, a substantial reduction in ash content and an increase in surface area are required in order to improve the quality of PT-char. Due to the high ash content, the use of both an acid and a base is important in order to extract the different ash components. Furthermore, surface modification is also required to increase the reactivity of the PT-char. Therefore, all these factors must be considered in order to improve the quality of PT-char as filler.

2.2. PP composite properties

2.2.1 PP composites and fillers properties

Composites are made up of two or more different parts, which are the matrix and the reinforcement [103, 104]. The matrix is the continuous phase, which normally forms the major component and has to be capable of binding with the reinforcement [103, 104]. The reinforcement is the discontinuous phase, which is used to provide strength and stiffness, inhibit crack propagation and reduce cost [103, 104]. Composite materials have bulk properties that are significantly different from those of any of the constituents [105]. Polymers are the most popular matrix for composites material and they are used in several applications due to their ability to be fabricated into any large complex shape [106].

Various additives are added into PP in order to stabilise the material during and after processing. The additives can be categorised into functional additives, reinforcements or fillers. Functional additives have specific functions in the polymer, e.g. antioxidants, UV stabilisers, hydroperoxide decomposers and flame retardants. Reinforcements are mainly used to carry the load applied to the composites, e.g. glass fibres, asbestos, wallostine and mica. Fillers are mainly used to lessen the expense of composites; nonetheless, they can still improve the processing characteristics and mechanical properties, e.g. talc, calcium carbonate, clay and CB [107]. Generally reinforcing fillers, are inorganic, solid materials that may be fibrous, platelets, flake-like or spherical in shape [106]. For both traditional and engineering materials, the cost of composites is a vital aspect [107]. The price of nanofillers (e.g. carbon nanotube) is usually higher than microfillers and sometimes even more expensive than the polymeric matrix. Hence in most cases the aim of their applications is usually to enhance the properties (mainly mechanical properties) of the composites [107].

There are diverse types of reinforcing fillers that are used to boost the performance of PP composites. The most common ones are, carbon fibre [108], calcium carbonate [69, 109, 110], silicon dioxide [111], talc [112, 113], mica [114], wallostine [115], dolomite [116] and CB [117, 118]. Particulate filled homopolymer PP composites can be found in automotive products, household appliances, packaging, consumer products as well as building and construction applications (see **Table 2.8**) [23, 24, 106]. Numerous fillers are blended with PP

for different applications depending on their characteristics. For instance, calcium carbonate and talc are generally used in automotive products and household appliances due to their ability to impart toughness and stiffness in addition to thermal stability [23, 24]. Furthermore, calcium carbonate and talc can be added to a higher content from 10 wt.% to 40 wt.%, thus reducing the cost of the composite [24]. Calcium carbonate filled PP composites can be found mainly in household appliances and in packaging due to its bright colour attribute [23, 24]. Due to its high temperature resistance, mica reinforced PP composites can also be found in automotive applications such as crash pad retainers, batteries and fan shrouds [24]. However, because it is dark in colour, mica is not suitable for light coloured applications [23, 24].

Table 2.8: Typical applications of PP composites.

Typical applications of PP composites	Required properties	Typical filler	Reference
Automotive Exterior: bumper fascia, mirror housing. Interior: door handles and pocket, pillar and trim.	High impact strength at low temperature, high tensile modulus and moderate tensile strength and high thermal stability.	Calcium carbonate, talc, mica, carbon fibres and CB	[23, 24, 106, 119, 120]
Appliances Small: body of iron and hairdryer, hand mixer and coffee maker. Large: refrigerator parts and washing machine parts (drum)	Good rigidity, impact strength and chemical resistance and high thermal stability.	Talc, mica, calcium carbonate, carbon fibres and wallostine	[23, 24, 120]
Packaging Dairy products, snack food packaging, plastic bottles, food storage containers.	Colourability, chemical resistance and thermal stability.	Calcium carbonate, carbon fibre	[23, 24]
Consumer Products Luggage, tables and chairs.	Good rigidity, impact strength, colourability,	Calcium carbonate,	[23, 24, 120]

	thermal and UV stability.	CB	
Building and construction Pipes and fittings	Chemical resistance and tensile modulus	CB, mica	[23, 24, 120]

Various filler characteristics (chemical composition, purity, particle size and distribution, surface area and filler loading) influence the properties of composites [107]. Traces of transition metal contamination reduce stability of the composite while inadequate purity can lead to discoloration [23, 107]. Furthermore, polymer oxidation is more pronounced on composites filled with mineral fillers with high surface area [23]. The fillers particle size, shape and distribution affect the dispersion and the interactions between the filler and the matrix [23]. Usually, nanofillers are commonly used in the reinforcing industry due to their more efficient reinforcement ability compared to large filler particles which simply detach from the PP matrix under loading [69, 121]. The superior reinforcement ability of nanofillers is due to their ability of transferring stress from the polymer matrix to the filler as a results of their large surface area and excellent adhesion ability with the polymer matrix [122].

Plate or flake-like fillers (e.g. talc and mica) reinforce polymers more than spherical fillers (e.g. calcium carbonate and CB) and their influence on fibrous reinforcements is even stronger due to their high aspect ratio [23, 106, 107, 123]. Even though nanocomposites are most preferred, a reduction in filler particle size influences particle aggregation because of the small distance between the particles [107]. Filler aggregation makes it difficult for the filler to disperse properly on the polymer matrix. **Table 2.9**, describe some of the filler particles reported in the literature.

Table 2.9: Various particle sizes and surface areas of fillers used in PP composites.

Typical fillers	Average particles size	Surface area (m^2/g)	Aspect ratio	Details	Reference
Calcium carbonate	0.1 µm	19.0		Spherical shape	[69, 124]
	0.7 µm	7.0			
	3.5 µm	3.0		Irregular shape	
	2.5 µm	3.6			[28, 125]
	0.7 µm	12.0			[126]

	0.8 µm				[109, 127]
CB	25.0 nm				[117]
	25.0 nm				[128]
Talc	13.0 µm		40		[129]
	19.0 µm				[130]
Silica	10.0 nm to 20.0 nm			Silica powder	[121]
	30.0 nm			Silica colloid	
	7.0 nm				[131]
	7.0 nm	390			[99]
	8.2 µm		2.9	Elongated particle shape	[132]
Mica	60.0 µm		1200		[114]
	8.1 µm		23.6	Flake particle shape	[132]
Barium sulphate	70.0 µm			Spherical particle shape. Agglomerates particle size of 100 µm.	[133]
Aluminium hydroxide	4.0 µm			Flake-like particle shape. Agglomerate particle size of 400 µm.	
Alumina	13.5 µm				[134]

Several researchers [69, 83, 110, 113, 117, 124, 131, 133, 135, 136], have previously used different filler loadings to investigate the properties of PP composites. The most important concept regarding the preparation of polymer composites is the dispersion state of the filler particles on the polymer matrix [83]. The matrix/filler and the particle/particle interactions which are both determined by the surface free energy (surface tension) of the filler, also have a major influence on the properties of composites [83, 107]. The matrix/filler interaction has a pronounced effect on the properties of the composites and the particle/particle interactions usually determine aggregation. [107]. Both interactions influence the dispersion of filler particles.

Very often at high filler loading, filler particle aggregates tend to occur making it difficult for the filler to disperse properly on the polymer matrix [69, 117]. At higher filler loadings, filler particle-particle interactions are stronger due to higher surface free energy and these stronger interactions consequently induce aggregation [69, 124]. This leads to poor matrix/filler interaction which then affects the properties of the composites [69, 110, 117, 124]. Agglomeration can also be caused by Van der Waals forces, water bridging, Lewis acid-base interactions and hydrogen bonds [50, 137, 138]. Filler agglomerates act as stress concentrators reducing the performance of PP composites [69, 110, 124]. Mechanical energy is required in order to separate filler particles. Sometimes mechanical mixing might not be sufficient and therefore, dispersants can also be used to reduce forces of attraction between the particles [137].

The properties of the final product depend not only on the characteristics of the filler but also on the operating conditions, such as type of moulding instrument (injection or compression) operating temperature and pressure for blending and moulding and the surface treatment conditions. Strong adhesion between the matrix and the filler is the primary condition for effective reinforcement [107]. Since fillers are different in nature, sometimes, blends of different fillers can improve mechanical properties more efficiently than composites filled with a single filler [132]. Moreover, blends of small and large filler particles or blends of different particle shapes of the same filler can also improve mechanical properties of PP composites much better than homogenous particles of the same filler [120]. Furthermore, variations in molecular structure of the PP grade used and the morphology arising from the processing conditions also affect the mechanical properties of PP composites. It is important to note that, if one property is improved it is generally at the expense of another. Therefore, it is important to choose the type of filler (according to particle size, shape, surface area, composition and whether it is modified or not) based on the application of interest.

2.2.2 Surface modification

It is documented that reinforcing fillers improve the properties and enlarge the application breadth of polymeric composites [69, 83, 110, 131–133, 135, 136, 139, 140]. Nonetheless, uniform dispersion and compatibility between the filler and the polymer matrix is a challenge for the preparation of polymer composites [141]. Most fillers are inorganic and polar in nature; hence problems originate from the poor compatibility with hydrocarbon polymers

[103]. In addition, most fillers particle, e.g. CB, have the tendency to aggregate due to high surface energy thus causing poor adhesion between the polymer matrix and the filler surface [128, 142]. Poor dispersion between the filler particles and the polymer matrix results in an insufficient reinforcement and poor mechanical properties [103]. In order to solve these problems, surface modifiers are normally used to increase the affinity and adhesion between the polymer matrix and filler surface [16, 29]. They are also used to protect the fillers while others can improve the flow property of the filler [103, 132, 143].

There are two main classes of surface modifiers which include the dispersants (non-coupling) and the coupling (coupling agents) modifiers. The non-coupling modifiers usually have strong interactions with the filler surface, but only very weak dispersive interactions with the polymer matrix chains [103]. The most widely used dispersant is fatty acid, e.g. stearic acid [103]. Coupling agents have strong interactions with both the filler and the polymer matrix [103]. Various coupling agents are used in the production of PP composites. Coupling agents can be categorised into three different types: organic, inorganic, and organic-inorganic. The organic group includes amides, isocyanates, anhydrides, acrylates, imides and polymers [144]. An example of a type of inorganic coupling agent is silicates [144]. Organic-inorganic agents include silane and titanate [103, 144].

Organosilanes [145–147] and organotitanates [99, 109, 127, 132, 143] and maleic anhydride grafted polypropylene (MAgPP) compatibiliser [148] are commonly used in polymeric composites due to their ability to improve the compatibility between the inorganic surface of the filler and the organic polymer matrix. Their molecules comprise functional groups that can chemically bond with each organic and inorganic material, thereby enhancing the interface between the filler and the polymer matrix [126, 128, 149, 150].

2.2.2.1 Organosilane

Silane coupling agents are extensively used worldwide due to their ability to migrate to the substrate interface and improve bonding in composites. In order to effectively couple the filler surface and the polymer matrix, the silane molecules must have bifunctional groups which will react with two phases forming a connection in between them [151].

The general structure of silanes is: $(RO)_3–Si–(R'X)$.

The alkoxy groups (RO) are typically ethoxy or methoxy while the organofunctional group (X) are typically amino, vinyl, methacryl, amine, mercapto and epoxy. Silanes are synthesised from trichlorosilane.

The silane, 3-methacryloxypropyltrimethoxysilane (3-MPTS) (**Figure 2.2**) is a commonly used coupling agent for polyolefins which is well established for fillers bearing –OH groups [125, 131, 152–155]. During silanisation the alkoxy groups (methoxy) bond with the filler surface by hydrolysing to silanol groups. The hydroxyl groups present on the surface of the filler attach and bond with the silanol groups [150]. The organofunctional group (methacrylate) of the silane reacts with the polymer matrix [150]. The way in which the organofunctional group and the polymer matrix interact depends mainly on the functionality's reactivity towards the polymer [156]. The alkyl group which is nonreactive has a similar polarity to the non-polar matrix. Therefore, it is capable of increasing the compatibility with the non-polar matrix [156]. The Si–C bond on the coupling agent is more stable and hence unreactive [157].

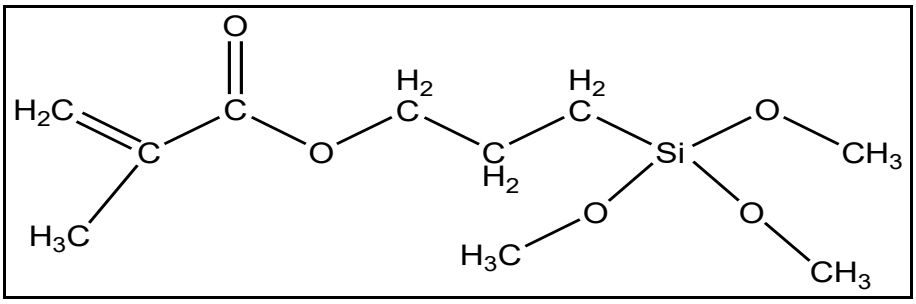

Figure 2.2: Chemical structure of 3-methacryloxypropyltrimethoxysilane.

As soon as 3-MPTS is joined with the inorganic surface of the filler, that surface takes on the surface chemistry features of the organic group attached to 3-MPTS [99, 132, 158] (**Figure 2.3**). The modified surface of the filler will display the surface energy of the organic group of the 3-MPTS, and consequently, the modified surface will become reactive [159].

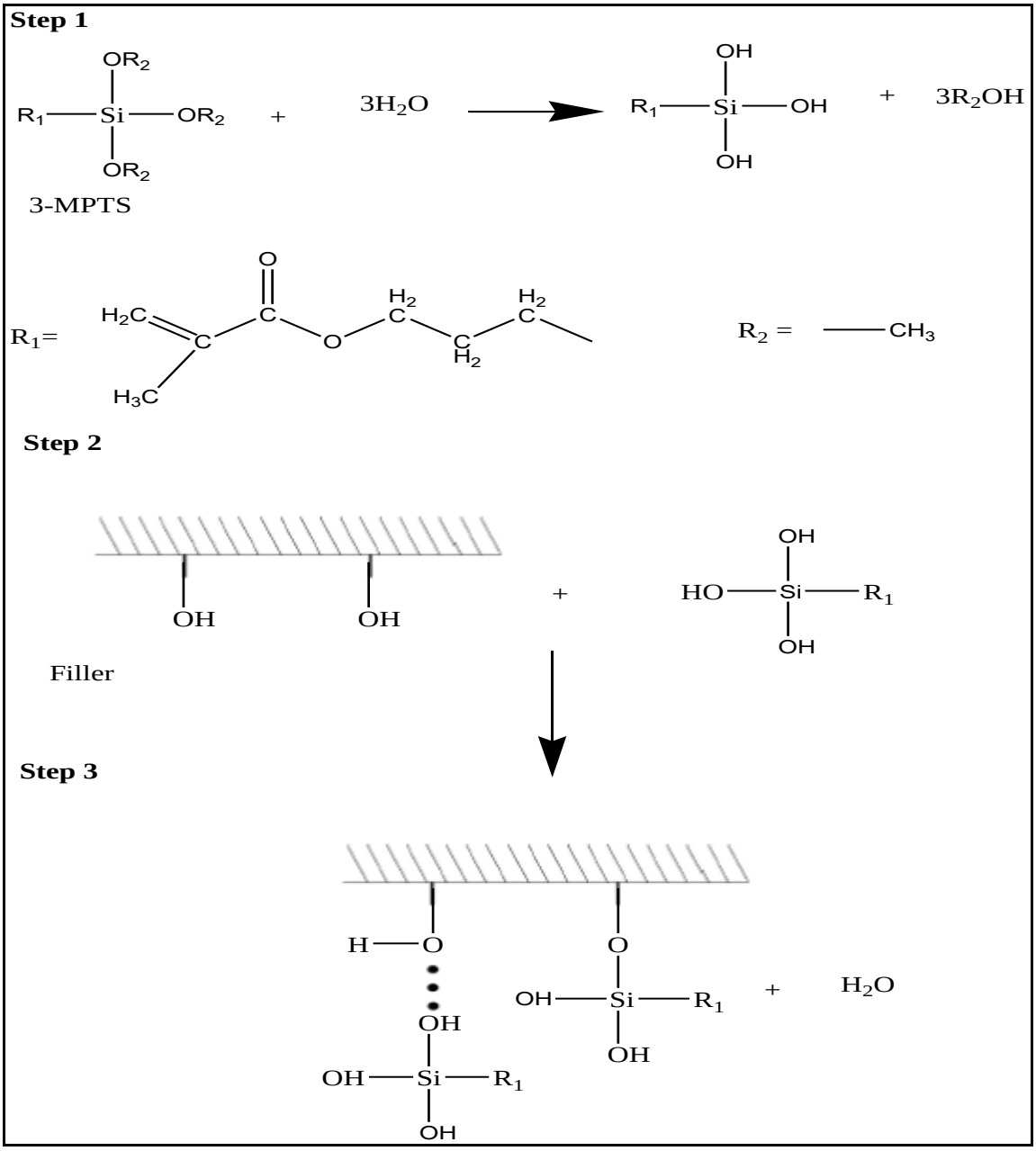

Figure 2.3: Reaction of silane with inorganic substrate (filler).

Silane coupling agents have the ability to increase the bond strength as well as, avoid debonding at the interface. Their unique properties make them, desirable for most applications [151]. Silane provides chemical coupling by reacting with hydroxyl groups of various fillers and they are well known to self-assemble into monomolecular and multimolecular layers on fillers. Generally, silanes chemically bond with fillers containing silica, like silicon dioxide, porcelain, and silicate glasses [149]. Silanes are not highly reactive with fillers like calcium carbonate, carbon black and graphite because they contain fewer hydroxyl (–OH) surface groups and no silanol (Si–OH) group. The sol-gel process is used to coat silica on the surface of the non-silane reactive fillers [152].

PT-char has been reported to contain high amounts of silica within the ash contents [17, 58]. Therefore silane is expected to bond with the PT-char. There are different kinds of silane coupling agents and they are each designed for use in a specific type of plastic [151] (see **Appendix A**). The 3-MPTS coupling agent is designed for use in polyolefin due to its organofunctional group which is compatible with PP [160].

2.2.2.2 Organotitanate

Titanates are unique coupling agents that are able to overcome many of the restrictions imposed by the use of silane coupling agents. They are able to join interfaces, which are generally nonreactive with a silane. These interfaces include calcium carbonate, carbon black and graphite, which require the addition of inorganic silica coated on the surface to enable the effective operation of the silane coupling agent [149, 152, 157].

The general structure of titanate coupling agents is: $RO–Ti–(OY)_{3,}$

The (RO) is the alkoxy group while the (OY) is the organofunctional fragment. The alkoxy group can be a monoalkoxy or neoalkoxy group and it is able to react with the inorganic substrate. The Y portion usually contains numerous and diverse groups which offer interactions between polar and non-polar thermoplastics, thermosets, and binder groups that can yield additional functions to the composite [161]. The Ti–O bond is capable of disassociation which enables various catalysis mechanisms such as repolymerisation, transalkylation and transesterification [157].

Titanates are quite different from silanes [149]. The former has one alkoxy group and three organofunctional groups providing more effective coupling to the polymer [149, 157] and the latter has three alkoxy groups and one organofunctional group [150, 156, 162]. The reaction mechanisms by which they couple to the inorganic surfaces of the filler vary. Silanes work via the hydroxyl groups of numerous fillers through water condensation, siloxane forming mechanisms while titanates work via proton (H^+) co-ordination mechanisms that need no water of condensation. This property enables titanates, to work on fillers such as carbon black, calcium carbonate, barium sulfate, graphite, aramid and organics that are non-reactive to silane.

The titanate, 2,2(bis-2-propenolatomethyl)butanolato,tris(dioctyl)phosphato-O (LICA 12) (**Figure 2.4**) is a commonly used coupling agent in the polyolefin composites for its ability to provide chemical bonding and a good dispersion between the filler surface and the polymer matrix [99, 109, 132, 143, 163]. These properties are responsible for improving the mechanical properties of the composites [149].

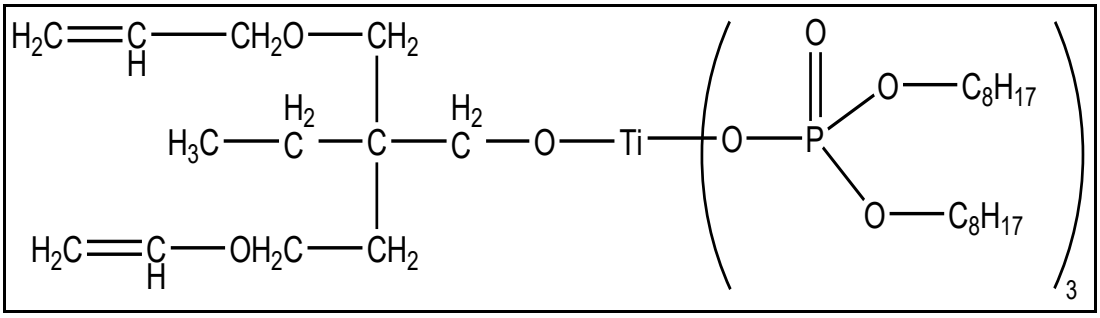

Figure 2.4: Chemical structure of titanium 2,2(bis-2-propenolatomethyl)butanolato,tris (dioctyl)phosphato-O

When the alkoxy groups (neoalkoxy) of LICA 12 react with free protons at the filler interface, the resulting organic titanium monomolecular layers [149, 157, 164] (**Figure 2.5**) are formed on the filler surface [149]. The presence of the monomolecular layer on the interface and also the chemical structure of titanates modify the surface energy of the filler in such a manner that the melt viscosity of the composites is less than those of the other coupling agents [165]. Titanates have excellent characteristics that allow them to be used as wetting agents, adhesion promoters, dispersant aids, super plasticisers, and surfactants [149]. They have higher hydrolytic stability than silane [162]. Other types of titanate coupling agents [164] are presented in **Appendix B**.

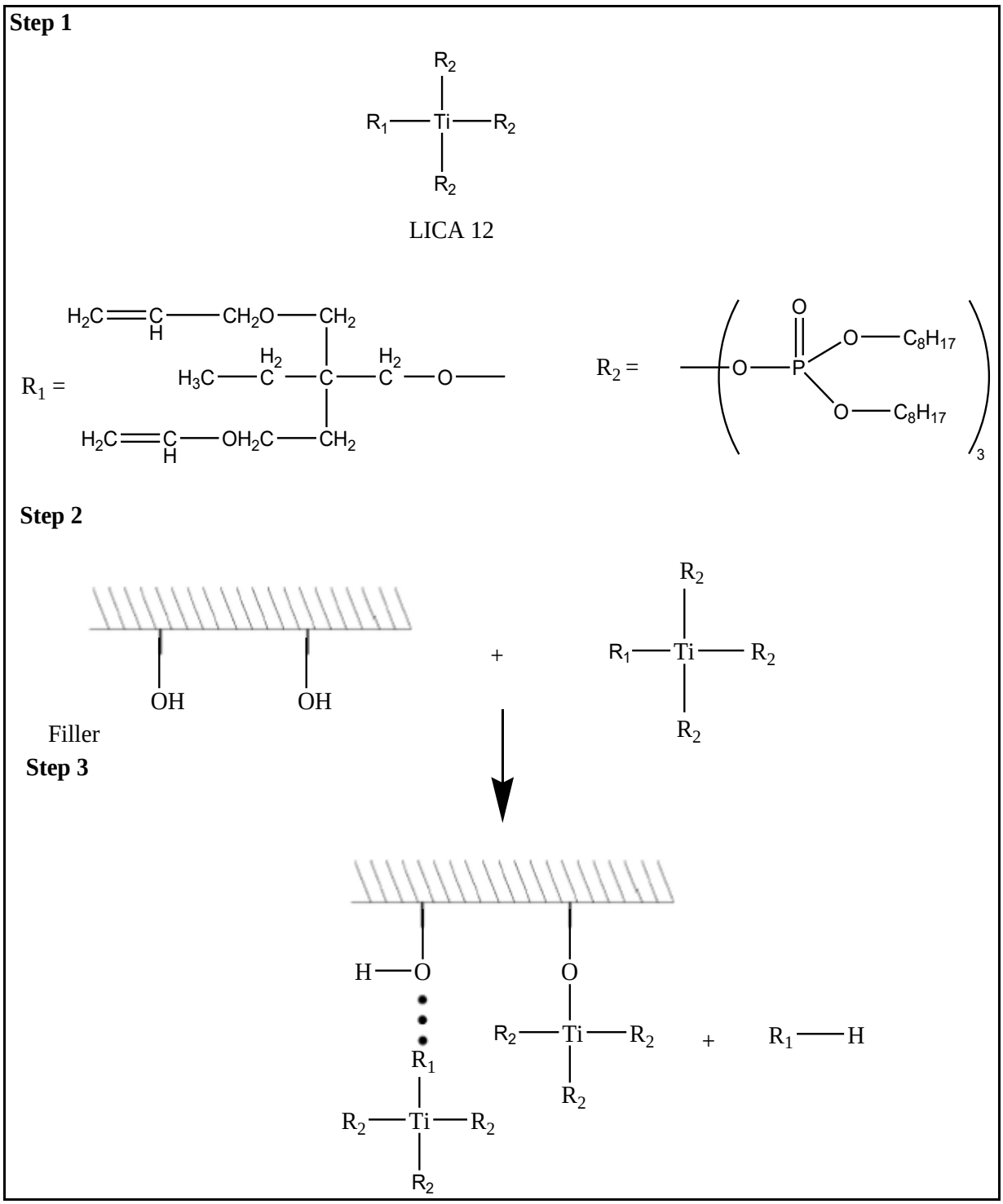

Figure 2.5: Diagrammatic representation of LICA 12 monomolecular formation.

2.2.2.3 Maleic anhydride grafted polypropylene (MAgPP)

MAgPP **(Figure 2.6**) is an α, β– unsaturated carbonyl compound which is broadly used as a compatibiliser in order to improve composite properties. Maleic anhydrides usually graft to the same polymer as that used as matrix to ensure compatibility. The hydroxyl groups on the

surface of the filler react with the anhydride groups of the copolymers and thus form ester bonds (**Figure 2.7**). The other end of the copolymer tangles with the polymer matrix due to their similar polarities [166]. Generally, MAgPP is used to modify the polymer matrix by graft copolymerisation [167].

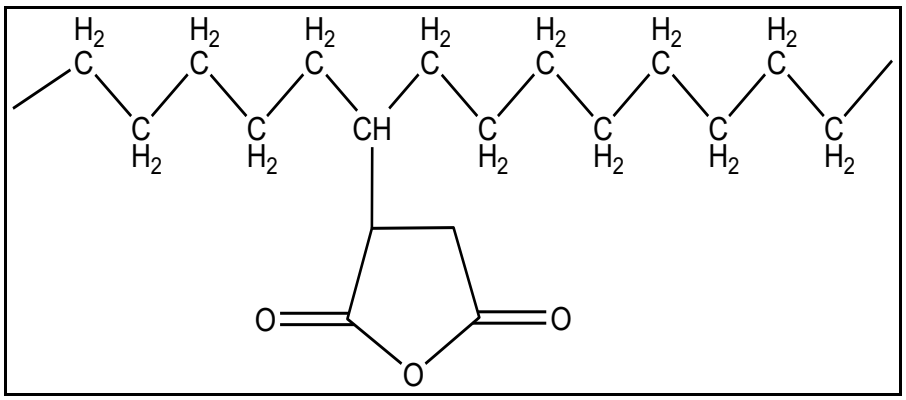

Figure 2.6: Chemical structure of Maleic-anhydride grafted Polypropylene.

MAgPP enhance PP-filler interface bonding via two simultaneous reactions. In the first reaction, the long molecular chains of MAgPP couple with PP matrix through chain entanglement. In the second reaction, the maleic anhydride (MA) groups bond with the hydroxyl groups present on the filler surface [168]. Different amounts of MAgPP have been used in several studies [126, 128, 168, 169] that have found the optimum concentration of MAgPP to be 5 wt.%. Concentrations of less than 5 wt.% have been reported to be insufficient for the esterification process to occur as there are not enough anhydride groups to bond with the hydroxyl groups present on the filler surface. However, concentrations of more than 5 wt.% lead to saturation of the functional groups present on the surface of the filler, which negatively affects the mechanical properties of PP composite [126, 168]. According to Li et *al*. [128], this might be due to the high melt flow index of MAgPP, which may lessen the shear viscosity of the whole PP matrix and that may lower the stress transfer from the matrix to the filler.

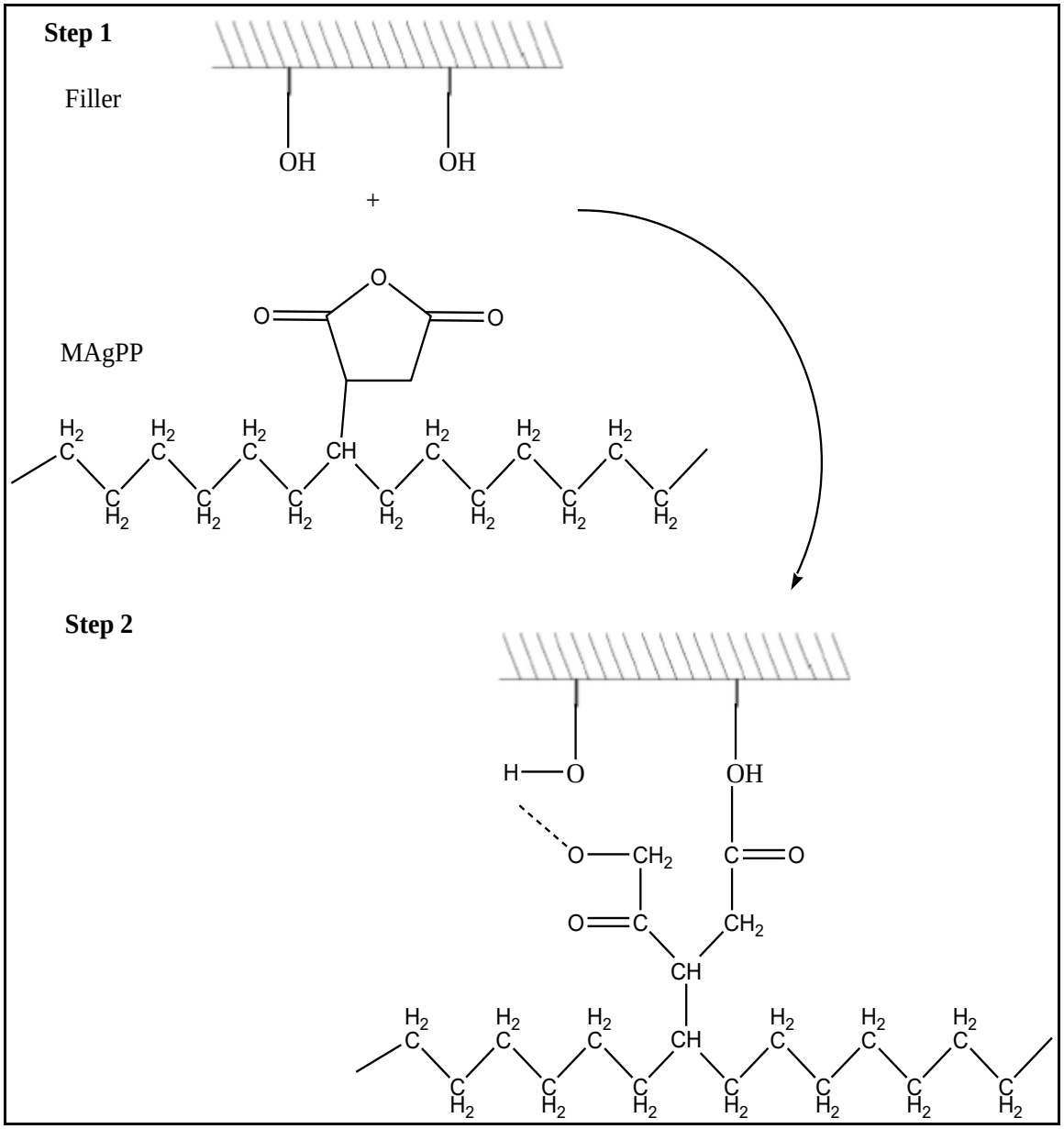

Figure 2.7: A reaction scheme between the filler surface and MAgPP.

2.2.3 Mechanical properties

The mechanical properties of PP composites are important factor for industrial application, as it is a multifunctional material. PP products are designed to serve different purposes with varying mechanical properties. Mechanical properties such as impact strength (IS), tensile properties i.e. tensile strength (TS), young modulus (YM) and elongation at break (EB) provide excellent measures of the degree of short-term reinforcement provided by the filler to the PP composite. The typical mechanical properties of homopolymer PP filled with various filler are presented in **Table 2.10**.

Table 2.10: Typical mechanical properties of homopolymer PP filled with various unmodified particulate fillers.

Homopolymer PP composites	Filler load	IS	TS (MPa)	YM (MPa)	EB (%)	Details	Ref
Calcium carbonate (vol.)	0	16.0	33.1	1437	121	Particle size of calcium carbonate is 0.07 µm. Samples were injected moulded and went through Izod notched test. IS measured in J/m. IS values approximated from the graph.	[69]
	5	19.0	27.2	1691			
	10	17.0	25.1	1871	87.4		
	20	16.0	21.5	1971	13.7		
	30	14.0	19.2	2697	5.9		
Calcium carbonate (wt.)	0	13.0	42	1300	23.0	Particle size of calcium carbonate is 5 µm. Samples were compression moulded and went through Charpy unnotched test. Values approximated from the graph. IS measured in kJ/m^2.	[170]
	10	7.0	36	1300	16.0		
	20	6.0	34	1400	14.0		
	30	5.0	30	1600	10.0		
	40	4.0	20	1800	7.0		
CB (wt.)	0	3.2	32.4			Particle size of CB is 25 nm. Samples were injected moulded and went through Charpy notched test. IS is measured in kJ/m^2.	[117]
	1	3.8	35.4				
	3	2.9	40.5				
	5	3.8	38.5				
	7	3.4	38.0				
	10	3.1	39.0				
CB (wt.)	10	39.0	32.5	750	10.0	Particle size of CB is 100 nm. Samples were injected moulded and went through Charpy unnotched test. Values approximated from the	[118]
	15	38.0	35.0	900	9.0		
	20	18.0	36.0	952	8.0		

	30	13.0	37.0	110	7.0	graph. IS in measured in kJ/m^2	
Mica (wt.)	0	0.24		1250	100	Particle size of mica is 60 µm. Samples were injected moulded. Values approximated from the graph. IS measured in kJ/m^2.	[114]
	0.5	0.2		1240	45.0		
	1	0.3		1310	35.0		
	1.5	0.3		1320	30.0		
	3	0.2		1325	25.0		
Mica (wt.%)	0			3.0	14.0	Average flake diameter of mica is 149 µm. Samples were injected moulded. Values were estimated from the graph. YM measured in GPa.	[171]
	1			3.1	12.0		
	3			3.2	11.0		
	5			3.5	9.0		
	10			3.9	8.0		
Talc (wt.)	0	3.5	33.0		28.0	Particle size of talc is 0.20 µm. Samples were injected moulded. Values approximated from the graph. IS measured in kJ/m^2.	[113]
	1	3.4	30.0		21.0		
	2	3.3	29.0		18.0		
	3	3.0	28.0		19.0		
	4	2.8	26.0		21.0		
Carbon nanotube-CN (wt.%)	0	2.7	28.3	648		Particle diameter of CN is 10 nm to 50 nm and length is 1 µm to 3 µm. Samples were compression moulded. Sample went through Izod notched test. IS measured in J/m.	[172]
	2	3.3	33.1	781			
	4	2.5	31.1	811			
	8	2.0	28.1	730			

As seen from **Table 2.10**, the mechanical properties of PP composites are significantly modified by the presence of the filler. The effect of each type of filler depends on its nature. Each composite system has a maximum load and once that amount is surpassed, the mechanical properties will be negatively affected [109, 110, 117, 118, 124, 135, 173]. This aspect is generally common with the impact properties of filled PP composites. Increasing filler loading causes filler particles to aggregate and consequently act as micro-crack initiators. Hence, poor dispersion is more pronounced at higher filler loading [114, 118]. Due to the tendency of the filler particles to agglomerate at higher filler loadings, the surface contact area of the filler is reduced. As a result, the effect of the filler in improving the mechanical properties tends to be minimal [110].

Restriction of the movement of the polymer chains, caused by the presence of the rigid filler, limits the ability of the polymer to adapt to deformation and consequently makes the polymer composite brittle [109, 173]. In order to reduce brittleness, a high rubber content is usually incorporated to increase toughness [24, 69], at the expense of decreased stiffness [69]. However, there are a few studies, that reported an increase in impact strength of PP composites upon addition of filler particles [69, 109, 121]. Nonetheless, their fracture mode was still brittle, with fracture energies less than 8 kJ/m^2.

General observations suggest that the filler's particle size, shape and distribution contribute to the mechanical properties of PP composites [133, 173, 174]. Tan and Tincer [133], found that PP composites filled with spherical particles of barium sulphate had higher impact strength than those filled with flake-like particles of aluminium hydroxide. Mareri *et al*. [173] also showed that a good dispersion of fine particles on the PP matrix makes plastic deformation easier and consequently increases the stress required for a microcrack to occur.

As seen from **Table 2.10**, the tensile strength of the PP composites is enhanced at lower filler loading, due to poor dispersion at higher filler loadings [117, 135], while the incorporation of filler increases the young modulus of the composites due to the stiffness of the filler [69, 117, 124, 131, 135, 173]. In a composite matrix that is well dispersed with filler, the volume of the affected area is large due to the short distance of the filler particles surrounding the matrix [174]. Consequently, this develops the percolation network which in turn increases the modulus of the composites [174]. Increasing filler reduces the elongation at break of the PP composites. This behaviour has been attributed to the presence of the filler particles which

limit the mobility of the PP chains [23, 28, 132, 135]. A low elongation figure signifies a brittle rupture, whereas a high elongation figure signifies a ductile rupture [23].

Other factors that have a profound influence on the mechanical properties are the rate of loading, temperature and time. These factors are usually associated with creep [23, 24]. The impact strength of PP composites usually decreases as the temperatures decrease and in the presence of a notch [23, 24, 69]. As the toughness decreases the material becomes less elastic and ductile [23]. An increase in temperature reduces the stiffness of a material [24]. Since fillers are different in nature, sometimes, blends of different fillers can improve mechanical properties more than composites filled with a single filler [132].

2.2.3.1 Effect of surface modification on mechanical properties

Interfacial adhesion between a filler and the PP matrix influences the resultant impact and tensile properties [23, 28, 135, 175]. A number of studies [28, 135, 175], have reported that a good interfacial adhesion results in efficient stress transfer from the polymer matrix to the dispersed filler, leading to improved properties. Surface modification of the filler, enhances the interface layer, leading to improved dispersion of the filler particles on to the matrix [28]. Changes in interfacial interactions between the filler and the polymer matrix can modify the debonding mechanism and failure behaviour [124]. During tensile stress, debonding of the filler particle is necessary as it changes the stress state of the polymer matrix [110, 121, 124].

Several researchers [131, 152], have reported that surface modification influences the tensile strength of the composites. Lin *et al.* [131] and Zhou *et al*. [152], reported remarkable increases in the tensile strength of composite surfaces modified with 3-MPTS silane coupling agents. However, Demjeng *et al*. [28, 125], found that 3-MPTS had no influence on the tensile strength of PP/$CaCO_3$ composites in spite of the fact that the methacryl functional 3-MPTS contains a reactive double bond. Nurdina *et al*. [132] and Lin *et al*.[99], also found an improvement in the tensile strength of PP composite surfaces modified with LICA 12 due to effective transfer of stress from the PP matrix to the filler.

A number of studies [28, 124, 176], have reported that the young modulus of PP composites does not depend on the surface modification of the filler. According to Laura *et al.* [176], the stiffness of the matrix depends only on the surface contact area of the filler. Lin *et al*. [131]

and Nurdina *et al*. [132], found that the young modulus of both the untreated and surface modified PP composites improved with increasing filler content, however, the composites modified with silane and titanate had higher tensile modulus than the untreated one. The application of surface modification with silane and titanate was found to decrease the elongation at break of the PP composites [28, 131, 132]. Contrary to previous reports Wah *et al.* [143], found that the effect of LICA 12 improved the elongation at break. Surface modification improve the impact strength of the PP composites [99, 109, 143] due to improved interfacial adhesion which consequently provides effective resistance to crack propagation.

2.2.4 Degradation stability

Throughout their processing, treatment and storage, polymers are exposed to conditions that tend to degrade their polymer chains and change their properties [120]. Polymer degradation is a change in the properties of polymers such as colour, shape, toughness and strength due to internal factors such as traces of solvents and catalyst [177–179], traces of metal (e.g. iron, nickel, etc) from processing equipment and additives [179–182] or environmental factors such as atmospheric oxygen, heat or sunlight [183]. Usually, polymer degradation is initiated by oxidation [184–186]. Oxidation starts at tertiary carbon atom due to the formation of free radicals [23, 187]. Polymer degradation is exothermic and as a result, the released heat and gases can further lead to an increase in the degradation rate [183]. Two common types of polymer degradation are thermal and photo-oxidative degradation.

Thermal-oxidative degradation is a combination of two models of degradation: the one activated by oxygen and the other is activated by high temperatures. Generally, PP is thermally stable in the absence of oxygen. Nonetheless, PP is vulnerable to attack by atmospheric oxygen especially at high temperatures [188]. At elevated temperatures, the constituents of the PP chain backbone start to separate and as a result, they react with each other to alter the PP properties [189]. In an inert atmosphere, PP normally start to decompose above 350 °C [190, 191]. The thermal properties of a polymer determine its processing characteristics as well as its low and high temperature applications. Applications where low temperature is required are refrigerator parts and food packaging for refrigerated shelves and high temperature applications are in steam sterilisation, microwave oven proof containers and parts for dishwashers and washing machines [24].

Photo-oxidative degradation of a polymer is caused by the absorption of photons, particularly at those wavelengths found in sunlight i.e. infrared radiation or ultraviolet light [180]. Photo-oxidative degradation is a combination of two models of degradations: the one activated by oxygen and the other one activated by UV or light [183]. This type of degradations may occur in the absence of oxygen [180]. When light is absorbed by the polymer, chromophoric groups present in the macromolecules of the polymer initiate photochemical reactions [180]. Photo-oxidative degradation creates chain scission similar to thermal-oxidative degradation and reduces the chain length, thus lowering the molecular weight of PP [189]. This changes the mechanical properties of PP resulting in extremely reduced ductility and embrittlement [24]. Furthermore, the optical properties of the plastic material get affected, hence yellowing of plastic occurs [180].

The main difference between thermal and photo-oxidative degradation is that the former happens through the bulk of the polymer and the latter happens at the surface of the polymer [192]. Photo-oxidative degradation usually affects outdoor applications such as PP car bumpers and dashboards, PP stadium seats, etc. In order to enable the processing plastic while maintaining its molecular weight and mechanical properties throughout its designed lifetime, it is necessary to protect it from degradative agents by adding essential ingredients such as antioxidants and stabilisers [120, 193].

Accelerated and natural weathering have been carried out by several researchers [194–196], who have reported the potential effect of the filler in inhibiting degradation. However, some researchers [26, 197–201], discovered that, the filler does not necessarily always inhibit degradation; but may in fact sometimes enhance it. For instance, according to a study carried out by Lu *et al*. [194], the untreated silica improved photodegradation stability of the PP composites due to its UV shielding effect, while the 3-MPTS modified silica, accelerated photodegradation due to the photo-initiating effect of the carbonyl groups present in the surface of the modified fumed silica. Contrary to the previous study, Li *et al*. [197], found that carbonyl groups present on the surface of the untreated calcium carbonate and silicon dioxide, act as chromophores which tend to be the source of initiation radicals.

Usually, the majority of polymers contain antioxidants such as hindered phenolic and secondary aromatic amines, which are widely known as radical scavengers, that inhibit degradation and ensure acceptable lifetimes under outdoor exposure conditions [23, 180].

However, several studies [199, 200, 202] have highlighted that the ability of these radical scavengers may be inhibited by their absorption into the mineral fillers, which consequently decreases the life-time of the composite material. Traces of transition metal iron on the surface of montmorillonite [199–201], as well as the formation of acidic sites on montmorillonite layers [201], have also been found to catalyse the oxidation of PP composites. Metal deactivators such as N,N'-dibenzaloxalyldihydrazide and phenolic antioxidant are some of the additives used to deactivate metal residues present in the formulation due to catalyst residues and impurities in additives [23].

Incorporation of MAgPP compatibiliser, has also been reported by several researchers [26, 201, 203, 204], to significantly reduce formation of photo-oxidation products in PP composites. This is particularly true for those filled with clay, mainly due to the ability of MAgPP to encapsulate the filler particle and thus slowing down degradation. In contrast to the reported studies, Mailhot *et al.* [205], found that, the addition of MAgPP instigated some photo-responsive groups which lead to the acceleration of photodegradation of PP/Montmorillonite composites. CB is well known as one of the industrial fillers with outstanding properties, such as heat and weather resistance, light weight, electro-conductivity, and low thermal expansion [117]. CB contains carboxyl, phenolic, hydroxyl, lactone, ketone and quinone groups [206], which makes it useful as a thermal and UV stabilising agent [207]. A previously reported study [21], suggested that the oxygenated functional groups can simultaneously act as the catalytic centre for oxidation.

During compounding, uncontrolled degradation reactions may occur. Rabello *et al*. [196], found that, talc-filled PP composites degraded faster than the unfilled PP at early stages of exposure. This is due to extra thermal history during compounding as well as additives that were added during processing of the PP composites, which may have accelerated degradation. Another factor which may cause degradation of polymer composite is the poor dispersion of the filler into the PP matrix which restricts the ability of the filler to stabilise degradation [197, 198, 208]. In addition to formation of defects at the interface, variation in the morphology of the filler may also accelerate polymer degradation. This was reported by Morrealle *et al*. [201], who found that nanosized calcium carbonate particles accelerate degradation more than the micro particles due to their smaller size and bigger interface area. From the reported results above, it is clear that the influence of filler on the degree of degradation differs extensively, according to the stabilisers and coupling agents used.

Interface properties between the filler and the PP matrix also play a vital role in the degradation stability of PP composites.

2.2.5 Concluding remarks

PP composite properties have been shown to be highly dependent on the filler's properties, such as its geometry (particle shape, size and size distribution) and surface area, as well as interactions between the fillers and the PP matrix. The literature further indicates that nanofillers have more reinforcing abilities than micro fillers due to their small size and greater interface area. Despite their reinforcing potentials, these fillers often have high surface energy which easily forms agglomerates, especially at higher filler content. The agglomerates can form before or during composite preparation, which will then cause processing and handling problems. Poor dispersion and incompatibility between the filler and polymer matrix result in poor polymer composite properties. To avoid poor compatibility the surface of the filler is modified with surface modifiers so as to develop greater compatibility. In order to understand the effect of filler in a composite, it is necessary to investigate its properties, since it contributes highly to the final properties of the composite material. Furthermore, it is also important to understand the influence of surface modification of the filler on the final properties of the composites.

CHAPTER 3: HYPOTHESIS AND OBJECTIVES OF THE STUDY

3.1. Research questions

The aim of this study is to investigate and analyse the feasibility of PT-char as a filler to improve the mechanical properties and degradation stability of PP composites. A critical analysis of the literature was done in order to investigate the possibility of using PT-char as filler. The following main questions sparked an interest, which when answered will provide valuable information required to achieve the above stated aim.

1. What is the effect of untreated PT-char on the mechanical properties and degradation stability of PP composites?
2. What is the effect of demineralisation on the mechanical properties and degradation stability of PP composites?
3. How will the different PT-char loadings affect the mechanical properties and degradation stability of PP composites?
4. What is the effect of different surface modifiers on the mechanical properties and degradation stability of PP composites?

3.2. Hypothesis

PT-char has the potential of becoming a useful filler in polymer composites. However, PT-char must be upgraded in order to have the appropriate characteristics required for the production of polymer composites. The untreated PT-char contains minerals added during tyre production which might have beneficial effects on the mechanical properties of PP composites, as most of them are currently used as fillers. However, these minerals might also have a detrimental effect on the degradation stability of PP composites because PP is sensitive to inorganic impurities [31]. As such, the differences in the geology of the untreated PT-char and the demineralised PT-char will give different properties to the final composite material. The PT-char loading will affect the dispersion of the PT-char into the PP matrix and consequently, the interfacial adhesion will influence the properties of the final composites. Furthermore, the performance of different surface modifiers will depend on the properties of the untreated and the demineralised PT-char.

3.3. Objectives

In order to answer the research questions stated above, the following objectives were identified:

- Analyse the properties of untreated PT-char and the demineralised PT-char and how they affect the mechanical properties and degradation stability of PP composites.
- Investigate the effect of PT-char loading on the mechanical properties and degradation stability of PP composites.
- Analyse the effect of surface modifiers on the mechanical properties and degradation stability of PP composite.

CHAPTER 4: EXPERIMENTAL METHODS AND PROCEDURE

4.1. Materials

1) PT-char

As mentioned, the PT-char was obtained from the pyrolysis process that was previously carried out in a different study and the detailed description of the pyrolysis is described elsewhere [30]. In summary: a mixture of waste tyre crumb, free of steel and fabric cords (provided by a local waste tyre recycler, Environmental Serve) was sieved to obtain particle size ranging from 2.8 mm to 3.4 mm. A total sample size of 1 kg of sieved waste tyre crumb was fed into a fluidised bed pyrolysis reactor at a feeding rate of 30 g/min. The reactor operated at 475 °C with a vapour residence time of a few seconds. The fast pyrolysis took place in the presence of a nitrogen atmosphere (3 m^3/h).

2) Polymer

PP homopolymer (HNR100) was used as a polymer matrix. HNR100 is a general purpose injection moulding grade with weight-average molecular weight (Mw) of 332393 g/mol, number-average molecular weight (Mn) of 60025 g/mol, melt flow rate (MFR) of 12 g/10 min (230 °C, 2.16 kg) and melting temperature (Tm) of 168 °C. HNR100 contains processing stabilisers and antioxidants to avoid oxidation during processing. The polymer matrix was supplied in pellet form by Sasol Polymers.

3) Acid-base lixiviants

Nitric acid and sodium hydroxide were used to remove impurities from the PT-char and their details are described in **Table 4.1**.

Table 4.1: Acid-base lixiviants used in the study.

Acid-base lixiviants	Assay	Density (g/cm^{-3})	Molar mass (g/mol)	Supplier	Catalogue number
Nitric acid (HNO_3)	70 %	1.42	63.0	Sigma Aldrich	438073
Sodium hydroxide (NaOH)	98.5 %	2.13	40.0	Sigma Aldrich	06306

4) Surface modifiers

Two different coupling agents and a compatibiliser were used to modify the surface of the PT-char and their details are described in **Table 4.2**.

Table 4.2: Coupling agents used in the study.

Coupling agent	Details	Supplier	Catalogue number
3-Methacryloxypropyltrimethoxy-silane (3-MPTS),	Colourless, transparent liquid, 98 % pure with a density of 1.05 g/ml at 25 °C.	Sigma Aldrich	440159
Titanium IV 2,2 (bis-2-propenolatomethyl)butanolato, tris(dioctyl)pyrophosphato-O (LICA 12)	Thick yellowish liquid with a boiling point of 71 °C and viscosity between 200 cP and 400 cP at 25 °C	KenRich Petro-chemical	
Maleic-anhydride-grafted polypropylene (MAgPP)	Packaged in pellet form, with a Mw of ~ 9100 g/mol, Mn of ~ 3900 g/mol, Tm of 156 °C, density of 0.93 g/ml at 25 °C, and the composition of maleic anhydride is between 8 wt.% and 10 wt.%.	Sigma Aldrich	427845

5) Additional materials

(i) **Ethanol (absolute):** was used as a solvent for hydrolysis of 3-MPTS [209]. Ethanol was supplied by Sigma Aldrich with a catalogue number of 32205.

(ii) **Toluene (99.5 %)**: according to the reference manual supplied together with LICA 12, toluene is used as a solvent to dissolve LICA 12 [99, 210]. Toluene was supplied by Sigma Aldrich with a catalogue number of 179418.

(iii) **Acetic acid (99.7 %)**: the purpose of using acetic acid was to make the silane solution slightly acidic as hydrolysis of silane takes place in a slightly acidic environment [131]. Acetic acid was supplied by Sigma Aldrich with a catalogue number of 695092.

4.2. PT-char characterisation

4.2.1 Particle size distribution of PT-char

The particle size distribution of PT-char was analysed by means of a Micromeretic Saturn Digisizer 5200 laser diffraction system. The refractive index of the carbon (2.42) was used since PT-char is mainly composed of carbon and because there is no exact value for PT char due to the heterogeneity of the samples.

4.2.2 Proximate, ultimate analysis and chemical composition of ash

The proximate analysis of PT-char was done using a Mettler Toledo TGA/DCC1. Proximate analysis was carried out at 950 °C according to the trend shown in **Appendix C**. The standard method used for the analysis was ASTM E1131-08. The ultimate analysis of PT-char was done using Vario EL Cube Elemental Analyser. Ultimate analysis of PT-char was carried out at 1800 °C and the oxygen content was not measured but calculated by percentage difference.

4.2.3 Surface morphology of PT-char

The microstructure and composition of PT-char were studied utilising a Zeiss EVO® MA15 Scanning Electron Microscope (SEM) fitted with an Oxford Instruments® X-Max 20 mm

EDX detector. The PT-char samples were first sputter-coated with gold before imaging for conductivity purposes and to reduce surface charging during surface irradiation. The analysis was done at accelerating voltage of 10 kV. The chemical composition of PT-char was identified using, EDX analysis [137].

4.2.4 Surface area of PT-char

The surface area of PT-char was determined from nitrogen adsorption measurements at 77 K by means of a Micromeretics 3Flex. The N_2 adsorption isotherms were used to calculate surface area using the Brunauer Emmett Teller (BET) and the pore dimensions were determined using the Barrett-Joyner-Halenda (BJH) method.

4.2.5 Surface chemistry of PT-char

The surface chemistry analysis of PT-char was performed according to ASTM D2734-94 using a Fourier Transform Infrared spectroscopy (FTIR) spectrometer (Nexus-Thermo Nicolet). The FTIR spectra of the unmodified and the modified PT-char samples were recorded in the scan range of 400 cm^{-1} to 4000 cm^{-1} with a resolution of 4 cm^{-1} and 64 scans were obtained. Prior to analysis, 5 mg of the sample was mixed with 95 mg of finely ground potassium bromide (KBr) [132, 211]. The mixture was compressed into thin pellets with a hydraulic press using 400 p.s.i of pressure and held for 3 min.

4.3. Demineralisation of PT-char

In order to reduce high amounts of ash, a sequential extraction method was used for the demineralisation process. Demineralisation was conducted by first preparing two separate solution of 1 M HNO_3 and 1 M NaOH. Then 10 g of PT-char was added into a 100 ml of 1 M HNO_3 solutions in a 200 ml schott bottle. The mixture was heated at 90 °C and agitated using a magnetic stirrer (at 800 rpm) hot plate for 24 h in a fume hood. Once the first demineralisation was completed, the mixture was filtered and washed with distilled water until the pH was neutral. The filtered, neutral solution was dried in a vacuum oven at 80 °C for 24 h to obtain the demineralised PT-char. The demineralisation procedure was repeated using 1 M NaOH solution under the same conditions in order to obtain a sequentially

demineralised PT-char (PT-DC) [18, 98]. To simplify the reading of the results, the subsequent terms were used: PT-UC stands for untreated PT-char and PT-DC stands for demineralised PT-char.

4.4. Surface modification of PT-char

4.4.1 3-MPTS treatment

3-MPTS was added into ethanol solution (ethanol to deionised water ratio 95:5) to make a final 2 wt.% solution of 3-MPTS. About 10 g of PT-char was added into the mixture and sonicated at room temperature for 1 h [131, 136, 212]. The pH value of the mixture was adjusted to 4.5 using acetic acid. The mixture was refluxed at 35 °C for 24 h. When the reaction was done, the modified PT-char was washed with ethanol to remove excess 3-MPTS. The product was dried in a vacuum oven at 80 °C for 24 h to remove excess ethanol [131, 142]. The quantity of 3-MPTS was based on the surface area of PT-char according to equation (1) below [211]. The minimum coating area of 3-MPTS is 314 m^2/g [213].

$$A_{3-MPTS} = \frac{A_f \times SA_f}{MCA_{3-MPTS}} \quad (1)$$

Whereby,

$A_{3\text{-}MPTS}$ = Amount of 3-MPTS (ml).

A_f = Amount of the filler (g).

SA_f = Surface area of the filler (m^2/g).

$MCA_{3\text{-}MPTS}$ = Minimum coating area of 3-MPTS (m^2/g).

4.4.2 LICA 12 treatment

LICA 12 was dissolved in toluene (100 ml) solvent at room temperature and the mixture was sonicated for 30 min. Then 10 g of PT-char was added into the solution of LICA 12 and toluene and the mixture were further sonicated for 1 h. After sonication, the modified PT-char was filtered and washed with toluene to remove excess LICA 12. The dispersion was dried in a vacuum oven at 80 °C for 24 h to remove excess toluene. The amount needed to treat the filler with LICA 12 usually lies between 0.5 wt.% and 2.5 wt.% [99, 211]. These amounts

have been recommended by the supplier (Kenrich Chemical) of the chemical. In this study, the quantity of LICA 12 coupling agent used was 2.5 wt.% based on the amount of the filler.

4.4.3 MAgPP treatment

There was no need for pre-treatment of the PT-char as MAgPP was directly blended with PP and PT-char since it is a solid form. 5 wt.% of MAgPP was added on the total formulation of PP and PT-char used [128, 168, 169].

4.5. Production of PP composites

4.5.1 Melt blending (Internal mixer)

PP composites were prepared using a Thermo Scientific, Haake PolyLab (QC) laboratory mixer fitted with roller rotors. The volume chamber of the internal mixer was 69 ml. The effect of different PT-char loadings, within the range reported in the literature [83, 117, 118, 122, 128, 214, 215] were investigated. The weight percentages of PT-char were chosen to avoid the tendency of fillers to aggregate at high loadings [83, 128, 216]. The volumes of the PT-char were: 0.5 vol.%; 1 vol.%; 2.5 vol.%; 5 vol.% and 10 vol.% and their respective weight are: 0.38 wt.%; 0.77 wt.%; 1.94 wt.%; 3.91 wt.% and 7.91 wt.%. The calculations were based on the volume of the chamber with the assumption that the density of the PT-char is 0.7 g/m^3. The final loadings were based on the weight percentages in order to be accurate and for comparison sake.

Various amounts of PP and PT-char (PT-UC, PT-UC+3-MPTS, PT-UC+LICA 12, PT-UC+MAgPP, PT-DC, PT-DC+3-MPTS, PT-DC+LICA 12 and PT-DC+MAgPP) were mixed together for 10 min at a set temperature of 165 °C (to avoid PP degradation) and a rotor speed of 15 rpm to form composites. The mixing torque and the temperature were measured using the PolySoft OS mixer software. Once PP composites were produced, they were cryogenically grinded in a cutting mill (Retch) using liquid nitrogen (to avoid thermal degradation of the PP) to obtain small pieces. The weight percentages, as well as the amounts used to blend PP and PT-char, are presented in **Appendix D**.

4.5.2 Injection moulding

PP composites were moulded into tensile and impact bars with a Thermo Scientific Haake Mini Jet II injection (type 557-2290). For impact and tensile testing, six composite samples of each treatment were moulded according to the conditions presented below:

Injections moulding conditions

- The temperature of the cylinder and the mould were 250 °C and 70 °C respectively.
- Both the injection pressure and the post pressure were each 250 bar respectively.

4.6. Determination of PP composites properties

4.6.1 Mechanical properties of PP composites

4.6.1.1 Impact test

The Charpy impact test (un-notched) was carried out using the pendulum impact instrument CEAST Torino (6546/000) according to ISO 179 [118, 168]. The impact test was carried out at room temperature and the composite samples were subjected to 15 J hammer weight (type 0.96) at a 90° angle. The test was done six times for each formulation and the average values were reported. **Figure 4.1** shows an image of the impact bar samples. Below are the impact test sample dimensions.

- **Impact bar**

Length = 60 mm
Width = 10 mm
Thickness = 1 mm

Figure 4.1: Typical sample of an impact bar.

4.6.1.2 Tensile Test

The tensile test was performed using LRX (Lloyd Instruments) at room temperature according to ASTM D638 [217] at a crosshead speed of 50 mm/min [152, 169, 210, 218]. The test was done six times for each treatment and the average value was reported. **Figure 4.2** shows an image of a tensile bar. Below are the tensile sample dimensions.

- **Tensile bar (dumbbell shapes)**

Gauge length = 88 mm

Width in the middle = 5.2 mm

Thickness = 1.6 mm

Figure 4.2: Typical image sample of a tensile bar.

4.6.2 Degradation stability of PP composites

4.6.2.1 Thermal-oxidative degradation

PP composite samples were exposed to hot air in a ventilated oven (United Scientific) at a temperature of 150 °C. PP composite samples were removed from the oven at different time intervals (0 h; 24 h; 48 h; 53 h; 72 h; 80 h and 96 h) and the changes due to thermal-oxidative degradation were monitored using attenuated total reflectance (ATR) FTIR.

4.6.2.2 Photo-oxidative degradation

A QUV fluorescent UV/condensation tester was employed to perform accelerated weathering. Samples were arranged parallel to the longitudinal axes of the lamp in a very settled position and the bulbs that were used of the UVB–313 type which provides the irradiation at a wavelength of 313 nm. The accelerated weathering took place at 45 °C in the presence of air. Photo-oxidative degradation of PP composites samples was monitored using

ATR-FTIR at different time intervals (0 h; 24 h; 48 h; 72 h; 96 h; 120 h; 144 h and 168 h) [195, 199].

4.6.2.3 Determination of PP composites degradation

Degradation of PP composite samples started with oxidation and was detected by monitoring the groups that were formed during degradation. In order to detect degradation, two ranges in the IR spectrum of the degraded PP composite sample were monitored. The ranges that were monitored were the carbonyl (C=O) range, which is from 1600 cm^{-1} to 1800 cm^{-1} and the hydroxyl (–OH) range which is between 3200 cm^{-1} and 3600 cm^{-1} [195]. The carbonyl groups are generally acids, ketones and esters and the hydroxyl groups are generally the hydroperoxides and alcohols [199].

In an FTIR spectrum of the degraded PP composite, the hydroxyl region is difficult to detect due to overlap with hydroxyl groups from the filler. Therefore the growth of the carbonyl band was used as a measure of the extent of degradation [219]. The carbonyl peak area was taken from 1600 cm^{-1} to 1800 cm^{-1} (with maximum absorption band at 1725 cm^{-1}) and the reference peak area was taken between 962 cm^{-1} and 983 cm^{-1} (with a maximum absorption band at 947 cm^{-1}). This peak was selected as a reference because it changed the least during degradation [184, 220]. The carbonyl growth in the composite sample was quantified using Carbonyl Index (CI) according to equation 2.

$$CI = \frac{Ac = o}{Ac - H} \tag{2}$$

Whereby,

$A_{C=O}$ is the area of the carbonyl peak.

A_{C-H} is the area of the reference peak

CI is generally the most used indicator due to its ability to measure the chemical oxidation of polymers [219, 221]. The degradation of PP composites was determined by ATR-FTIR method. A Thermo Nicolet iS10 FTIR, fitted with a smart single bounce diamond ATR cell, was used for this analysis. The PP composite samples spectra were recorded in a scan range of 400 cm^{-1} to 4 000 cm^{-1} and 64 scans were recorded at a resolution of 4 cm^{-1}.

4.7. Experimental design

4.7.1 Statistical experimental design

In order to simplify and facilitate results analysis, it is important to design experiments efficiently. The experimental data must express the relationship between the variable factor and the response variable. Factorial designs are efficient and they have the advantage of improving the accuracy of the comparisons between the composites by removing the inconsistency among the PT-char loadings of the composites. In this study, an investigative experimental strategy was followed where the use of PT-char as a filler in PP composites was studied. Planning and conducting of the experimental approach included the incorporation of variable factors, such as type of PT-char, type of coupling agent and PT-char loadings as well as response variables, such as mechanical properties (impact strength, tensile strength, young modulus and elongation at break) and degradation stability (thermal and photo-oxidative degradation). **Table 4.3**, below presents the factors and their levels.

Table 4.3: Factors and their levels.

Factor	Factor levels	Number of levels
PT-char	PT-UC	1
	PT-DC	2
Coupling agent	None	1
	3-MPTS	2
	LICA 12	3
	MAgPP	4
PT-char Loading	0.38 wt.%	1
	0.77 wt.%	2
	1.94 wt.%	3
	3.91 wt.%	4
	7.91 wt.%	5

An impact test was conducted first since it is very quick and convenient. This test was conducted in order to eliminate variables that did not make any significant impact on the mechanical properties of PP composites. Therefore, a full factorial design [222] type $2^1 4^1 5^1$,

which represents 3 factors with different levels (2, 4 and 5) and provides 40 experimental runs, was used to analyse the impact strength of the PP composites. Thermal-oxidative degradation studies were carried out following the impact strength test. However, the 4^{th} and the 5^{th} (3.91 wt.% and 7.91 wt.%) loadings were eliminated since they were detrimental to the composite system. With that said, a full factorial design of type $2^1 4^1 3^1$ which represents 3 factors with different levels (2, 4 and 3) and provides 24 experimental runs, was used to analyse thermal-oxidative degradation. The tensile properties test and the photo-oxidative studies were carried out following thermal-oxidative degradation studies. In both these tests, the influence of MAgPP compatibiliser was not considered since it significantly reduced the impact strength and accelerated thermal-oxidative degradation of PP composites. With that said, a full factorial design of type $2^1 3^1 3^1$, which represents 3 factors with different levels (2, 3 and 3) and provides 18 experimental runs, was used to analyse the tensile properties and photo-oxidative degradation. The full factorial design for mechanical properties and degradation study is presented in **Appendix E**. **Figure 4.3** below is a flow diagram of the experimental work performed in this study.

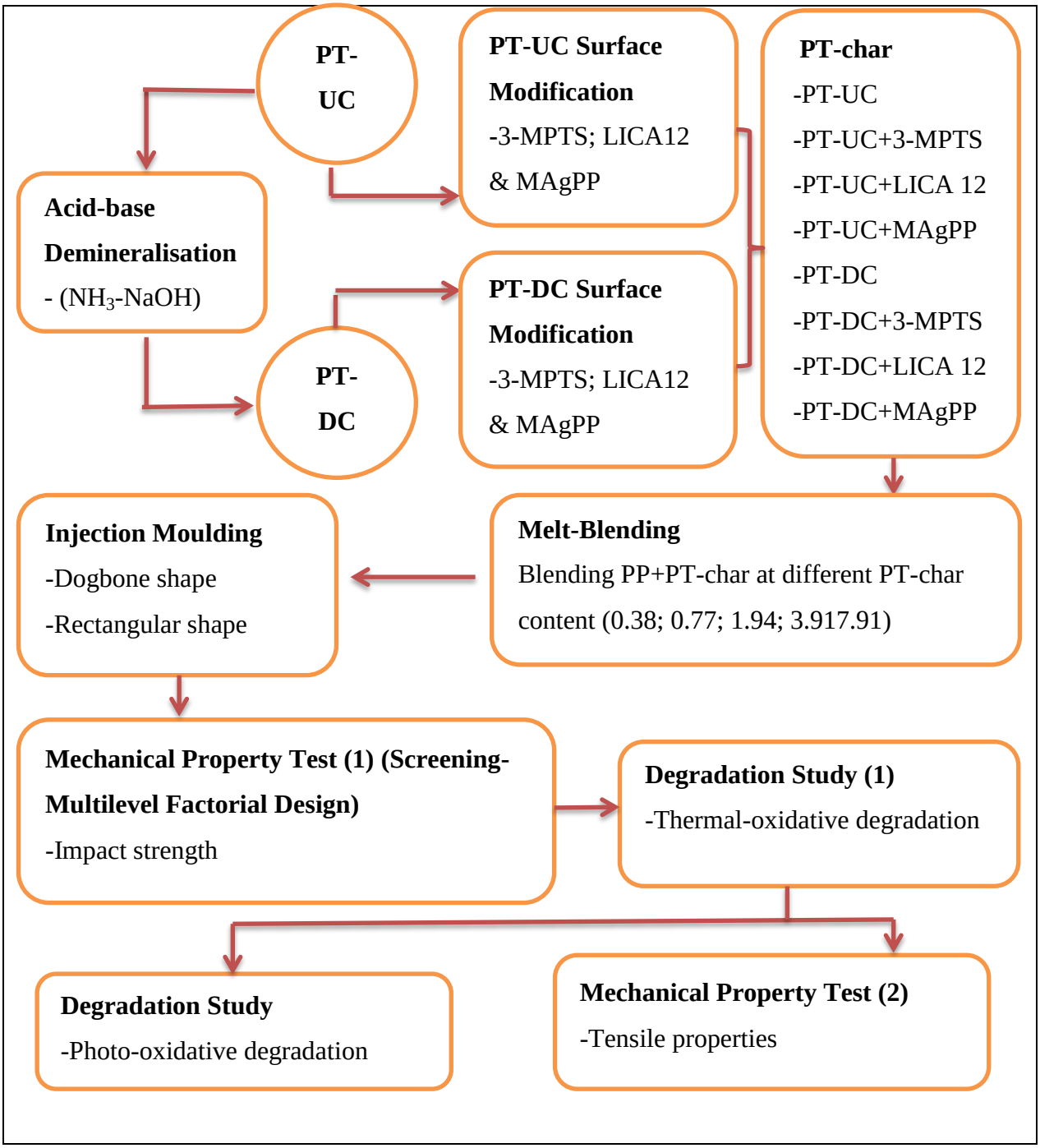

Figure 4.3: Experimental flow diagram.

In the first part of the experiments, the PT-UC was demineralised with HNO_3-NaOH in order to remove inorganic impurities. Transition metals impurities in fillers are known to accelerate degradation of PP [31], and therefore it is important to remove them. PT-DC was obtained after the demineralisation stage. The two different PT-chars (PT-UC and PT-DC) were moved to the surface modification stage. Both PT-UC and PT-DC were surface modified with two different coupling agents (3-MPTS and LICA 12) and a compatibiliser (MAgPP) to improve the filler reactivity towards the polymer. The difference between these surface

modifiers is that two (3-MPTS and LICA 12) are used to pre-treat PT-char before blending with PP while MAgPP can be directly blended without pre-treatment of the PT-char.

In order to get a homogenous mixture/disperse PT-char onto the polymer matrix, PP composites were prepared by utilising a melt blending instrument at different PT-char loadings (0.38 wt.%; 0.77 wt.%; 1.94 wt.%; 3.9 wt.% and 7.91 wt.%) in order to evaluate the effects of filler loading on the properties of PP composites. The blends were then moulded using injection moulding in order to produce the test composite samples for evaluation of the mechanical properties and for degradation studies. Multiple samples of each different combination were moulded and were used to make replicate measurements

The moulding stage was followed by the screening of the composite impact strength using a Multilevel Factorial Design. Composites with the best impact strength were selected to move to the next stage, which was the thermal-oxidative degradation study. This was followed by analysis of the tensile properties and the photo-oxidative degradation studies. The effect of PT-char, demineralisation of PT-char, surface modification of PT-char and the PT-char loadings on different PT-char composites was studied. The purpose was to determine the feasibility of PT-char as filler and whether it requires surface modification or not.

4.7.2 Statistical analysis

Three-way analysis of variance (ANOVA) was conducted in order to obtain the mean values of the response variable. The p-values designate which of the effects (main/interactions) is/are statistically significant. A p-value of less than or equal to 0.05 was considered to be statistically significant.

CHAPTER 5: EXPERIMENTAL RESULTS AND DISCUSSIONS

5.1. PT-char particle characterisation

5.1.1 Particle size distribution of PT-char

Since the particle size of filler is a primary factor for reinforcement, the particle size distribution of PT-UC and PT-DC was measured on a volume frequency basis. **Table 5.1**, below presents the average particle size of PT-UC and PT-DC.

Table 5.1: Average particle size of PT-UC and PT-DC (µm).

	PT-UC		PT-DC	
	Value	Standard deviation	Value	Standard deviation
Average	89.9	3.54	11.0	0.55

The average particle size of PT-UC is larger than that of PT-DC because the ash and the carbonaceous deposits within PT-UC were removed during demineralisation [20]. Demineralisation significantly reduced the particle size of PT-UC due to digestion of large particles into small particles. The average particle size of PT-UC and PT-DC are larger than the PT-char particle size reported by Zhou *et al*. [20] and Martinez *et al*. [51], due to variations in the pyrolysis conditions. The particle size of PT-UC and PT-DC are larger than that of commercial CB [83, 117, 128]. However, the average particle size of PT-DC is comparable to some of the previously reported fillers such as calcium [28, 69, 201], talc [129, 130] and silica [132]. The average particle size of PT-UC is possibly too large for PP composite applications as the particles might act as stress concentrators and consequently cause the final composite to have poorer mechanical properties [223]. **Figure 5.1** and **Table 5.2** show the particle size distribution of PT-char before and after demineralisation.

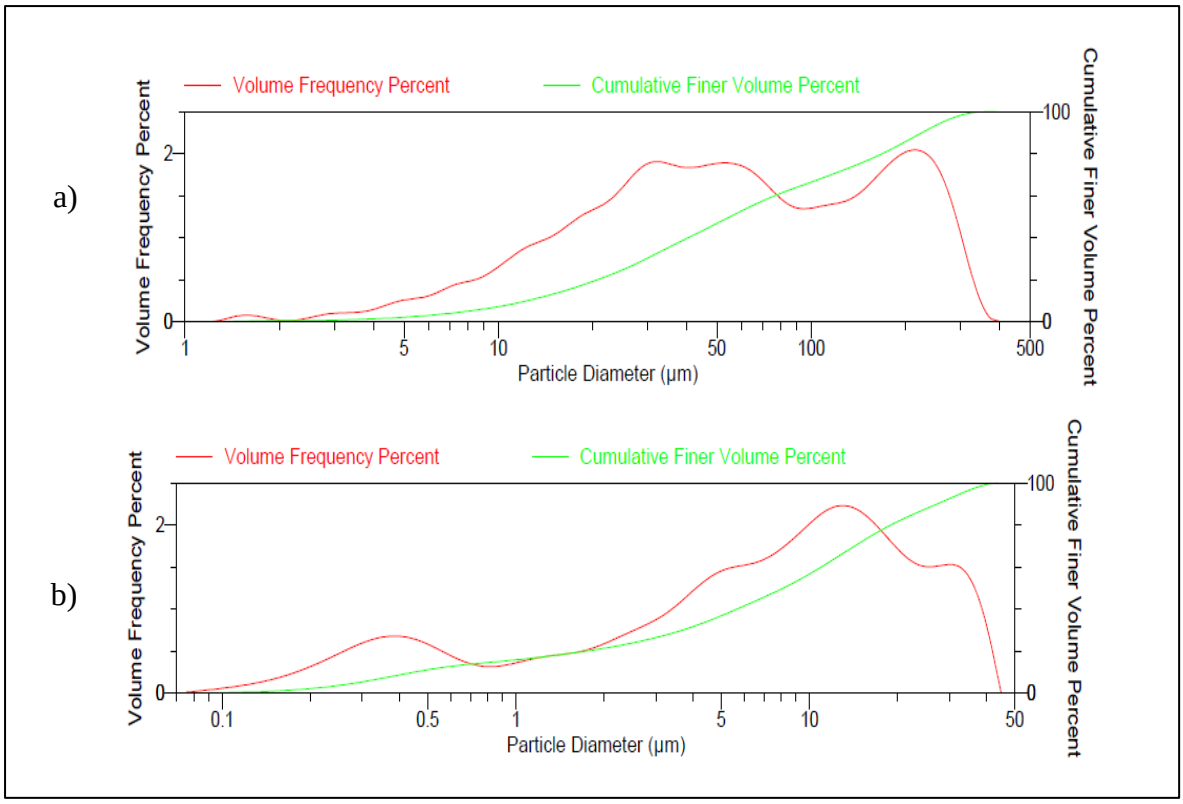

Figure 5.1: Particle size distribution of a) PT-UC and b) PT-DC.

Table 5.2: Particle size, cumulative distribution of PT-UC and PT-DC.

Particle size range (µm)	PT-UC (%)	PT-DC (%)
> 100	31.9	0
100-50	19.8	0
50-20	27.7	17.6
20-10	12.9	25.0
10-2	7.70	35.4
< 2	0	22.0

As indicated in **Figure 5.1**, both PT-UC and PT-DC show a bimodal particle size distribution. The particle size distribution of both PT-UC and PT-DC is heterogeneous with PT-UC having the highest percentage (31.9 %) of particles greater than 100 µm. After demineralisation, the PT-UC particles were drastically reduced in size in such a way that there were no particles greater than 50 µm amongst the PT-DC particles. This indicates that the demineralisation process digests the PT-UC particles. A large amount of PT-DC particles lies between 2 µm and 50 µm in size. About 22.0 % of PT-DC particles are less than 2 µm of which 11.0 % is less than 0.5 µm in size and the majority of industrial reinforcement products

are derived using this specific size [50]. Heterogeneous particle size is essential in polymer composites since it enhances packing and flow rate during composite production.

From the results presented it is clear that demineralisation has a major effect on the particle size of PT-char. The results further indicate that the particle sizes of PT-UC and PT-DC are larger than that of the commercial CB used in the tyres [50, 51], mainly due to re-polymerisation reactions taking place during pyrolysis. Generally, fillers with small particle size are most preferred within the reinforcement industry because the strength of the reinforcement tends to increase with a decrease in the particle size of the filler [50]. Usually, the larger the particle size of the filler, the lower the surface area and the poorer the material obtained [17]. Therefore, of the two fillers analysed in this study, PT-DC is most likely to be the more suitable filler for reinforcement applications.

5.1.2 Surface morphology of PT-char

The SEM micrograph images of both PT-UC and PT-DC are presented in **Figure 5.2**. As seen from **Figure 5.2**a) and b), both PT-UC and PT-DC consist of spherically shaped particles [224]. The spherical filler shape is useful in composites as it gives a uniform distribution of stress, an increase in melt-flow and lower viscosity [223]. The particle size distribution of both PT-UC and PT-DC is heterogeneous. Furthermore, PT-UC has larger particles than PT-DC due to its ash and carbonaceous deposits content [20]. **Figure 5.2**a) further shows that PT-UC is composed of grey areas and bright spots and the bright spots suggest the presence of zinc oxide which was added during tyre manufacturing [91]. As seen from **Figure 5.2**c), demineralisation reduced the particle size of PT-UC. The PT-DC particles are finer than PT-UC particles and the presence of bright spots is reduced due to the reduction of ash and tarry product content in the surface of PT-UC. The porosity structure of both PT-UC and PT-DC was not visible. As seen from **Figure 5.2**d), formation of aggregates is observed in PT-DC particles. Stress concentrations on composites normally take place in these aggregated regions and this could have a detrimental effect on composite properties [182].

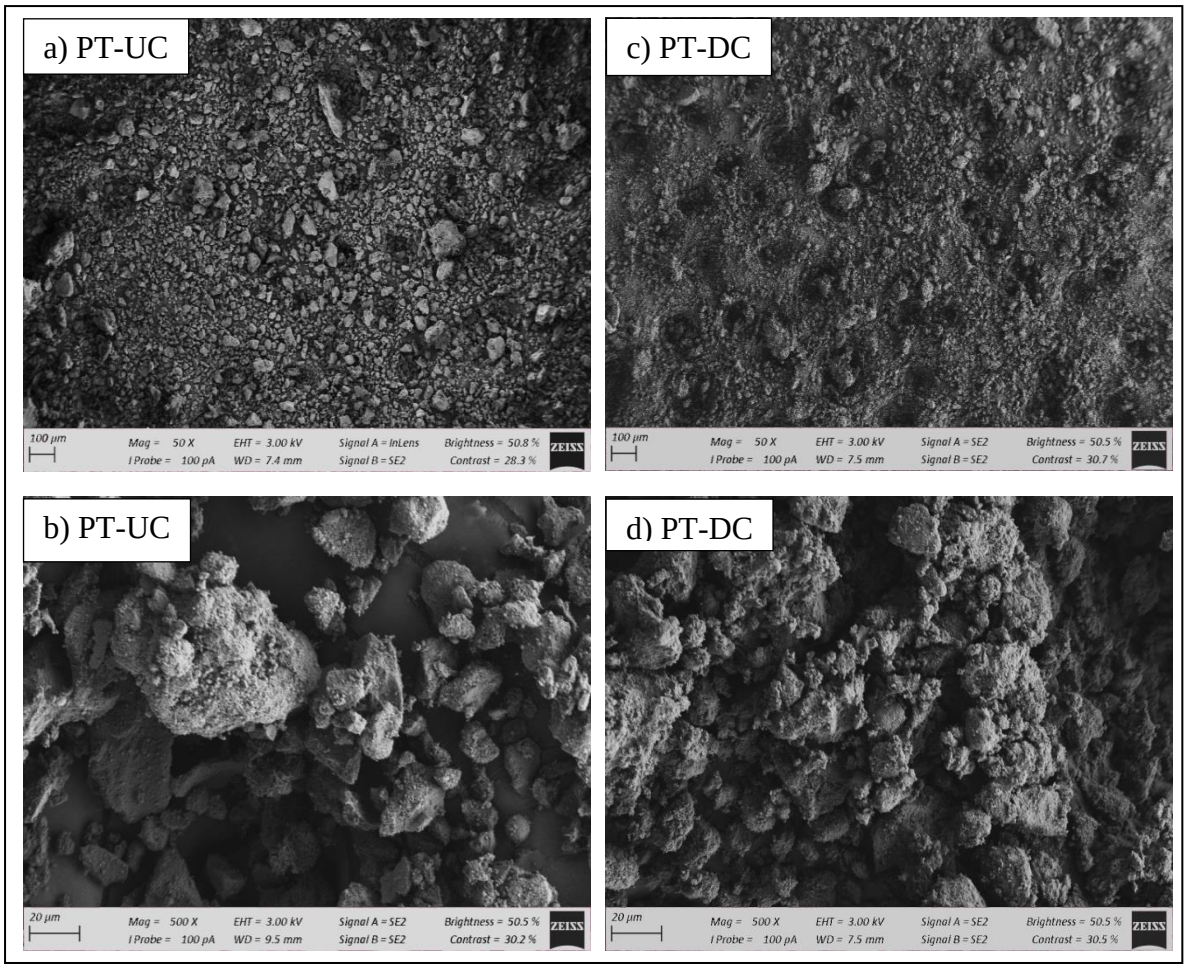

Figure 5.2: Surface morphology of PT-UC and PT-DC particles at different magnifications: a) and c) at 50X magnification and b) and d) at 500X magnification.

5.1.3 Proximate, ultimate analysis and chemical composition of ash

Proximate analysis was performed on both PT-UC and PT-DC. The analysis was repeated twice in order to spot anomalies (see **Appendix F**). **Table 5.3** below shows the proximate analysis results obtained for PT-UC and PT-DC.

Table 5.3: Proximate Analysis of PT-UC and PT-DC (wt.%).

	PT-UC		PT-DC	
	Value	Standard deviation	Value	Standard deviation
Moisture content	0.45	0.35	1.45	0.07
Volatiles + Organics	7.80	< 0.05	9.60	0.14
Fixed Carbon	75.3	0.49	86.3	0.07
Ash	16.5	0.14	2.70	0.14

PT-UC has a considerably higher ash content (16.5 wt.%) but still within the reported values [45, 46, 48, 58, 71, 73]. This high ash content is due to the variety of inorganic components added to the tyre in order to improve its properties, accelerate vulcanisation and reduce the cost. The amount of inorganics significantly depends on the formulations used by the manufacturers of the rubber tyres. The moisture, fixed carbon as well as the volatile and organic values found for PT-UC are in agreement with the ones reported in the literature [21, 45, 46, 48, 71, 73]. Demineralisation leads to an increase in fixed carbon with a final percentage of 86.3 wt.%, which is due to the removal of inorganics present. About 83.6 % of ash was successfully reduced from PT-UC due to the combined use of an acid and a base [17, 88]. Demineralisation increased the moisture content to 1.45 wt.%. An increase in the volatiles and organic content was unexpected. This peculiar behaviour might be caused by the breaking down of the polymer chains during demineralisation, giving rise to smaller molecules that appear in TGA at lower temperatures. The ultimate analysis was also performed on both PT-UC and PT-DC (see **Appendix G**) and the results are presented in **Table 5.4** below.

Table 5.4: Ultimate analysis of PT-UC and PT-DC (wt.%).

	PT-UC		PT-DC	
	Value	Standard deviation	Value	Standard deviation
N	0.28	< 0.05	0.46	< 0.05
C	76.6	0.64	90.8	0.41
H	0.68	0.01	0.71	0.01
S	2.38	0.34	0.95	0.01
Ash	16.5	0.14	2.70	0.14
O	3.61		4.36	

The carbon content of PT-UC was found to be 76.6 wt.%, which is virtually the same as the fixed carbon content result obtained from the proximate analysis of PT-UC. However, this value is less than the values reported by several researchers [5, 10, 11, 39, 46, 54, 58, 73, 77, 78], which could be due to differences in pyrolysis temperatures and possibly due to the high ash content (as shown in **Table 5.3**) which results in a lower carbon content. The removal of inorganic impurities during demineralisation increased the carbon content to 90.8 wt.% [50]. The carbon is mainly derived from the CB filler while some small portion of it is derived from the rubber [76]. The values of nitrogen and hydrogen contained within PT-UC were

found to be 0.28 wt.% and 0.68 wt.% respectively and these values are within the range of the reported values in the literature [10, 17, 18, 39, 54, 58, 77, 225]. The hydrogen is derived from the undegraded rubber and to some extent from the chemisorbed water. The nitrogen is derived from nitrogen containing organic compounds such as accelerators used during tyre manufacture [76]. Demineralisation had the effect of slightly increasing the nitrogen and hydrogen content to 0.46 wt.% and 0.71 wt.% respectively. The increase in the hydrogen content is consistent with the increase in the volatile content. The increase in nitrogen is the result of the demineralisation treatment performed using nitric acid. The sulphur content was reduced to about 38.9 % of its initial value due to the effect of nitric acid [21]. The reduced sulphur content is comparable to the sulphur content reported in commercial CB [19, 226]. The sulphur is derived from the sulphur that was added as a vulcanising agent. The concentration of the organic oxygen within PT-UC was found to be 3.61 wt.% which is slightly lower than the values reported in literature [5, 73, 74, 77]. However, due to the effect of demineralisation, it increased to 4.36 wt.%. The oxygen within PT-char is derived from the oxygen surface intermediates formed during waste tyre pyrolysis [76]. The oxygen surface intermediates are from oxygen functional groups such as hydroxyl and carbonyl groups, which are contained within the surface of PT-char as revealed by the FTIR analysis which will be reported later in this chapter. The mineralogy study was performed (**see Appendix H**) in order to analyse the inorganic, or ash composition within PT-char (PT-UC and PT-DC) and the results are presented in **Table 5.5** .

Table 5.5: Chemical composition of the ash within PT-UC and PT-DC

	PT-UC			PT-DC		
	$Mass_a$	$Mass_b$	Standard deviation	$Mass_a$	$Mass_b$	Standard deviation
C	23.2	3.82	0.04	30.0	0.81	0.09
O	29.0	4.78	0.03	40.6	1.10	0.02
Mg	0.44	0.07	< 0.01	0.17	< 0.01	< 0.01
Al	1.18	0.19	< 0.01	0.52	0.01	< 0.01
Si	7.95	1.31	0.02	2.04	0.06	0.02
P	ND			0.06	< 0.01	< 0.01
S	0.49	0.08	< 0.01	9.10	0.25	0.03
Cl	ND			0.03	< 0.01	< 0.01

K	0.47	0.08	< 0.01	0.56	0.02	< 0.01
Ca	0.83	0.14	< 0.01	0.32	< 0.01	< 0.01
Fe	0.48	0.08	< 0.01	0.26	< 0.01	< 0.01
Co	0.34	0.06	< 0.01	ND	ND	
Cu	0.46	0.08	0.01	0.37	0.01	< 0.01
Zn	31.9	5.27	0.02	0.41	0.01	< 0.01
Total	100	16.5	0.17	100	2.70	0.22

ND = Not detected.

$Mass_a$ = The wt.% of the element within the ash content.

$Mass_b$ = The actual wt.% of the element within the carbon matrix.

As mentioned, the chemical composition of PT-char was analysed using the EDX method. Therefore, the results are subjected to experimental error since the EDX method is semi-quantitative. As said, the ash within PT-UC contains significant amounts of oxygen, silicon and zinc. Carbon was found within the ash content and it is believed that it must have been derived from the carbon tape that was holding the sample during the EDX analysis.

The inorganic oxygen within the ash is derived from metal oxide since metals contained within the tyre can be in their elemental form or in their corresponding oxides forms [33]. For instance, sodium is not found in nature as an element but as a compound. Therefore, it exists within the ash as sodium oxide. Furthermore, aluminium and magnesium both instantly form oxide layers upon exposure to air. Therefore, a small portion of these elements will be in their oxide forms. Since zinc substantially represents 1 wt.% to 2 wt.% of the tyre, the ash contains significant amounts of zinc [33, 227]. Zinc is possibly present as zinc oxide, since it was added as zinc oxide during tyre. A small portion of zinc might also be present as zinc sulphide, as previously reported [62, 71, 228]. Due to the addition of significant amount of silicon dioxide as a replacement for CB filler in some tyres [37], silicon might be present in its oxide form in a substantial amount within the ash. Thus, a large portion of the inorganic content of the ash is in the oxide form.

Some inorganics, such as phosphorus and chlorine were not detected on the surface of PT-UC. However, they were detected on the surface of PT-DC. This was not due to the introduction of inorganic compounds by acid-base lixiviants, but rather due to the high

amount of other inorganics on the surface of PT-UC, which might have covered phosphorus and chlorine. A similar behaviour was also observed with sulphur. Although the sulphur content of the ash is very low, a significant amount of sulphur is retained within the carbon matrix.

Demineralisation successfully reduced zinc content by 92.3 % and silicon content by 95.8 %. The removal of zinc in zinc oxide form was successful due to its amphoteric nature, which makes it able to react with both nitric acid and sodium hydroxide. Due to its slightly acidic nature, silicon must have been substantially removed by sodium hydroxide. Due to the small amount of cobalt present in the surface of PT-UC, demineralisation removed all the cobalt that was present on the surface of PT-UC. Demineralisation only slightly reduced copper. This could have been because acid-base lixiviants were only able to diffuse through some of the particles or might have removed only the copper which was on the surface of PT-UC. Due to its basic nature, iron oxide was also slightly removed by nitric acid only and not by sodium hydroxide. Calcium was greatly reduced by about 93.4 % probably by nitric acid and not sodium hydroxide since it requires a temperature of 600 °C to dissolve [229].

The proximate and elemental analysis as well as the results of the chemical composition analysis of the ash showed more or less similar values to those obtained by various researchers [17, 39, 45, 46, 48, 55]. Since PT-UC is derived from a mixture of truck tyres, it was expected to have a diverse chemical composition. The amounts of organic and inorganic compounds contained in the PT-UC depend on the formulations used by different tyre manufacturers. Furthermore, these results indicate that sodium hydroxide and nitric acid are efficient in reducing certain inorganic compounds. For instance, the inorganic oxides, such as those of zinc, aluminium and iron, have amphoteric character and can dissolve in sodium hydroxide [17], while other inorganic oxides such as those of calcium, copper, are easily dissolved in nitric acid due to their basic nature. Some inorganic additives in the tyre are strongly connected with the matrix in such a way that it is difficult to remove them [230]. As stated in the literature, sequential demineralisation with the use of an acid and a base is an efficient way to counteract such differences in the nature of the inorganic compounds [79].

5.1.4 Surface area of PT-char

The surface area of the PT-char is one of the most important properties to consider when evaluating the filler since it determines the degree of interaction between the PT-char and the PP matrix. The PT-UC went through a demineralisation process in order to recover active sites and increase surface area in the resulting PT-DC. **Table 5.6** and **Table 5.7** below present the surface area and the pore analysis results of PT-UC and PT-DC.

Table 5.6: The surface area analysis of PT-UC and PT-DC (m^2/g).

	PT-UC	PT-DC
BET surface area	73.9	76.7
BJH adsorption cumulative pore surface area	69.9	71.1
BJH desorption cumulative pore surface area	68.2	70.2

Table 5.7: The pore size analysis of PT-UC and PT-DC.

	Unit	PT-UC	PT-DC
BJH adsorption cumulative pore volume	cm^3/g	0.51	0.56
BJH desorption cumulative pore volume	cm^3/g	0.52	0.57
BET adsorption average pore diameter	nm	28.1	29.9
BET desorption average pore diameter	nm	28.1	29.9
BJH adsorption average pore width	nm	29.0	31.5
BJH desorption average pore width	nm	30.2	32.3

The BET surface area of PT-UC was found to be 73.9 m^2/g which is supported by literature since the surface areas of PT-char usually vary from 30 m^2/g to 90 m^2/g [10, 22]. The BJH adsorption pore surface area of PT-UC is 69.9 m^2/g and is less than its BET surface area which means that the pores do not cover the entire surface area. In addition, it may also be due to some residual volatiles entrapped in the surface of PT-UC [230]. Demineralisation slightly increased the BET surface area of PT-DC to 76.7 m^2/g as a result of the removal of inorganic compounds [55]. Demineralisation slightly increased the porosity of PT-UC. As seen from **Table 5.7**, the pore volume, diameter and width slightly increased. Such results were unexpected due to the remarkable reduction in particle size of PT-char. However, this could be the result of the inability of acid-base lixiviants to penetrate through the active sites of PT-char in order to remove residual volatiles trapped within the PT-char pore surface [75].

Nonetheless, the surface areas of PT-UC and PT-DC are high and comparable to commercial CB used in rubber products such as N351; N650; N660; N550; N774; N772; N750 and N440 [19, 51, 58, 227, 231]. The pore sizes of both PT-UC and PT-DC correspond to the mesopore range (further indication in **Appendix I**). Several researchers [54, 59–62], have also reported PT-char with mesoporous structure.

5.1.5 Surface chemistry of PT-char

The surface chemistry of the filler is very important as it determines the strength of the matrix-filler interactions. In order for PT-char to be uniformly distributed in the PP matrix, PT-char and PP need to be compatible with each other to improve the properties of PP composites. Therefore, PT-UC and PT-DC were surface modified with 3-MPTS and LICA 12 coupling agents. Since PT-char contains a high amount of carbon arising from CB filler which was added during tyre manufacturing, it was very challenging to get a spectrum (of both PT-UC and PT-DC) with good signal to noise ratio. This is due to CB being a strong absorber in the infrared region of the light spectrum. Therefore, in order to avoid this, the PT-char samples were diluted with large amounts of potassium bromide. **Figure 5.3**, below shows the FTIR spectra of PT-UC and PT-DC.

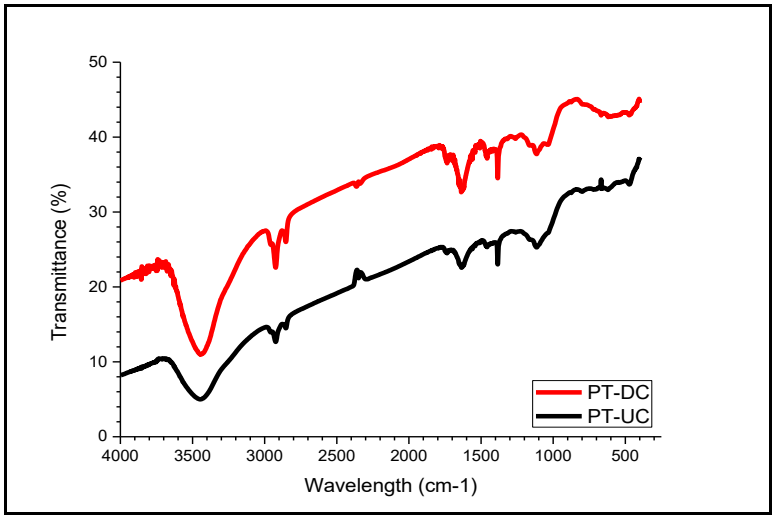

Figure 5.3: FTIR spectra of PT-UC and PT-DC.

The spectra of PT-UC and PT-DC are almost the same due to the presence of carbonyl, carboxylic acid and hydroxyl group transmission band in both the spectra. The peaks at 472 cm^{-1}, 620 cm^{-1} and 1034 cm^{-1} results from Si–O–Si bond which belongs to the silica present

inside PT-char. The band at 800 cm^{-1} results from C-H bending found in the carbon skeleton [232]. The peaks at 1114 cm^{-1} for PT-UC and 1115 cm^{-1} for PT-DC belong to C–O stretching vibrations of the secondary alcohols. There is a medium sized peak at 1384 cm^{-1}, a small peak at 1457 cm^{-1} and other small peaks at 1635 cm^{-1} and 1735 cm^{-1} in both spectra and these are attributed to –OH bending of alcohols or carboxylic acids, C–H bending of alkane from methylene and methyl groups, C=O stretching of conjugated ketones [232] and C=O stretching vibrations of carboxylic acids. Both spectra show weak peaks at 2363 cm^{-1} and 2400 cm^{-1} arising from perturbation due to the presence of CO_2. There are strong bands at 2853 cm^{-1} and 2923 cm^{-1}also, which could possibly be overtone bands of carboxylic groups [232].

Lastly, a broad peak at 3447 cm^{-1} was observed in both spectra, and this peak can be attributed to the –OH stretching vibrations of hydroxyl groups in the structure of alcohols or phenols [209, 232]. The –OH peak is intense in the spectra of PT-DC due to the changes brought about by acid-base lixiviants. These results indicate that the objective of entering –OH groups in the surface of the PT-char, by using nitric acid and sodium hydroxide as acid-base lixiviants seems to be successful. Filler with –OH groups on its surface is advantageous for silanisation. Silanes react readily with hydroxide-rich surfaces [232]. Since, the spectra of PT-UC and PT-DC (**Figure 5.3**) are almost completely the same, there was only a slight difference of PT-UC and PT-DC treated with either 3-MPTS or LICA 12 (**Figure 5.4** and **Figure 5.5**).

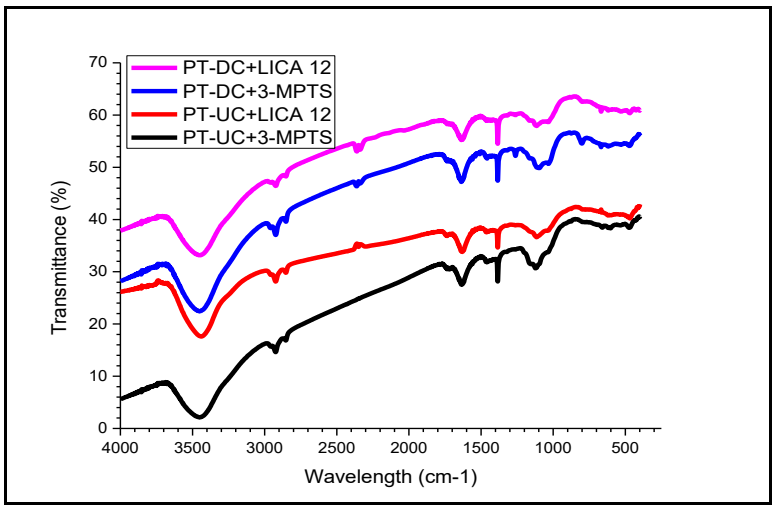

Figure 5.4: FTIR spectra of PT-UC and PT-DC coupled with 3-MPTS or LICA 12.

In the spectra of PT-UC+3-MPTS and PT-DC+3-MPTS, an intense peak (**Figure 5.4** and **Figure 5.5)** was observed at 801 cm^{-1} which is due to the Si-OH bond [131]. Further peaks were also observed at 472 cm^{-1}, 1033 cm^{-1} and 1122 cm^{-1} which belong to Si–O–Si groups [131, 152] and these were already present before the treatment. The absence of the Si–OH stretching band for both PT-UC+3-MPTS and PT-DC+3-MPTS at ~ 950 cm^{-1} indicates that all of the hydroxyl groups reacted with the silanol groups of 3-MPTS [131]. The Si–O bond at 1384 cm^{-1} could not be verified for either PT-UC+3-MPTS or PT-DC+3-MPTS since the peak also appear in the spectra of both PT-UC and PT-DC. The presence of phosphate group peaks at 2853 cm^{-1} and 2923 cm^{-1} [211, 233] could not be verified also for either PT-UC+LICA 12 or PT-DC+LICA 12 since these peaks also appear in the spectra of both PT-UC and PT-DC.

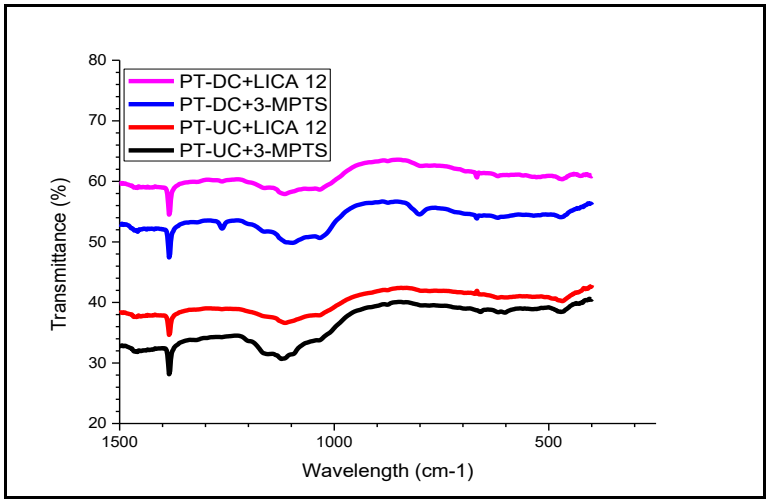

Figure 5.5: FTIR spectra of PT-UC and PT-DC with 3-MPTS and LICA 12.

In the spectra of PT-UC+LICA 12 and PT-DC+LICA 12 there is an absence of Ti–O transmission bands at 904 cm^{-1} and 990 cm^{-1}. The absence of the titanium transmission bands could be due to the low intensity of the spectrum. This is related to the presence of high amount of carbon (arising from CB filler) which makes it difficult for the peaks to have high intensity since carbon is a strong absorber of the infrared region of the light spectrum. The FTIR spectra of coupling agents are also provided in **Appendix J**.

From the results discussed above, it is clear that PT-UC already has many functional groups, before any treatment, including the oxygen containing functional groups (e.g. the carbonyl, carboxylic acid, phenolic and lactonic groups). Although the measurement of oxygen functional groups was not covered, an increase in their content during demineralisation was

indicated by the increase in oxygen content as shown by the elemental analysis. The presence of these oxygen functional groups contributes immensely to the reactivity of PT-char [21, 76]. Furthermore, many peaks arising from the addition of coupling agents overlapped with the ones already present on the surface of the unmodified PT-char. Moreover, surface modification of PT-char will enhance the interface between the PT-char and the PP matrix. Altering the surface chemistry of PT-char is necessary, since PP properties are highly dependent on the interface, which consequently influences the dispersion state of the filler into the PP matrix.

5.1.6 Concluding remarks

PT-UC and PT-DC were found to have spherical particles with heterogeneous particle size distributions. The formation of aggregates was observed in the PT-DC particle, which could have detrimental effects on composites properties. Demineralisation significantly reduced the particle size and the ash content within PT-UC. However, the surface area and the porosity of PT-DC were slightly improved due to the removal of some carbon residuals entrapped in the surface of PT-UC. Due to a significant reduction of the ash content within PT-UC, the oxygen contained in the ash was reduced while the oxygen present on the carbon surface increased as shown by the elemental and FTIR analysis. Furthermore, the effect of demineralisation significantly reduced rich elements such as zinc and silica. The surface chemistry of PT-UC already had many functional groups (including oxygenated groups) present before any treatment. This, however, made it difficult to investigate whether surface modification introduced functional groups on the surface of PT-UC, since the functional groups of the surface modifiers overlapped with the ones that has already been present in the surface of PT-UC before treatment.

5.2. Melt blending characteristics

PP and the PT-char were first mixed in a one-step process, but as the PT-char loading increased, the blades could not turn due to the high viscosity of the blend. Therefore, a two-step process was chosen to allow the blades to turn and to avoid also breaking the internal mixer. The one step process entails mixing PP simultaneously with PT-char and the two-step process entails mixing PP first for 2 min and then immediately adding the PT-char for the

remaining 8 min. The values of mixing torque for pure PP and composites filled with UC and DC obtained at 10 min mixing time are shown in **Figure 5.6** below.

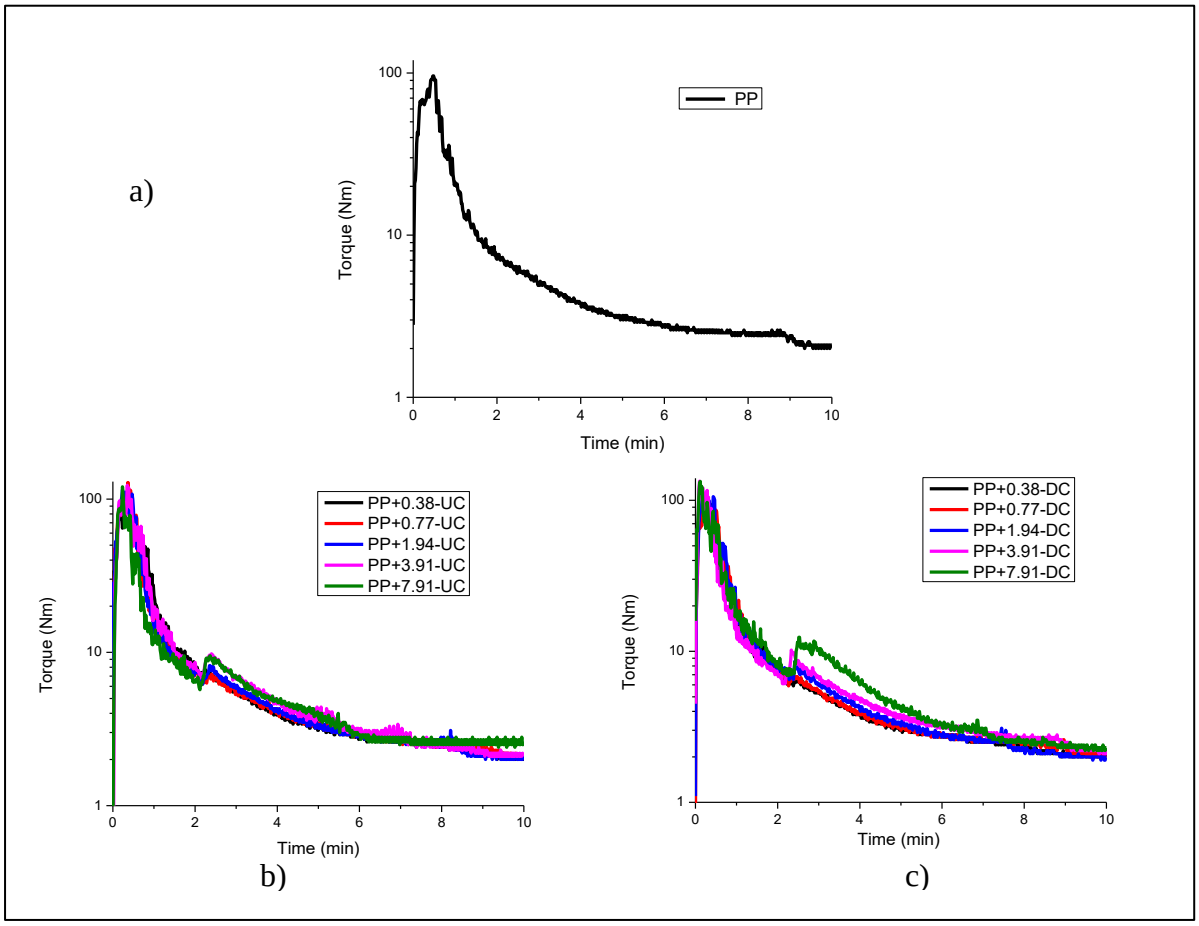

Figure 5.6: Mixing torques vs time for (a) pure PP, (b) unmodified PP composites filled with UC and (c) unmodified PP composites filled with DC.

As seen from **Figure 5.6**a), the mixing torque rapidly increased within the first minute of mixing due to the shear stress experienced by the PP. An increase in temperature (see **Appendix K**) and continuous shearing force due to mixing friction caused the PP to melt and resulted in a lower mixing torque [234]. As seen from **Figure 5.6**b), after 2 min of mixing, the addition of PT-char into the molten PP caused the mixing torque to increase due to the dispersive resistance provided by the PT-char [234]. An increase in PT-char loading increased the mixing torque due to a reduction in the ability of the PP matrix to flow. During composites mixing, the presence of the rigid PT-char particles limits the molecular motion of the PP matrix, resulting in an increase in mixing torque [235].

PP composites filled with DC had slightly higher mixing torque after 2 min (especially at 3.91 wt.% and 7.91 wt.%) than those filled with UC. This was caused by the increase in surface area of DC which led to an increase in interfacial area in the composites melt [124]. Furthermore, the small particle size of DC results in greater particle-particle interactions during mixing which lead to an increase in mixing torque. With increasing mixing temperature, the mixing torque of the composite melt decreased gradually as the PT-char is dispersed on the PP matrix. Mixing torques for 3-MPTS modified PP composites at various PT-char loadings are presented in **Figure 5.7.**

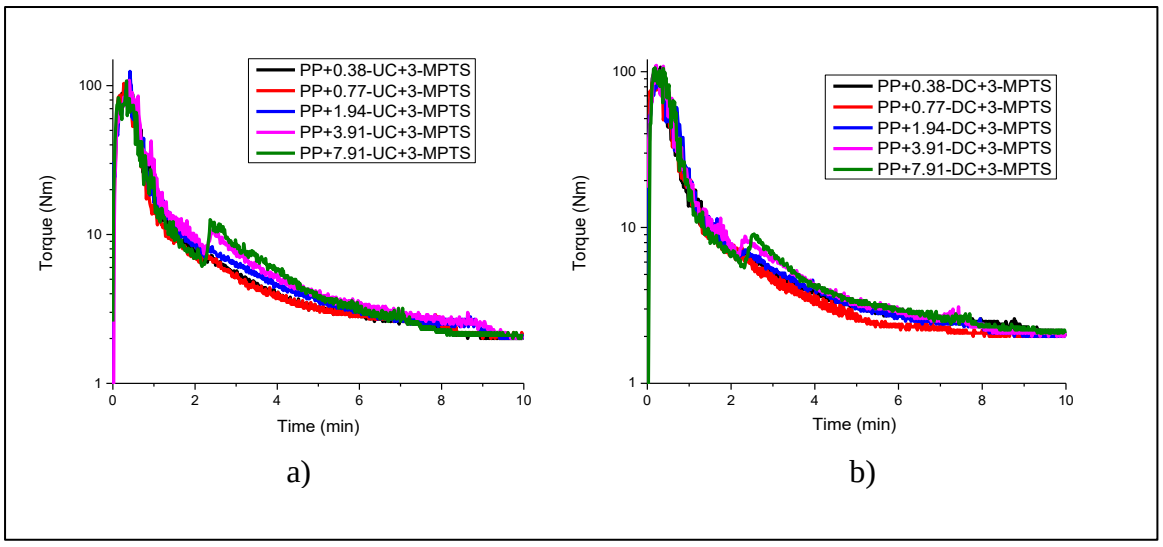

Figure 5.7: Mixing torques for 3-MPTS modified PP composites.

The increase in mixing torque is slightly more pronounced in **Figure 5.7**a) compared to **Figure 5.6**b). During melt blending, interfacial interactions between a surface treated PT-char and the PP chains form and as a result they may cause a slight increase in the mixing torque of the composites melt. This attribute results from enhanced adhesion of the PT-char particles into the PP matrix, facilitated by the presence of the silane. The UC contains fairly high amounts of silica as compared to the DC and silica contains a high density of the silanol groups. Therefore, the ethoxy groups of the silane coupling agents react with the silanol groups forming siloxane bonds. Therefore, the organofunctional fragments of the silanes react with the PP chains to form crosslinks between the PT-char and the PP. These chemical bonds, limit the movement of the polymer chains resulting in the increase in the mixing torque.

The increase in the mixing torque is less pronounced as DC loading is increased in **Figure 5.7**b) as compared to **Figure 5.6**c). This was caused by silane modification, which reduced the particle-particle interactions that normally lead to agglomeration of the DC particles [235].When the desired bonding between PT-char and PP melt was stabilised, the mixing torque decreased. Fillers play a vital role in the rheological behaviour of the PP composites. According to Marti-Ferrer *et al*. [235], the filler arranges itself according to the applied direction of the shear force. Thus, the torque differences are a result of the motion of the filler during its arrangement on the PP matrix. Mixing torque values for LICA 12 modified PP composites at various PT-char loadings are presented in **Figure 5.8**.

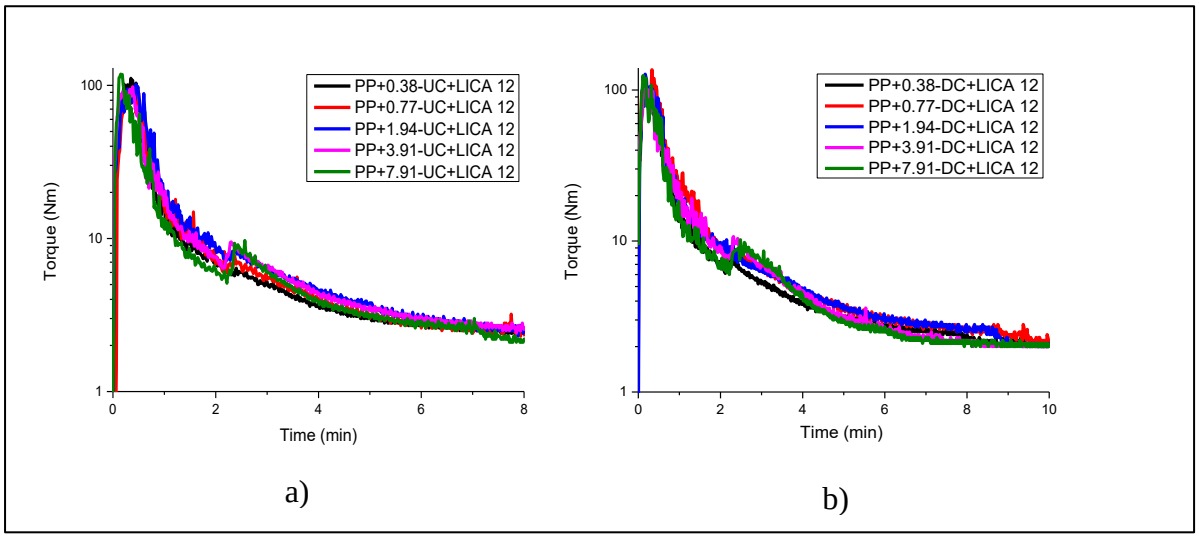

Figure 5.8: Mixing torques for LICA 12 modified PP composites.

No significant difference was observed between LICA 12 modified PP composites filled with UC and DC. Nonetheless, contrary to **Figure 5.6**c), the addition of LICA 12 reduced the mixing torque of PP composites filled with DC. This trend is similar to the work reported by several researchers [132, 143, 236]. The decrease in the mixing torque is due to the plasticising effect induced by the titanate coupling agent, which reduced the friction resistance of the unmodified PT-char. Mixing torque values for MAgPP modified PP composites at various PT-char loadings are presented in **Figure 5.9.**

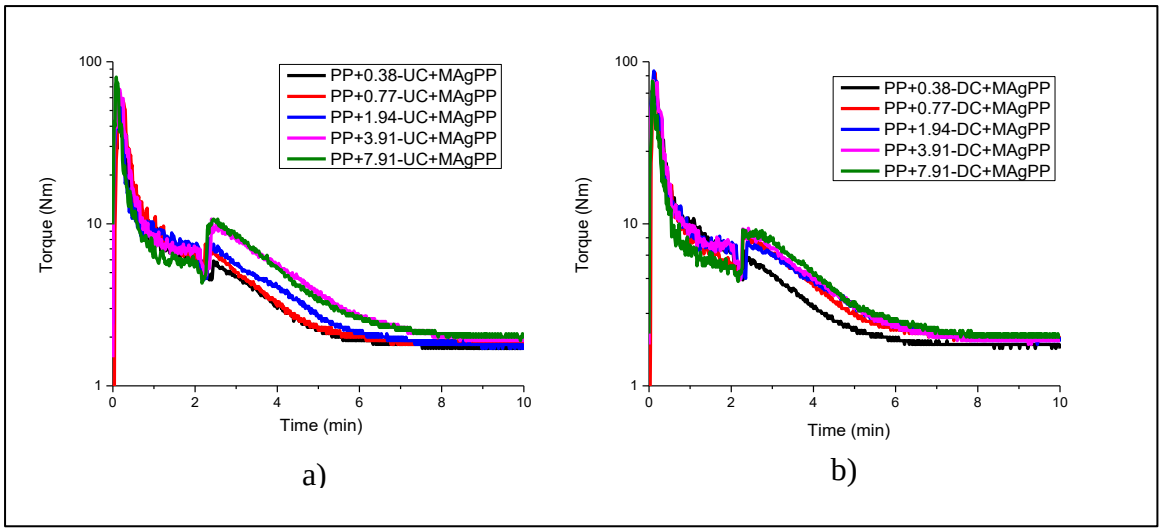

Figure 5.9: Mixing torques for PP composites modified with MAgPP at various PT-char loadings.

As seen from **Figure 5.9**a) and b), the mixing torque of PP composites modified with MAgPP were higher (more pronounced after 2 min) than those of PP composites modified with silane and titanate coupling agents which might be due to the differences in the treatment methods. This behaviour could possibly mean that there was no chemical bonding between the hydroxyl groups of the PT-char and the anhydride moieties of the grafted PP. Instead of lubricating the PT-char during mixing the addition of MAgPP possibly created hindrance between the spherical particles of PT-char and the PP matrix thereby causing more frictional resistance. This behaviour consequently leads to defects in the composite system.

5.2.1 Concluding remarks

The PT-char particle size and surface area, the presence of agglomerates and the interactions between the filler and the matrix influenced the mixing torque of the polymer melt. Incorporation of PT-char increased the mixing torque of the composites melt due to rigid PT-char particles which limited the movement of PP chains. The mixing torque of the PP composites increased with an increase in PT-char loading due to the presence of agglomerates. Surface modification, enhanced the interface between the filler and the PP matrix thereby reducing the mixing torque. However, when the adhesion between the PT-char and the PP matrix was stronger, it led to an increase in the mixing torque of the composites melt.

5.3. PP composites impact strength and surface fracture

5.3.1 PP composites impact strength

Three-way ANOVA was conducted in order to obtain the mean values of the impact strength of the PP composites (**Figure 5.10)**. The purpose of ANOVA was to find statistically significant factors and their interactions. The p-values designate which of the effects (main/interactions) is/are statistically significant. A p-value of less than or equal to 0.05 was considered to indicate statistical significance. The main and the interaction effects plots are presented in **Appendix L.**

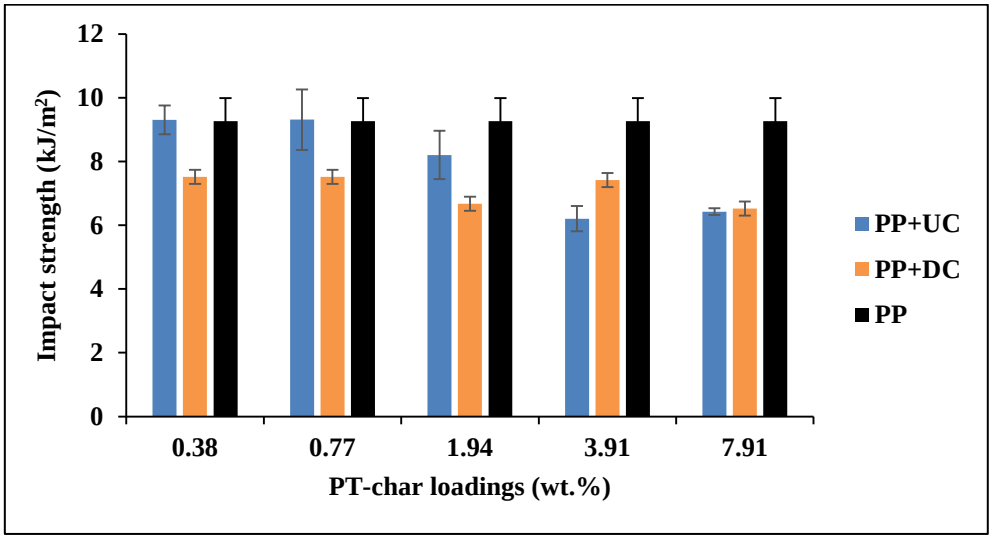

Figure 5.10: Impact strength of pure PP and the unmodified PP composites.

Table 5.8: Analysis of variance of the impact strength of the PP composites.

	p-value
PT-char	< **0.05**
Coupling agent	< **0.05**
Loading	< **0.05**
PT-char * Coupling agent	0.112
PT-char * Loading	0.158
Coupling agent *Loading	0.730
PT-char * Coupling agent * Loading	0.440

Bold value = p-value is significant.

According to **Table 5.8**, both PT-char and the loading were significant, with no interaction effect between the factors. As seen from **Figure 5.10**, there was no significant improvement in impact strength of PP composites upon addition of unmodified PT-char. This means that the interfacial region was not able to resist crack initiation effectively due to poor adhesion between the PT-char and the PP matrix [121]. Demineralisation reduced the impact strength of PP composites. The reduction in minerals such as calcium carbonate and silicon dioxide within DC might have resulted in a decrease in the toughness of the composite since combination of such minerals has been reported to have a beneficial effect in mechanical properties [28, 99, 124]. In addition, the presence of aggregates within DC (as shown in **Figure 5.2**) might have increased the level of stress concentrations which ultimately induced crack initiation [69, 113, 173].

The impact strength of PP composites decreases after reaching a maximum load, a similar behaviour which was found by several researchers [118, 173, 237]. According to Maiti *et al*. [237], as the filler concentration is increased the presence of the filler restricts the mobility and deformability of the matrix and so makes the composite more brittle, hence a decrease in the impact strength. In addition, the formation of agglomerates at high filler loading also contributes to mechanical failure [69, 124]. **Figure 5.11** below presents the impact strength of the modified PP composites filled with UC.

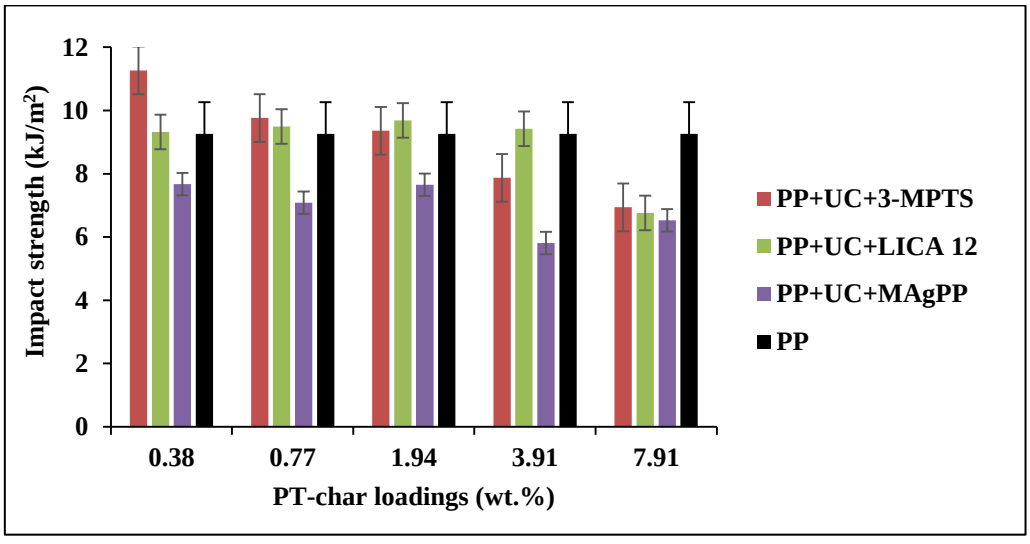

Figure 5.11: Impact strength of pure PP and the modified PP composites filled with UC.

Surface modification significantly improved the impact strength of PP+UC composites. This is due to improved interfacial adhesion facilitated by the addition of 3-MPTS and LICA 12,

which subsequently provide effective resistance to crack propagation [99, 109, 143]. However, only few modified composites filled with UC had slightly higher impact strength than the pure PP. This attribute is due to the presence of the small organic molecules (surface modifiers) on the surface of PT-char particles which act as adhesives, thereby enhancing the interface and reducing the brittleness [117]. At higher PT-char loading, the influence of surface modification was overcome by the formation of PT-char agglomerates.

The addition of MAgPP reduced the impact strength of PP composites. Since MAgPP was directly blended with PP and PT-char, it is possible that esterification between the anhydride moieties of the grafted PP and the hydroxyl groups on the surface of UC did not occur during mixing and thus the compatibiliser did not achieve its goal [238, 239]. **Figure 5.12** below presents the impact strength of the modified PP composites filled with DC.

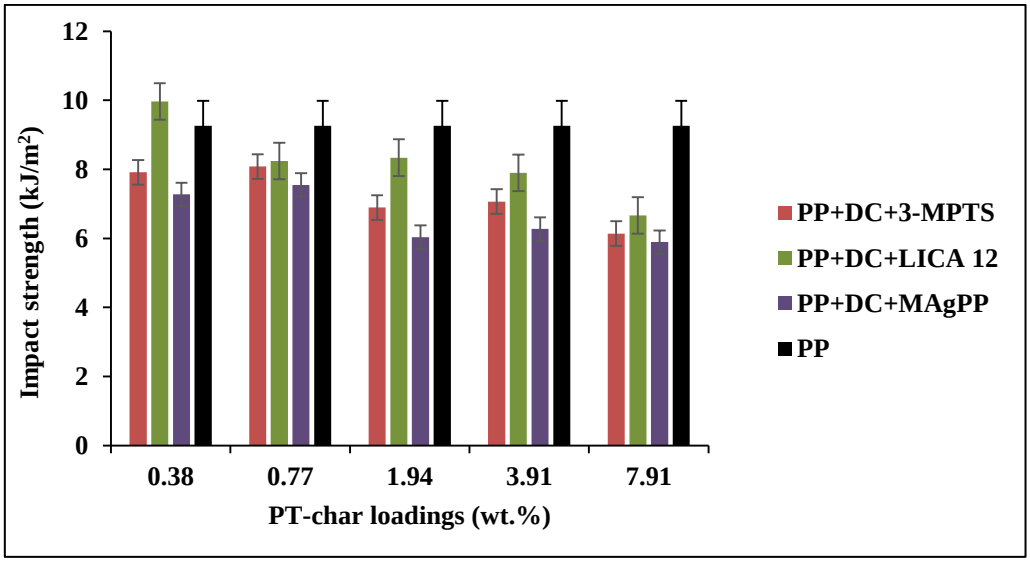

Figure 5.12: Impact strength of pure PP and the modified PP composites filled with DC.

As seen from **Figure 5.12**, the use of DC affects the impact strength of the modified composites. However, the impact strength of modified PP+DC composites did not surpass that of the pure PP except PP+0.38-DC+LICA 12. As mentioned earlier, the small particle of DC results in greater particle-particle interactions as compared to the UC. This led to the formation of agglomerates which caused defects in the composites system.

Furthermore, the influence of surface modification on the UC and the DC particles is not the same due to the difference in the surface chemistry of UC and the DC. UC contains fairly

high amounts of silica as compared to the DC and silica contains a high density of the silanol groups. Therefore, the 3-MPTS coupling agent will enhance adhesion of the UC particles more than that of the DC particles, hence a slight effect on the impact strength of the PP+DC+3-MPTS composites. The addition of LICA 12 surpassed the impact strength of pure PP only at 0.38 wt.% PT-char loading, nonetheless, the influence of LICA 12 was much stronger than 3-MPTS and MAgPP. This is due to the plasticising effect of titanate coupling agents. There was no sign of improvement in the impact strength of PP+DC composites modified with MAgPP which could possibly be due to the same reason as mentioned previously (**Figure 5.11**).

5.3.2 PP composites surface fracture

The impact test fracture surface images of the PP composites are presented in **Figure 5.13, Figure 5.14** and **Figure 5.15** in order to evaluate the dispersion morphology of PT-char in the PP matrix. **Figure 5.13** presents the fracture surface images of PP+UC and PP+DC composites at 0.38 wt.% and 7.91 wt.% and pure PP and their impact values (Iv).

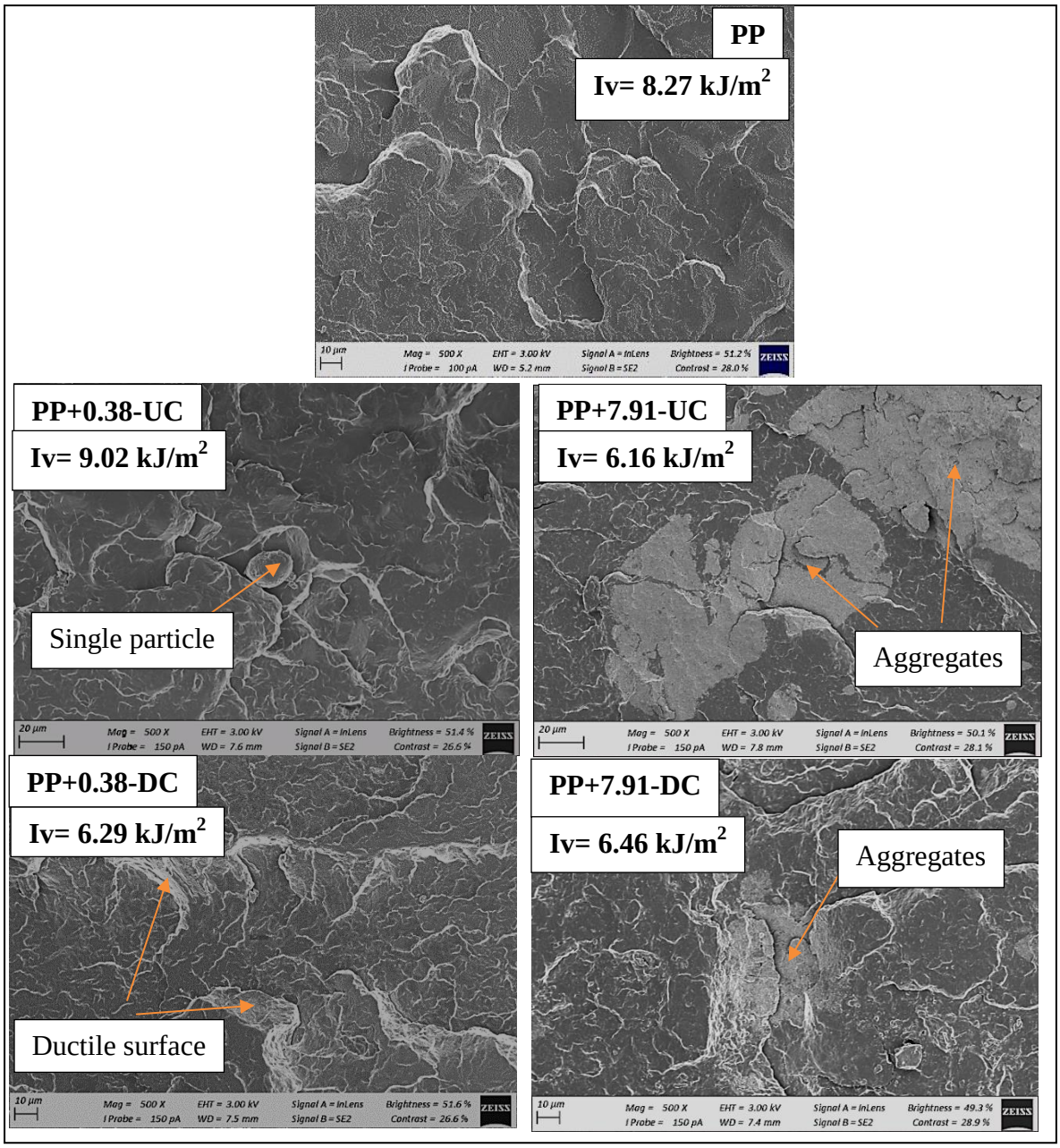

Figure 5.13: Fracture surface images of pure PP, PP+UC and PP+DC composites at different PT-char loadings (0.38 and 7.91 wt.%).

The SEM micrograph image of PP matrix presents a smooth surface without the presence of cracks/pores. The PP pellets were well mixed together during compounding. Nonetheless, a ductile behaviour was observed. Ductile fracture is categorised by plastic deformation, as indicated by a dull and fibrillary structure [132]. At 0.38 wt.%, both PP+UC and PP+DC composites show ductile behaviour which presents a good dispersion of the PT-char particles in the PP matrix. The spherical particles of PT-char were homogeneously distributed in the PP matrix, thus providing a uniform distribution of stress during impact [223]. However, at

high PT-char loading (7.91 wt.%), both PP+UC and PP+DC composites show a weak adhesion between the PT-char and the PP matrix owing to formation of aggregates.

Aggregation makes it difficult to homogeneously disperse PT-char into the PP matrix because it creates voids during loading and result in de-bonding of the PT-char particles from the PP matrix [118, 124]. **Figure 5.14** below presents the fracture surface images of PP+UC and PP+DC composites modified with 3-MPTS and LICA 12 coupling agents at 0.38 wt.%. Additional fracture surface images of PP composites (at 1.94 wt.%) are provided in **Appendix M**.

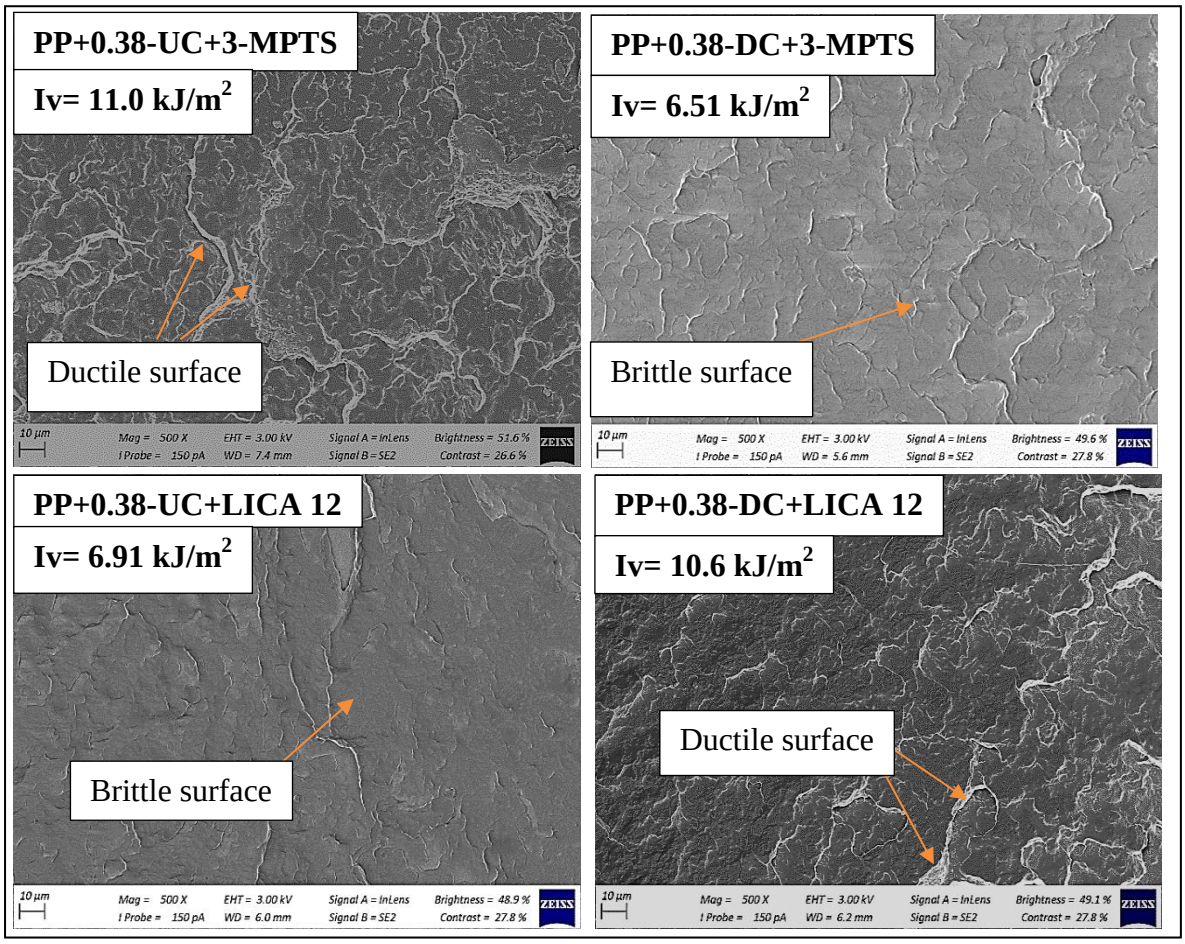

Figure 5.14: Fracture surface image of PP+UC and PP+DC composites, modified with 3-MPTS and LICA 12 at 0.38 wt.%.

Surface modification improved the adhesion between PT-char and the PP matrix. The micrographs image of the PP+0.38-UC+3-MPTS composite shows a ductile failure at the PT-char and PP matrix interface. This might be caused by the enhanced affinity between the organic groups present on the modified UC and the PP matrix [194]. The micrograph image

of PP+0.38-DC+3-MPTS composite shows a brittle failure characterised by the appearance of a smooth fracture surface and the presence of a crack/void. The adhesion of DC particles modified with 3-MPTS on the PP matrix may not have been enough for DC particles to be embedded inside the PP matrix. This might be due to the reduction of silica within the DC which is important for silanisation.

The composite modified with LICA 12 shows a significant improvement in the PT-char-PP matrix interface, as suggested by the absence of the holes/voids in the PP matrix [143]. This attribute could be due to the plasticising effect of LICA 12 [143, 157]. However, the PP+0.38-UC+LICA 12 composite show a brittle behaviour while the PP+0.38-DC+LICA composite shows a ductile behaviour. The improved surface area of DC enabled LICA 12 to enhance the interface and improve the adhesion of PT-char particles into the PP matrix. Consequently, this caused the modified DC particles to be embedded inside the PP matrix. This behaviour is in correspondence with the impact values of 3-MPTS and LICA 12 modified composites (both at 0.38 wt.%) obtained as indicated in **Figure 5.11** and **Figure 5.12**. **Figure 5.15** below shows fracture surface images of PP+DC+MAgPP composite at 0.38 wt.% and 7.91 wt.% PT-char loadings.

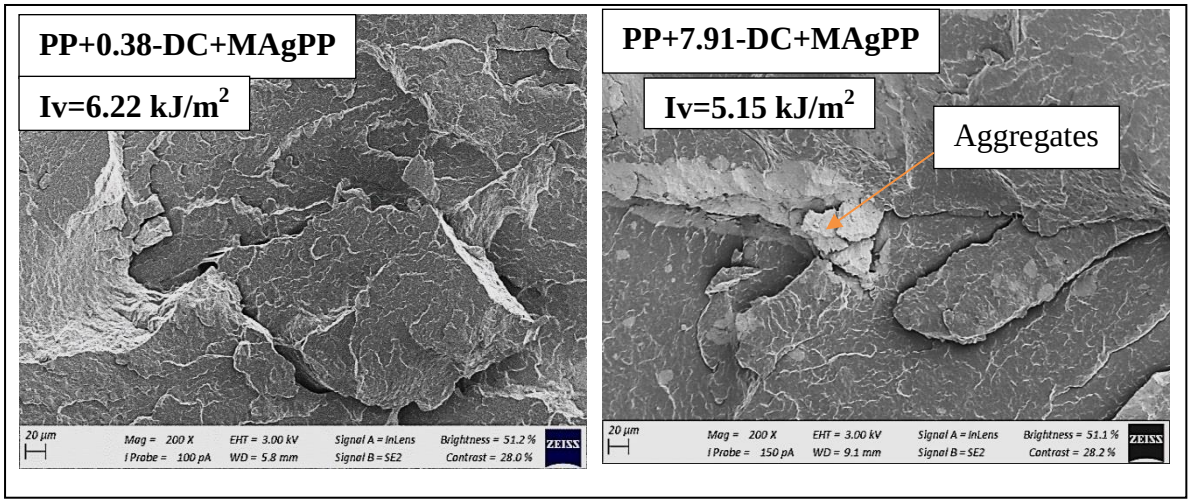

Figure 5.15: Fracture surface images of PP+DC+MAgPP composites at 0.38 and 7.91 wt.%.

Both the PP+DC+MAgPP composites (0.38 wt.% and 7.91 wt.%) show very loose structures. In the PP+7.91-DC+MAgPP composite, the PT-char particles tend to be exposed and loosely spread on the fracture surface, with some formation of PT-char particle agglomerates. This clearly indicates a weak PT-char/PP matrix interaction. The addition of MAgPP did not prevent the PT-char from aggregating. Hence the compatibilised DC particles were not well

dispersed and embedded in the PP matrix. These results contradict reports of previous researchers [26, 126, 128, 200], which found a good dispersion of the filler onto the PP matrix facilitated by the presence of MAgPP. The addition of MAgPP did not improve the interface between the PT-char and the PP matrix. It might be possible that there was insufficient time for reaction of anhydride groups with the –OH groups of PT-char, thus preventing the esterification process from occurring.

5.3.3 Concluding remarks

The addition of PT-char did not improve the impact strength of PP composites. However, the improvement in the impact strength of PP composites was achieved thanks to the addition of coupling agents (3-MPTS and LICA 12) which enhanced the interface thereby improving the dispersion of the unmodified PT-char onto the PP matrix. The performance of MAgPP compatibiliser was very poor due to an insufficient esterification process between the anhydride groups of the MAgPP and the hydroxyl groups of the PT-char. The impact strength of PP composites decreased after reaching a maximum load. At low PT-char loadings the differences in the composites impact strength are small but at high PT-char loading the properties are typical of those polymers filled with high amounts of inorganic fillers. Fracture surface images of PP composites revealed good dispersion of PT-char particles in the PP matrix at low PT-char loadings. At higher PT-char loading the micrographs revealed the presence of the PT-char particles aggregation.

5.4. Thermal-oxidative degradation

Thermal degradation studies were carried out to investigate the thermal degradation of PP composites. The highest PT-char loadings (3.91 wt.% and 7.91 wt.%) were removed due to their aggregation tendency at higher PT-char loadings which results in failure of the composites. Although MAgPP did not have any substantial effect on the mechanical properties of PP composites, it was of interest to investigate its effect on the thermal stability of the PP composites. **Figure 5.16** below shows the FTIR spectrum of thermally degraded pure PP at different time intervals.

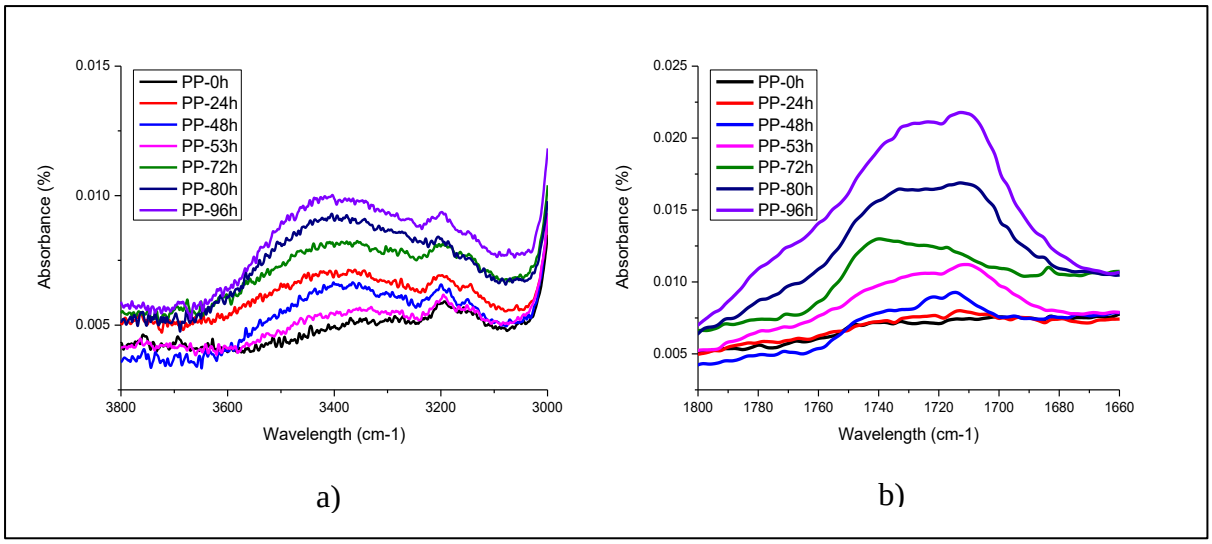

Figure 5.16: FTIR spectrum of thermally degraded pure PP under different time intervals: a) hydroxyl region and b) carbonyl region.

As seen from **Figure 5.16**a) and b), the area of the carbonyl region (with a maximum absorption band at about 1725 cm^{-1}) and the hydroxyl region (at about 3400 cm^{-1}) increase slowly with the duration of exposure, while the PP is experiencing intense continuous thermo-oxidative degradation. Once degradation has started, degradation products accelerate the degradation in the composite material. The carbonyl region indicates the production of carboxylic acids, ketones, esters and phenolic compounds, while the hydroxyl region indicates production of hydroperoxide and alcohols [240]. As mentioned, the hydroxyl region was not detected due to overlap with the hydroxyl groups from the filler. The growth of the carbonyl band was used as a measure of the extent of degradation. The carbonyl growth was quantified using CI as described in section 4.6.2.3. The increase in the CI is proportional to the increase in the formation of the carbonyl groups. **Figure 5.17** and **Table 5.9** below present the CI of thermally degraded pure PP and unmodified PP composites

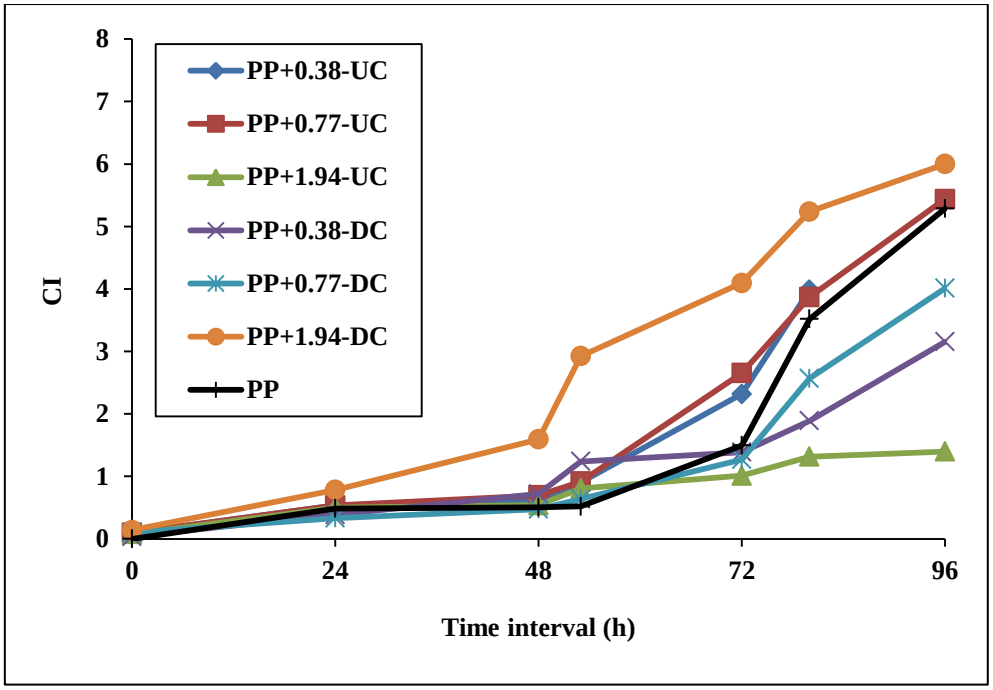

Figure 5.17: CI versus time plots of thermally degraded pure PP and unmodified PP composites.

Table 5.9: CI of thermally degraded pure PP and unmodified PP composites.

Composite	PT-char loading (wt.%)	(CI) No exposure	(CI) 48 h	(CI) 96 h
Pure PP		0	0.51	5.29
PP+UC	0.38	0.10	0.61	5.87
	0.77	0.10	0.70	5.44
	1.94	0.08	0.54	1.39
PP+DC	0.38	0.04	0.72	3.16
	0.77	0.10	0.48	4.01
	1.94	0.14	1.59	6.00

Table 5.9, indicates that no degradation took place on the pure PP before any thermal exposure. As mentioned, this general purpose homopolymer PP contains processing stabilisers and antioxidants. It is generally known from the literature that stabilisers and antioxidants inhibit oxidation during processing [24, 120, 193]. An exponential trend was observed on the unmodified composites consistent with the pure PP (**Figure 5.17**). For the first 53 h of thermal exposure of the pure PP, the carbonyl growth is very slow. During this period, the processing antioxidants contained in the PP matrix plays their stabilising role, reducing the rate of thermal-oxidative degradation. Once the antioxidant is consumed as a sacrificial additive, the carbonyl growth starts to increase exponentially till the last hour of

thermal exposure. **Table 5.9**, indicates that the addition of either UC or DC leads to minor initiation of thermal-oxidative degradation of PP composite before any thermal exposure. This indicates that, PT-char had a slight pro-degradant effect. This attribute is due to the presence of metal within PT-char, which is in agreement with previous studies [179, 182]. Once the composite samples are exposed to heat, the addition of PT-char leads to retardation of thermal-oxidative degradation except for the PP+1.94-DC composite. This degradation retardation could result from the interaction between the antioxidant contained in the PP matrix and the PT-char, which delays degradation of the PP composite. The CI of the PP+1.94-DC composite was high relative to the rest of the PP composites due to the aggregation tendency of small particles at high PT-char loading that caused defects in the composite system. Nonetheless, demineralisation improved thermal stability of PP composites at 0.38 wt.% and 0.77 wt.% which is due to DC having less transition metal pro-degradants in its surface. **Figure 5.18** and **Table 5.10** below present the CI of the thermally degraded pure PP and 3-MPTS modified PP composites

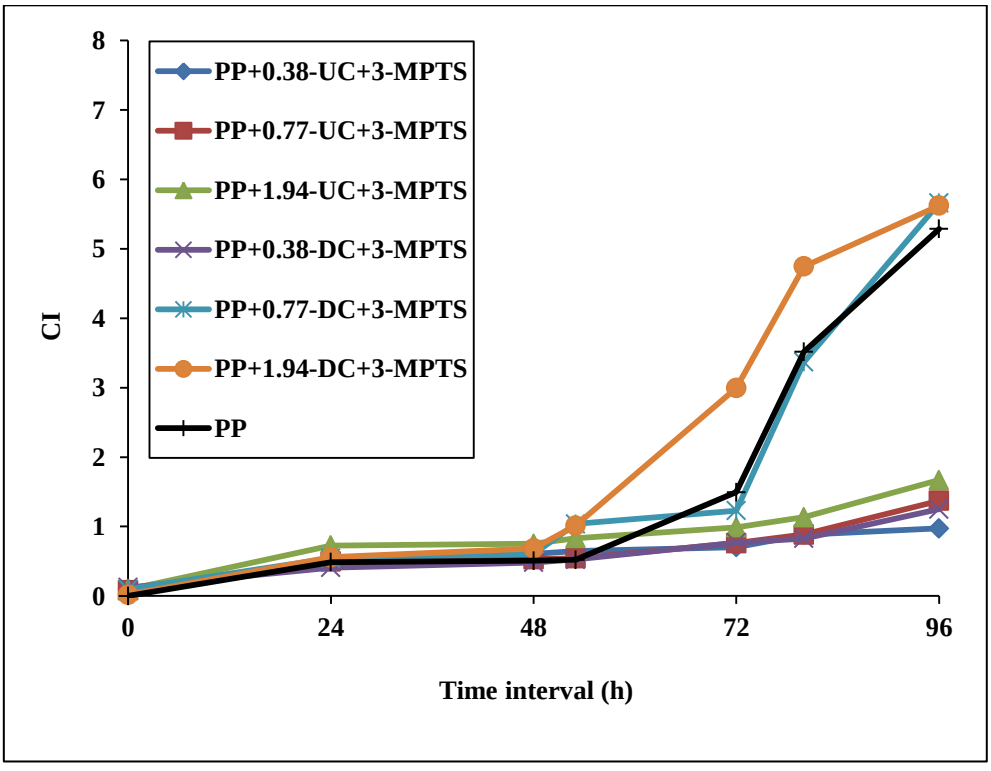

Figure 5.18: CI versus time plots of thermally degraded pure PP and 3-MPTS modified PP composites.

Table 5.10: CI of thermally degraded pure PP and 3-MPTS modified PP composites.

Composite	PT-char loading (wt.%)	(CI) No exposure	(CI) 48 h	(CI) 96 h
Pure PP		0	0.51	5.29
PP+UC+ 3-MPTS	0.38	0.10	0.61	0.97
	0.77	0.08	0.53	1.37
	1.94	0.09	0.75	1.67
PP+DC+ 3-MPTS	0.38	0.12	0.48	1.25
	0.77	0.10	0.60	5.66
	1.94	0.02	0.69	5.63

Table 5.10, indicates that, the addition of 3-MPTS leads to minor initiation of thermal degradation of the PP matrix before any thermal exposure, which is consistent with the results obtained from **Table 5.9**. In this case it cannot be concluded that the addition of 3-MPTS leads to the initiation of degradation. Once the carbonyl growth was established, the addition of 3-MPTS led to significant retardation of degradation with the exception of the PP+0.38-UC and PP+1.94-UC composites. This degradation retardation by 3-MPTS, could be due to the creation of an enhanced interface between the PT-char and the PP matrix. By the end of thermal exposure, 3-MPTS modification significantly improved thermal-oxidative stability of most of the PP composites. This was not true for the PP+0.77-DC+3-MPTS and PP+1.94-DC+3-MPTS composite, which is due to the tendency of small particles of PT-char to aggregate especially at high PT-char loading. Nonetheless, the CI of the PP+1.94-DC+3-MPTS and PP+0.77-DC+3-MPTS composites were slightly higher than that of the pure PP, which further indicates that 3-MPTS leads to significant retardation of thermal-oxidative degradation. Contrary to a previous report [85], the presence of metal impurities on the surface of the modified UC did not affect the performance of 3-MPTS to inhibit thermal-oxidative degradation. This attribute could be due to a substantial amount of silica present on the surface of UC which enabled 3-MPTS to encapsulate the metal impurities on the surface of the filler and thus slow down thermal-oxidation product formation. **Figure 5.19 and Table 5.11** below present the CI of the thermal degraded pure PP and LICA 12 modified PP composites

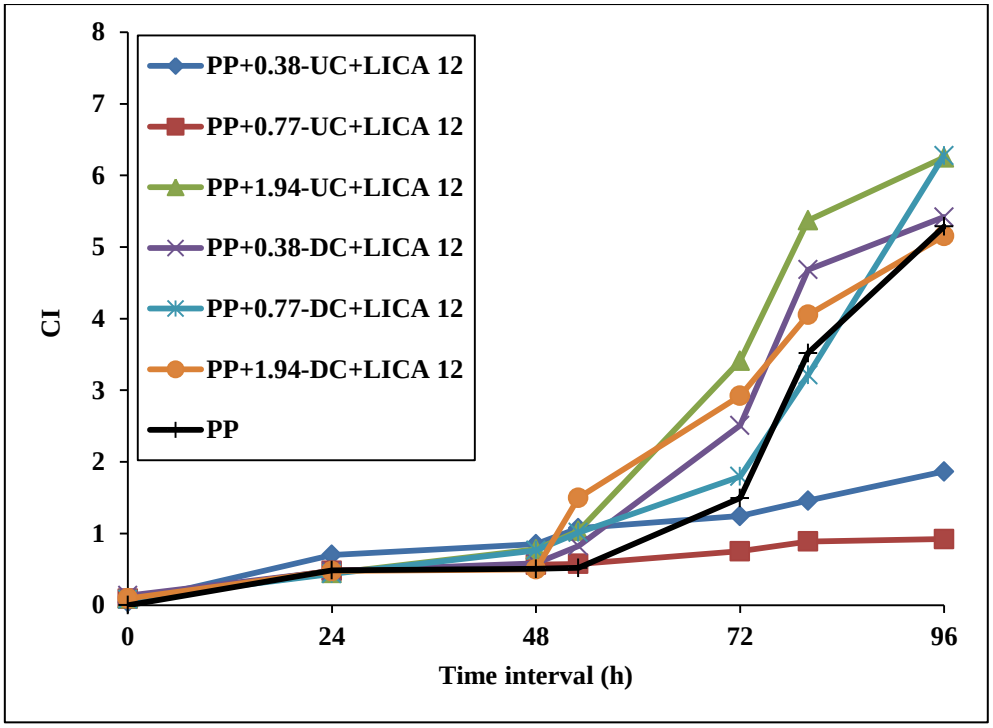

Figure 5.19: CI versus time plots of thermally degraded pure PP and LICA 12 modified PP composites.

Table 5.11: CI of thermally degraded pure PP and LICA 12 modified PP composites.

Composite	PT-char loading (wt.%)	(CI) No exposure	(CI) 48 h	(CI) 96 h
Pure PP		0	0.51	5.29
PP+UC+ LICA 12	0.38	0.04	0.85	1.87
	0.77	0.09	0.56	0.92
	1.94	0.09	0.78	6.25
PP+DC+ LICA 12	0.38	0.13	0.58	5.42
	0.77	0.08	0.76	6.28
	1.94	0.10	0.50	5.16

Table 5.11, indicates that, the addition of LICA 12 also leads to minor initiation of thermal degradation of the PP matrix before any thermal exposure, which is also consistent with the results obtained from **Table 5.9**. Once the carbonyl growth was established, the extent of degradation of LICA 12 modified composites was higher relative to the pure PP till the last hour of thermal exposure, except for the PP+0.38-UC+LICA 12 and PP+0.77-UC+LICA 12 composites. Although, DC contains relatively more oxygen functional groups and less transition metal than UC, LICA 12 did not inhibit thermal-oxidative degradation on the DC composites once the carbonyl growth was established. This is in agreement with previously

reported studies that confirmed that oxygenated functional groups on the surface of the filler can simultaneously act as the catalytic centres for oxidation [21, 84]. **Figure 5.20** and **Table 5.12** below present the CI of the thermally degraded pure PP and MAgPP modified PP composites

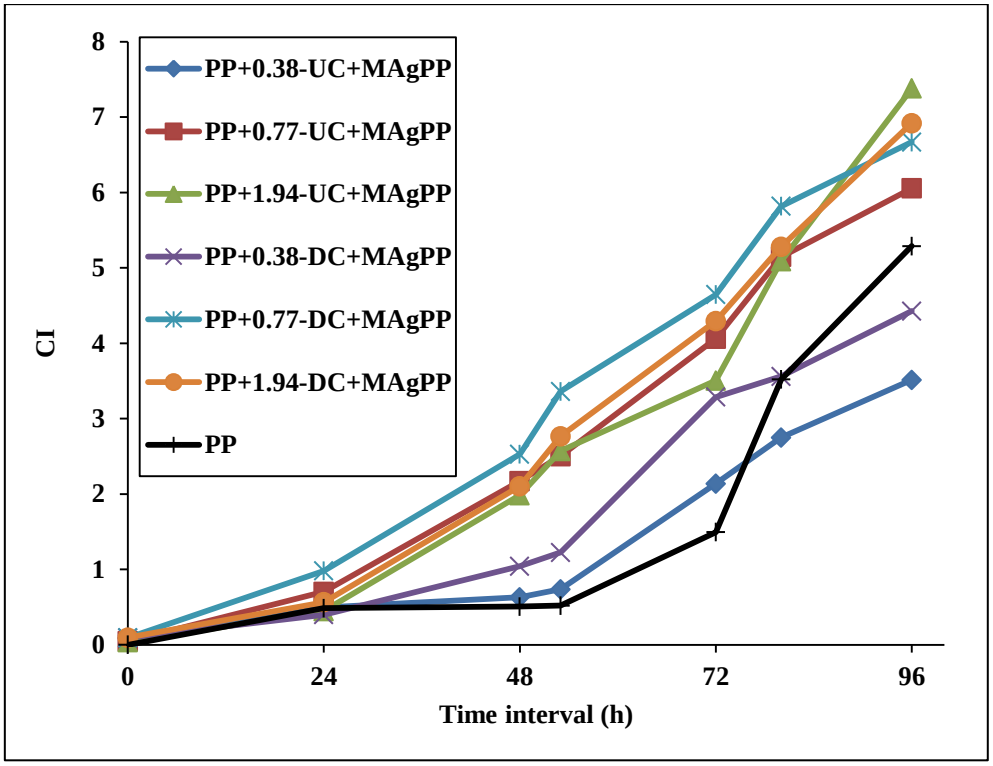

Figure 5.20: CI versus time plots of thermally degraded pure PP and MAgPP modified PP composites.

Table 5.12: CI of thermally degraded pure PP and MAgPP modified PP composites.

Composite	PT-char loading (wt.%)	(CI) No Exposure	(CI) 48 h	(CI) 96 h
Pure PP		0	0.51	5.29
PP+UC+ MAgPP	0.38	0.09	0.63	3.51
	0.77	0.05	2.17	6.05
	1.94	0.04	1.99	7.38
PP+DC+ MAgPP	0.38	0.09	1.04	4.43
	0.77	0.09	2.53	6.67
	1.94	0.09	2.10	6.92

Within 48 h of thermal exposure, all the MAgPP modified composites had a higher CI than the pure PP (**Table 5.12)**. The acceleration of degradation is more pronounced with MAgPP

modified composites at 0.77 wt.% and 1.94 wt.% PT-char loading. However, from 80 h onwards of thermal exposure (**Figure 5.20**), the addition of MAgPP was able to stabilise the thermal-oxidative degradation rate of PP+0.38-UC+MAgPP and PP+0.38-DC+MAgPP composites. Contrary to the trends observed with 3-MPTS and LICA 12 surface modification, the addition of MAgPP accelerates thermal-oxidative degradation. This could be due to differences between the MAgPP treatment method compared to the other surface modifications (3-MPTS and LICA 12). There was not sufficient time for esterification to occur between the anhydride groups of the maleic anhydride with the hydroxyl groups of the PT-char surface, since the PT-char was not first pre-treated with MAgPP. As a result, the addition of MAgPP was unable to improve the dispersion of PT-char on the PP matrix, thus allowing thermal-oxidative degradation to protrude the PP composite. Furthermore, the MAgPP might have also activated some thermo-responsive groups that led to acceleration of thermo-oxidative degradation of the composites. Thermo-responsive group such as carboxylic acids result from a partial hydrolysis of maleic anhydride [199, 205].

5.4.1 Concluding remarks

Thermal-oxidative degradation results indicate that the formation of carbonyl groups (carboxylic acids, ketones and phenols) increases in proportion with residence time during thermal exposure of PP composite samples. An exponential trend was observed on both unmodified and modified PP composites. The sharp exponential trend is credited to rapid increase of the carbonyl groups [241].

The addition of PT-char leads to minor initiation of thermal-oxidative degradation of the PP composite before any thermal exposure regardless of surface modification. This indicates that, PT-char has a slight pro-degradant effect before any thermal exposure, which could be due to the presence of metal impurities. However, once the carbonyl growth is established, the addition of PT-char leads to retardation of thermal-oxidative degradation. Demineralisation improved the resistance of PP composites to thermal-oxidative degradation only at lower PT-char loading, independent of surface modification. At high PT-char loading, the addition of PT-char accelerates thermal-oxidative degradation, particularly with demineralised PT-char, due to the presence of aggregates which cause defects in the composite system. Surface modification improved the resistance of PP composites to thermal-oxidative degradation with 3-MPTS treatment producing excellent results. However,

LICA 12 treatment leads to significant retardation of thermal-oxidative degradation only during the early stages of degradation. The addition of MAgPP accelerated thermal-oxidative degradation due to anhydride groups which did not react with PT-char and subsequently intensified the degradation.

Therefore, the use of PT-char as filler in PP can be useful in applications that require low thermal-oxidative stability. However, the use of PT-char as filler may not be useful in applications that require high thermal-oxidative stability since it has a pro-degradant effect due to the presence of metal impurities. The use of suitable surface modifiers such as 3-MPTS will lead to improved thermal-oxidative stability.

5.5. PP composites tensile properties

A tensile test was carried out in order to determine how the composite material will react to forces being applied in tension. Since the impact test results were very poor for all the composites at high loadings (3.91 wt.% and 7.91 wt.%), the study was continued ahead only with the lower loadings (0.38 wt.%, 0.77 wt.% and 3.94 wt.%). In addition, the effect of MAgPP on the tensile properties of PP composites was also not investigated further since its performance on the impact test and degradation studies was very poor.

5.5.1 PP composites tensile strength

Figure 5.21 below shows the tensile strength of the PP composites at various PT-char loadings and **Table 5.13** present the p- values of the main and interaction effects and their plots are presented in **Appendix N**.

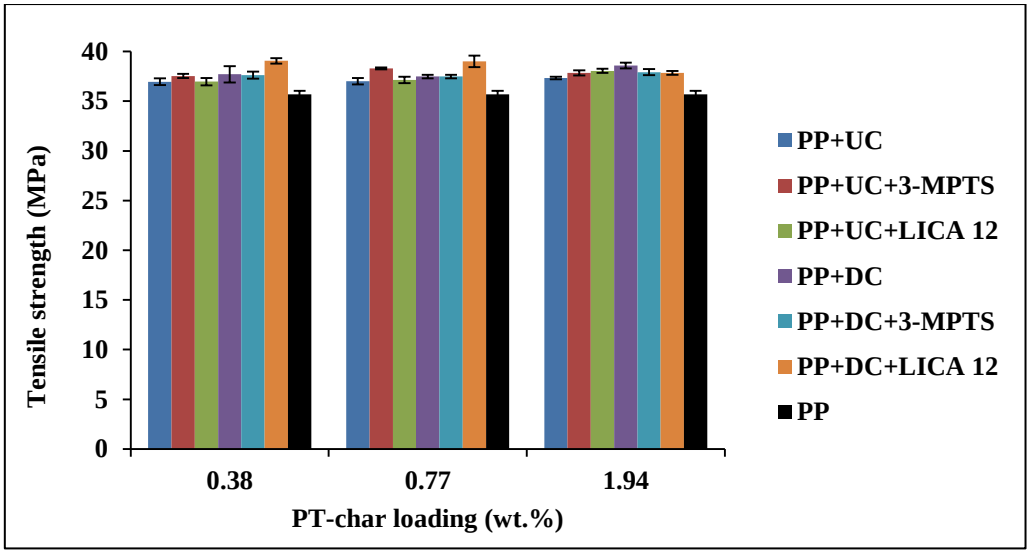

Figure 5.21: Tensile strength of PP composites at different PT-char loadings.

Table 5.13: Analysis of variance of the tensile strength of the PP composites.

	p-value
PT-char	< **0.05**
Coupling agent	**0.049**
Loading	0.326
PT-char * Coupling agent	**0.001**
PT-char * Loading	0.287
Coupling agent * Loading	0.397
PT-char * Coupling agent * Loading	**0.008**

Bold value = p-value is significant.

According to **Table 5.13**, the interaction effect between the PT-char, the coupling agent and the loading was significant, exhibiting a p-value of 0.008. In comparison with the pure PP, the addition of PT-char improves the tensile strength of the PP composites in all PT-char loadings irrespective of demineralisation or surface modification. The presence of PT-char allows the efficient transfer of load from the PP matrix to the filler, thereby, improving the tensile strength of the PP composites. Although demineralisation improved the tensile strength of the PP composites, the PP+UC composite was found to be indistinguishable from PP+DC composites in all PT-char loadings. The spherical particles of PT-char allowed the even distribution of stress transfer through the interface, irrespective of the reduction in the PT-char particle size.

Contrary to a previous report [211], surface modification with 3-MPTS and LICA 12 improved the tensile strength of PP composites. The surface modifiers improved the interfacial bonding between the PT-char and the PP matrix. The highest tensile strength was found with LICA 12 treated composites, which could be attributed to the plasticising effect of organotitanate treatment [143, 242, 243]. The tensile strength of the PP+DC+LICA 12 composite was significantly higher than that of the PP+UC+LICA 12 composite only at 0.38 wt.% and 0.77 wt.%, which could be due to poor dispersion at high filler loading. The tensile strengths of PP+UC+3-MPTS and PP+DC+3-MPTS composites were not significantly different from one another at all PT-char loadings, which could be due to an enhanced interface.

5.5.2 PP composites young modulus

Figure 5.22 shows the young modulus of the PP composites and **Table 5.14** present the p-values of the main and interaction effects and their plots are presented in **Appendix N**.

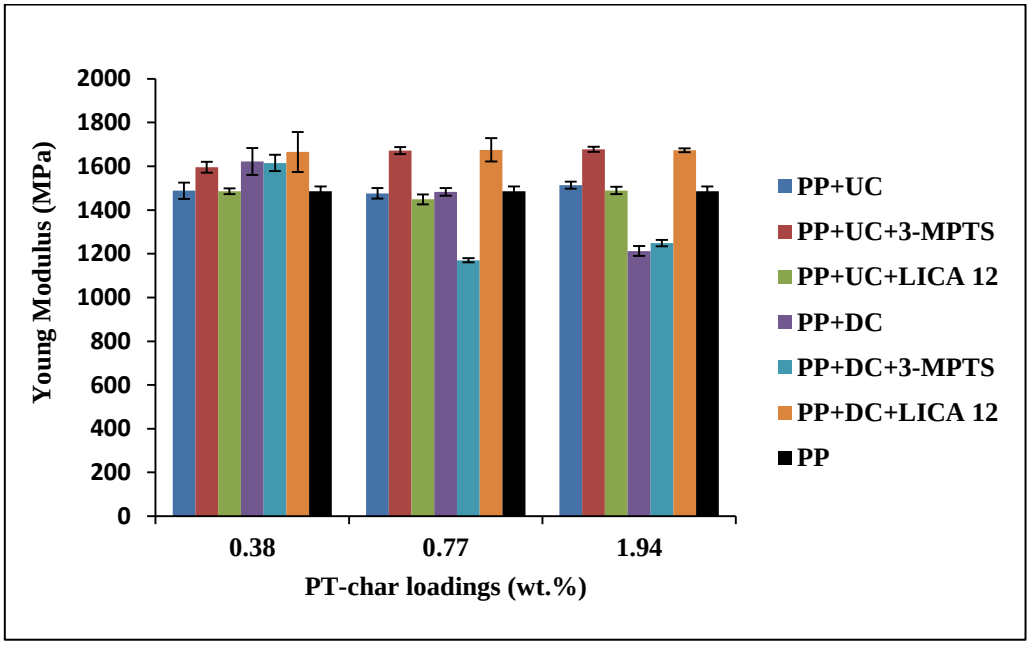

Figure 5.22: Young modulus of PP composites at different PT-char loadings.

Table 5.14: Analysis of variance of the young modulus of the PP composites.

	p-value
PT-char	< **0.05**
Coupling agent	< **0.05**
Loading	< **0.05**
PT-char * Coupling agent	< **0.05**
PT-char * Loading	< **0.05**
Coupling agent * Loading	< **0.05**
PT-char * Coupling agent * Loading	< **0.05**

Bold value = p-value is significant

As seen from **Table 5.14**, the interaction between the PT-char, the coupling agent and the loading was significant. As seen from **Figure 5.22**, the majority of the composites young modulus was higher than that of pure PP. The improvement is due to the stiffness of the filler [234]. According to Guerrica-Echevarria *et al*. [135] an increase in young modulus is the result of PP being replaced by the rigid filler particles and the fact that the presence of the filler introduces mechanical strains in order to limit the movement and deformability of the matrix.

The incorporation of the unmodified UC improves the young modulus of the PP composites more than the incorporation of the unmodified DC at 0.77 wt.% and 1.94 wt.%. Due to the fact that the stiffness of the matrix depends on the surface contact area of the filler and the fact that the BET surface area of the DC is greater than that of the UC, the young modulus was expected to be improved by the addition of DC [176]. However, it was observed that the young modulus of the matrix depends more on the particle size of the filler than on the surface area. The young modulus of the PP+UC composites increased with an increase in PT-char loading while those of the PP+DC composites decreased with an increase in PT-char loading. Due to the reduction in particle size effect rendered by demineralisation, the small particles of DC aggregate easily at high PT-char loading thereby reducing the adhesion between the PT-char and the PP matrix [234].

In agreement with several researchers [131, 132], surface modification improved the young modulus of the PP composites. This tremendous effect was due to a good distribution of PT-char particles which enables them to effectively exert an influence on the overall stiffness of

the PP composite. The presence of LICA 12 improved the young modulus of PP composites filled with DC more than PP composites filled with UC at all loadings. This attribute could be caused by an increased surface contact area in the case of DC usage [176]. The addition of 3-MPTS improved the young modulus of the UC filled PP composites more than those of the DC filled PP composites due to high quantities of silica present in UC, which makes it favourable for reaction with 3-MPTS [149, 244].

5.5.3 PP composites elongation at break

Figure 5.23 below shows the elongation at break of PP composites and **Table 5.15** presents the p-values of the main and interaction effects and their plots are presented in **Appendix N**.

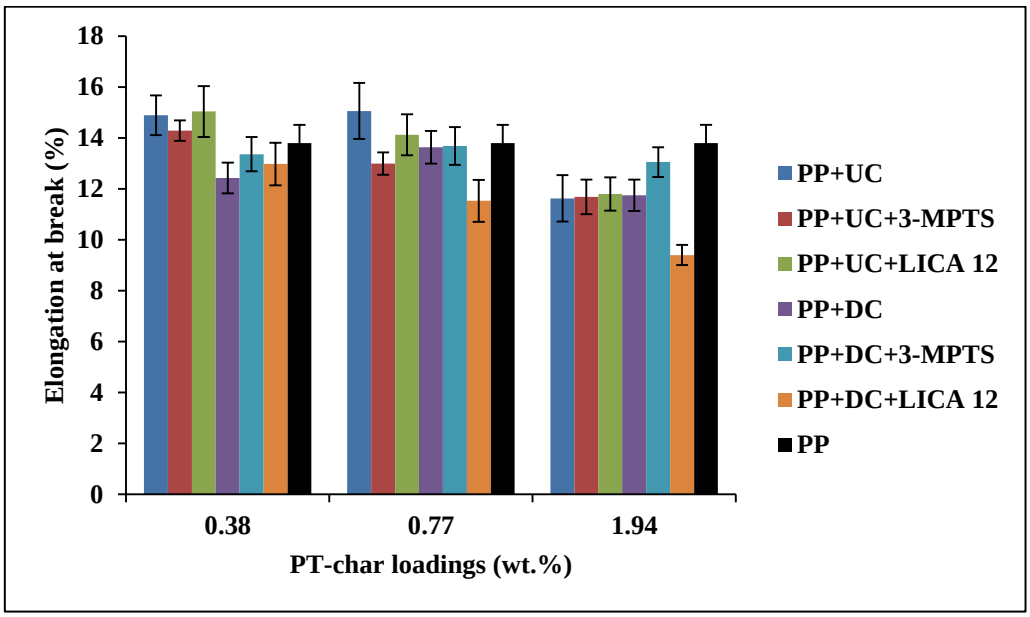

Figure 5.23: Elongation at break of PP composites at different PT-char loadings.

Table 5.15: Analysis of variance of the elongation at break of the PP composites.

	p-value
PT-char	**0.003**
Coupling agent	0.152
Loading	**< 0.05**
PT-char * Coupling agent	**0.005**
PT-char * Loading	0.227
Coupling agent * Loading	0.154

PT-char * Coupling agent * Loading	0.641

Bold value = p-value is significant

According to **Table 5.15**, the effect of PT-char loading is significant, presenting a p-value of less than 0.05. The elongation at break of PP composites decreases with an increase in PT-char loadings. Usually, the incorporation of particulate filler weakens the level of elongation [99, 129]. The addition of PT-char restricts the motion of PP chains [118, 132]. As seen from **Figure 5.23**, the elongation at break of PP+UC composites (0.38 wt.% and 0.77 wt.%) is much higher than PP+DC composite as well as the pure PP. The presence of minerals within the UC increased the ductility of the PP+UC composites.

The only significant interaction was found between the PT-char and the coupling agent exhibiting a p-value of 0.005. The elongation at break of PP+UC+LICA 12 composite are significantly higher than PP+DC+LICA 12 composites due to the quantity of minerals contained within UC which enhances ductility. However, the elongation at break of PP+DC+3-MPTS composites is higher than that of PP+UC+3-MPTS composite at 0.77 wt.% and 1.94 wt.%. This is due to the quantity of silica within UC which strengthen the interfacial bonding between the PP and the UC+3-MPTS thereby reducing the ductility. According to Akanbi *et al*. [116], the enhanced interfacial interactions between the filler and the PP matrix can result in a stronger interfacial bonding which ultimately enhances rigidity and reduces ductility.

5.5.4 Concluding remarks

Incorporation of PT-char significantly affects the tensile properties of PP composites. The addition of PT-char improved the tensile strength and the young modulus of PP composites. However, elongation at break decreased. This is related to the addition of particles into the polymer matrix as the filler particles act as stress absorbents but at the same time they restrict the movement of the polymer chains. The small particle size of DC gave aggregation problems especially at higher PT-char loadings and the effect was subsequently detrimental to the tensile properties. Surface modification improved the tensile strength and the young modulus of the PP composites due to enhancement of the interface between the PT-char and the matrix. However, with regard to elongation at break, stronger interfacial bonding enhanced rigidity and reduced ductility.

5.6. Photo-oxidative degradation

Figure 5.24 below shows a comparison of CI of photo-degraded pure PP and PP composites at different PT-char loadings. The values of CI obtained before and after exposure (48 and 168 h) are given in **Table 5.16**.

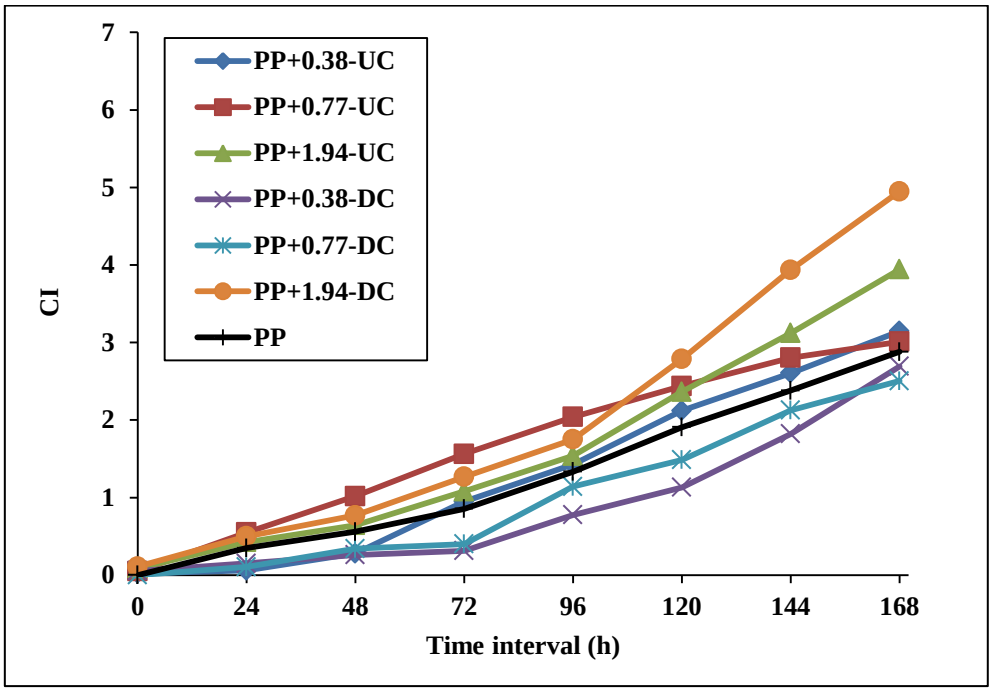

Figure 5.24: CI versus time plot of photo-degraded pure PP and unmodified PP composites.

Table 5.16: CI of photo-degraded pure PP and unmodified PP composites.

Composite	PT-char loading (wt.%)	(CI) No exposure	(CI) 48 h	(CI) 168 h
Pure PP		0	0.35	2.88
PP+UC	0.38	0.02	0.28	3.15
	0.77	0.05	1.02	3.01
	1.94	0.09	0.64	3.94
PP+DC	0.38	0	0.26	2.69
	0.77	0.05	0.34	2.51
	1.94	0.11	0.77	4.95

As seen from **Figure 5.24**, the rate of photo-oxidation of the pure PP is almost linear with the irradiation time and there was no induction period. **Table 5.16**, shows that, the addition of DC at 0.38 wt.%, before any photo-oxidative exposure, did not affect the initiation of photo-

oxidative degradation of PP composites as compared to the rest of the PP composites. However, the addition of PT-char led to minor initiation of photo-oxidative degradation for the rest of the PP composites which could be due to the presence of metal impurities. The rate of degradation of the PP+DC composite (0.38 wt.% and 0.77 wt.%) was lower than that of the pure PP and the rest of the PP composites till the last day of exposure. There are several reasons for this behaviour: i) DC performs much better than UC because transition metal impurities present in the fillers have been known to accelerate degradation of PP [26, 31, 199–201, 245], ii) at lower PT-char loading (0.38 wt.% and 0.77 wt.%) the small particle of DC were well dispersed on the PP matrix; thereby reducing the effect of photo-oxidative degradation. However, at high PT-char loading (1.94 wt.%), the extent of the degradation of PP composites was more pronounced, especially for DC filled PP composites. This effect is due to poor dispersion of PT-char at high PT-char loading particularly for small particles of DC due to its aggregation tendency. A similar behaviour was also observed by Li *et al*. [197] who found that increasing calcium carbonate and silicon content increased the rate of degradation of the composites due to poor adhesion of filler particles caused by agglomeration of filler particles. **Figure 5.25** and **Table 5.17** and below shows a comparison of CI of photo-degraded pure PP and 3-MPTS modified PP composites at different PT-char loadings.

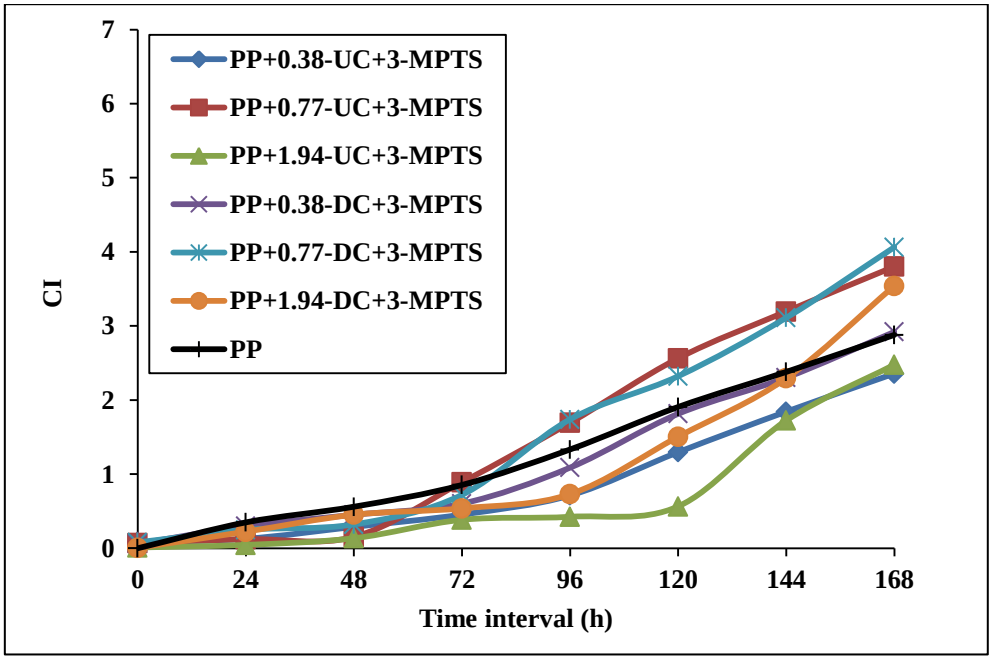

Figure 5.25: CI versus time plots of photo-degraded pure PP and 3-MPTS modified PP composites.

Table 5.17: CI of photo-degraded pure PP and 3-MPTS modified PP composites.

Composite	PT-char loading (wt.%)	(CI) No exposure	(CI) 48 h	(CI) 168 h
Pure PP		0	0.56	2.88
PP+UC+ 3-MPTS	0.38	0.08	0.29	2.36
	0.77	0.07	0.15	3.80
	1.94	0.01	0.14	2.48
PP+DC+ 3-MPTS	0.38	0.06	0.45	2.92
	0.77	0.08	0.32	4.06
	1.94	0.05	0.45	3.54

Table 5.17, shows that, the addition of surface modified PT-char led to a minor degradation before any exposure. Once the carbonyl growth has been established, a significant improvement in photo-oxidative stability was observed on all 3-MPTS modified composites. This exceptional improvement was due to the enhancement of the interface between the PP matrix and the filler. Furthermore, 3-MPTS surface modification significantly improved photo-oxidative stability of PP composites (except PP+0.77-UC+3-MPTS and PP+0.77-DC+3-MPTS) till the last hour of exposure. These results contradict the ones reported by Lu *et al*. [194], who found that 3-MPTS accelerated photo-oxidative degradation of PP/fumed silica composite, due to the photo-initiating effect of the carbonyl groups present on the surface of the modified fumed silica. The presence of silica on the surface of PT-char enabled 3-MPTS to encapsulate the metal impurities on the surface of the filler and thus slow down photo-oxidation product formation **Figure 5.26** and **Table 5.18** below compares of the CI of photo-degraded pure PP and PP composites modified with LICA 12.

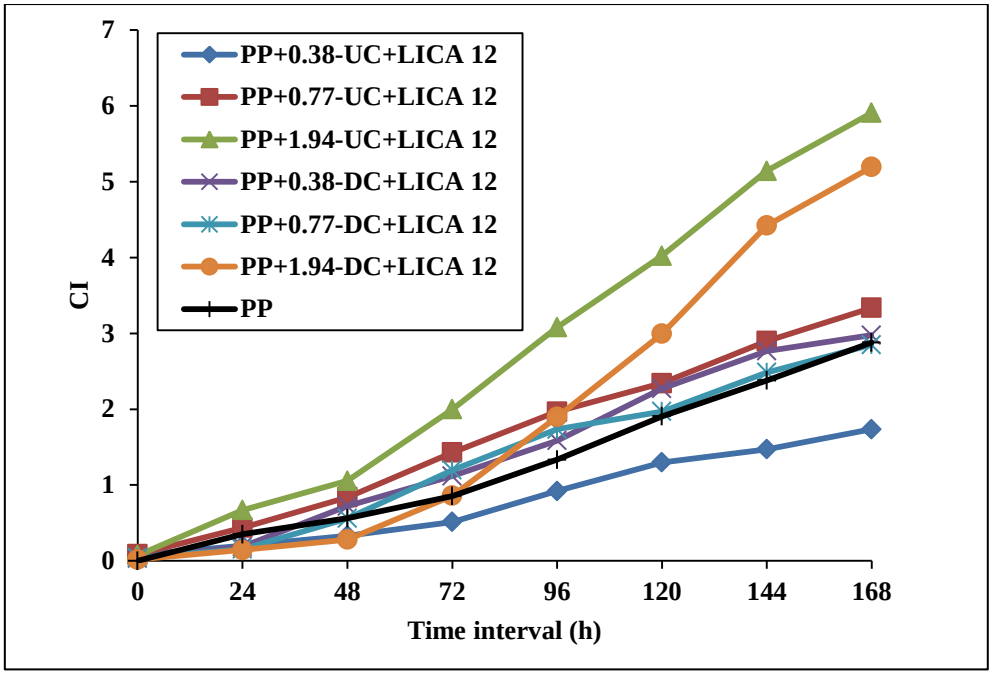

Figure 5.26: CI versus time plots of photo-degraded pure PP and LICA 12 modified PP composites.

Table 5.18: CI of photo-degraded pure PP and LICA 12 modified PP composites.

Composite	PT-char loading (wt.%)	(CI) No exposure	(CI) 48 h	(CI) 168 h
Pure PP		0	0.56	2.88
PP+UC+ LICA 12	0.38	0.08	0.33	1.73
	0.77	0.09	0.84	3.34
	1.94	0.07	1.06	5.91
PP+DC+ LICA 12	0.38	0.03	0.72	2.98
	0.77	0.04	0.56	2.85
	1.94	0.02	0.28	5.20

As seen from **Figure 5.26** and **Table 5.18**, LICA 12 surface modification leads to significant increase in the CI within 48 h of exposure, except for the PP+0.38-UC+LICA 12 and PP+1.94-DC+LICA 12 composites. After 72 h of exposure, the rate of carbonyl growth of PP composites modified with LICA 12 was higher than that of the pure PP till the last hour of exposure, except for the PP+0.38-UC+LICA 12 composite which remained low. Contrary to previous reports [211, 246], the performance of LICA 12 was not effective in inhibiting photo-oxidative degradation of PP composites. The presence of transition metals and the organic-titanium monomolecular layers formed on the PT-char surface might have catalysed the acceleration of photo-oxidative degradation of the PP composites [157].

5.6.1 Concluding remarks

The addition of PT-char leads to minor initiation of photo-oxidative degradation of PP composites before exposure regardless of surface modification. This is due to the presence of metal impurities in the PT-char. Demineralisation of PT-char leads to significant retardation of photo-oxidative degradation only at lower PT-char loading, due to the reduction in metal impurities. At high PT-char loading, the addition of PT-char accelerates photo-oxidative degradation. This is particularly true for the demineralised PT-char due to the presence of aggregates which cause defects in the composites system. Surface modification with 3-MPTS leads to significant improvement in resistance to photo-oxidative degradation of PP composites, due to the formation of an enhanced interphase between PT-char and the PP matrix. Surface modification with LICA 12 delays photo-oxidative degradation during early stages of degradation. However, once the oxidation got underway, the addition of LICA 12 leads to acceleration of photo-oxidative degradation. This is due to the presence of metal impurities and the catalytic effect of the organic-titanium monomolecular layers formed on the PT-char surface. Overall, the use of PT-char as filler in PP may not be useful for outdoor applications since it has a pro-degradant effect, due to the presence of metal impurities. However, the use of suitable surface modifiers such as 3-MPTS will lead to improved photo-oxidative stability.

CHAPTER 6: CONCLUSIONS

6.1. Summary

The aim of the study was to investigate and analyse the feasibility of using PT-char as a filler so as to improve the mechanical properties and degradation stability of PP. The research study consisted of three major experimental stages: the first stage included demineralisation with the use of acid-base lixiviates in order to reduce the inorganic impurities. It also included modification of the surface of the PT-char with the use of surface modifiers to enhance the compatibility of PT-char and PP; the second stage consisted of the production of PP composites using different treatments at different PT-char loadings; and the third stage was to analyse the effect of different treatments on the mechanical (impact and tensile) and degradation (thermal and photo-oxidative) of PP composites.

6.2. PT-char characterisation

PT-UC and PT-DC were found to have spherical particles with heterogeneous particle size distribution. Demineralisation greatly reduced the particle size and the ash content within PT-UC. The surface area and the porosity of PT-DC were slightly improved due to the removal of some carbon residuals entrapped in the surface of PT-UC. Most of the elements present on the surface of PT-UC, such as zinc and silicon, were removed to a large extent. Due to a significant reduction in the ash content of PT-UC, the oxygen contained in the ash was reduced while the oxygen present on the carbon matrix increased. PT-UC had many functional groups (carbonyl and hydroxyl) present before any treatment and demineralisation increased their prevalence.

6.3. Mechanical properties

The addition of PT-char influenced the mechanical properties of PP composites. The untreated PT-char showed moderate improvements in some mechanical properties (tensile properties) due to the presence of minerals and its heterogeneous spherical particle shape which gave uniform distribution of stress. On the other hand, the demineralised PT-char reduced the mechanical properties of PP composites due to the reduction in mineral

compounds contained within PT-char which are beneficial for mechanical properties of PP composites. High PT-char loadings reduced the mechanical properties of PP composites, particularly with demineralised PT-char due to the aggregation tendency of small particle sizes which caused defects in the composite systems. Fracture surface images revealed the presence of aggregates at high PT-char loading which resulted in problems with the dispersion of the PT-char on the PP matrix. Surface modification with 3-MPTS and LICA 12 coupling agents improved the mechanical properties of PP composites due to the enhancement of the interface between PT-char and the PP matrix. However, the performance of MAgPP compatibiliser was very poor due to an insufficient esterification process between the anhydride groups of the MAgPP and the hydroxyl groups of the PT-char.

The mechanical properties of PT-char filled PP composites showed small differences at low PT-char loading as compared to the mechanical properties of unfilled PP. However at high PT-char loading the mechanical properties of PT-char filled composites are typical of those PP composites filled with high amount of inorganic mineral fillers. Therefore, PT-char cannot replace commercial reinforcing fillers at equal parts. However, it may be added in small amounts and modified with coupling agents to enhance the interface between the PT-char particles and PP and further reduce aggregation of the PT-char particles in order to improve the mechanical properties of PT-char filled PP composites.

6.4. Degradation

The addition of PT-char leads to minor initiation of thermal and photo-oxidative degradation of PP composite before any exposure, regardless of surface modification. This indicates that, PT-char has a slight pro-degradant effect which is due to the presence of metal impurities. However, once the carbonyl growth is established, the addition of PT-char leads to retardation of thermal-oxidative degradation. Demineralisation of PT-char leads to significant retardation of photo-oxidative degradation only at lower PT-char loading due to reduction in metal impurities. At high PT-char loading, the addition of PT-char accelerates thermal and photo-oxidative degradation, particularly with demineralisation. This is due to the aggregation tendency of PT-char particles, which causes defects in the composites system.

Surface modification with 3-MPTS leads to significant improvements in thermal and photo-oxidative degradation stability of PP composites due to an enhanced interphase between PT-char and PP.

Surface modification with LICA 12 delays thermal and photo-oxidative degradation during early stages of degradation. However once the oxidation got underway the addition of LICA 12 leads to acceleration of photo-oxidative degradation. This is due to the presence of metal impurities and the catalytic effect of organic-titanium monomolecular layers that are formed on the PT-char surface. Surface modification with MAgPP leads to acceleration of thermal-oxidative degradation due to insufficient time for esterification to occur between the anhydride groups of the maleic anhydride with the hydroxyl groups of the PT-char surface.

Therefore, the use of PT-char as filler in PP can be useful in applications that require low thermal and photo-oxidative stability. Utilisation of appropriate filler surface modifiers such as silane, will lead to improved thermal and photo-oxidative stability. However, the use of PT-char as filler may not be useful in applications that require high thermal-oxidative stability and for outdoor applications, since it has a pro-degradant effect due to the presence of metal impurities. Furthermore, the use of PT-char as filler is not suitable for food and medical applications, since the presence of transition metals in the PT-char can significantly increase the toxicity of the PP.

CHAPTER 7: RECOMMENDATIONS

Based on the results and the discussion the following recommendations are made for future study.

1. **Effect of demineralisation**

Demineralisation of PT-char was not effective in improving the properties of PP composites. However, only one level of combination was analysed. Therefore, it is recommended that an optimisation study should be carried out, in order to find the optimum condition that will enhance the properties of PP composites.

2. **Surface Chemistry**

The performance of the surface modifiers is highly dependent on the surface chemistry of the PT-char. Therefore, the surface modifier has to be chosen depending on the surface chemistry of the filler, i.e. surface chemistry analysis should be performed on the filler. If this analysis indicates that the surface contains a lot of silica groups, a silane coupling agent should be used, since it favours silica containing fillers. If the filler contains more hydroxyl and carbonyl groups on the surface of the PT-char, the titanate coupling agent should rather be used.

3. **Determine the quantity of functional groups (such as -OH and oxygen functional groups)**

The coupling effectiveness of the surface modifier treatment depends on the presence of -OH groups. The oxygen containing functional groups, such as the quinone and the phenolic hydroxyl groups, function as effective thermal antioxidant. It is therefore recommended that their quantities should be determined in order to understand their significance during degradation.

4. **Optimise the use of coupling agent and compatibiliser and consider peroxide as an initiator when pre-treating PT-char with coupling agents.**

For effective surface modification of PT-char with coupling agents, an initiator, such as peroxide, should be used during treatment to achieve a good coupling effect. This could improve the performance of the coupling agents.

It is also recommended that an optimisation study of the coupling agents and the compatibiliser should be carried out in order to find the optimum amount, so that the coupling at the interface can boost the properties of PP composites.

5. **Several studies can be done to further analyse the properties of PP composite**

The mechanical properties of the PP composites are mainly controlled by the crystallisation of PP. Fillers tend to perform the role of nucleation agents for PP and can cause either α or β PP which have different properties and behaviour. Therefore, it is recommended that crystallisation studies should be carried out, in order to understand the effect of PT-char on the crystallinity of PP composites.

The study can be extended by performing a three or four point bending test in order to evaluate the ability of PP composites to withstand the bending force. The study can also be extended by performing long term mechanical tests (such as creep) in order to analyse how PP composites filled with PT-char responds to fatigue arising from oscillating stresses.

Flammability tests should also be performed to determine how easily the PP composites material will ignite when it is placed next to a heat source. This will determine if the PP composites material made of PP and PT-char can be used without contributing to the fire. Natural weathering tests should also be performed instead of accelerated weathering in order to compare these with conditions found in real life, such as: rain, wind, cold and hot temperatures.

6. **Make use of waste PP instead of virgin PP**

The study can be extended by making use of waste PP (waste PP from the PP manufacturing industry), instead of virgin PP. In this way the viability of producing a 100% green product, obtained by recycling two different waste materials, can be tested.

CHAPTER 8: REFERENCES

[1] E.L.K. Mui, D.C.K. Ko, G. McKay, Production of active carbons from waste tyres-A review, J. Carbon. 42 (2004) 2789–2805. doi:10.1016/j.carbon.2004.06.023.

[2] G.R. Defoliart, D.M. Watts, P.R. Grimstad, Changing patterns in mosquito-borne arbovirus, J. Am. Mosq. Control Assoc. 2 (1986) 437–455.

[3] M.B. Hahn, R.J. Eisen, L. Eisen, K.A. Boegler, C.G. Moore, J. McAllister, H.M. Savage, J.P. Mutebi, Reported distribution of Aedes (Stegomyia) aegypti and Aedes (Stegomyia) albopictus in the United States, J. Med. Entomol. 53 (2016) 1169–1175. doi:10.1093/jme/tjw072.

[4] K.S. Fan, C.H. Lin, T.C. Chang, Management and performance of Taiwan's waste recycling fund, J. Air Waste Manag. Assoc. 55 (2005) 574–582. doi:10.1080/10473289.2005.10464647.

[5] G. Li, B. Shen, F. Lu, The mechanism of sulfur component in pyrolyzed char from waste tire on the elemental mercury removal, J. Chem. Eng. 273 (2015) 446–454. doi:10.1016/j.cej.2015.03.040.

[6] M. Sienkiewicz, J. Kucinska-Lipka, H. Janik, A. Balas, Progress in used tyres management in the European Union: A review, Waste Manag. 32 (2012) 1742–1751. doi:10.1016/j.wasman.2012.05.010.

[7] R. Murillo, E. Aylón, M.V. Navarro, M.S. Callén, A. Aranda, A.M. Mastral, The application of thermal processes to valorise waste tyre, J. Fuel Process Technol. 87 (2006) 143–147. doi:10.1016/j.fuproc.2005.07.005.

[8] S. Seidelt, M. Müller-Hagedorn, H. Bockhorn, Description of tire pyrolysis by thermal degradation behaviour of main components, Anal. Appl. Pyrolysis. 75 (2006) 11–18. doi:10.1016/j.jaap.2005.03.002.

[9] J.D. Martinez, N. Puy, R. Murillo, T. Garcia, M.V. Navarro, A.M. Mastral, Waste tyre pyrolysis - A review, J. Renew. Sustain. Energy Rev. 23 (2013) 179–213. doi:10.1016/j.rser.2013.02.038.

[10] M. Kyari, A. Cunliffe, P.T. Williams, Characterization of oils, gases, and char in relation to the pyrolysis of different brands of scrap automotive tires, J. Energy Fuels. 19 (2005) 1165–1173. doi:10.1021/ef049686x.

[11] O.S. Chan, W.H. Cheung, G. McKay, Preparation and characterisation of demineralised tyre derived activated carbon, J. Carbon. 49 (2011) 4674–4687. doi:10.1016/j.carbon.2011.06.065.

[12] J. Hopewell, R. Dvorak, E. Kosior, Plastics recycling: Challenges and opportunities, Philos. Trans. R. Soc. B Biol. Sci. 364 (2009) 2115–2126. doi:10.1098/rstb.2008.0311.

[13] N. Antoniou, G. Stavropoulos, A. Zabaniotou, Activation of end of life tyres pyrolytic char for enhancing viability of pyrolysis - Critical review, analysis and recommendations for a hybrid dual system, J. Renew. Sustain. Energy Rev. 39 (2014) 1053–1073. doi:10.1016/j.rser.2014.07.143.

[14] H. Sato, H. Ogawa, Review on development of polypropylene manufacturing process, Process Prod. Technol. Center. Sumitomo Chem. Co., Ltd. 2 (2009) 1–11.

[15] D. Bikiaris, Microstructure and properties of polypropylene/carbon nanotube nanocomposites, J. Mater. 3 (2010) 2884–2946. doi:10.3390/ma3042884.

[16] I. Chun, R.. Woodham, Use of processing aids and coupling agents in mica-reinforced polypropylene, J. Polym. Compos. 5 (1984) 250–257. doi:10.1002/pc.750050404.

[17] A. Chaala, H. Darmstadt, C. Roy, Acid-base method for the demineralization of pyrolytic carbon black, J. Fuel Process. Technol. 46 (1996) 1–15. doi:10.1016/0378-3820(95)00044-5.

[18] S. Manocha, G.R. Prasad, P. Joshi, R.S. Zala, S.S. Gokhale, L.M. Manocha, Preparation and characterization of activated carbon from demineralized tyre char, AIP Conf. Proc. 1538 (2013) 109–112. doi:10.1063/1.4810039.

[19] C. Roy, A. Chaala, H. Darmstadt, The vacuum pyrolysis of used tires End-uses for oil and carbon black products, J. Anal. Appl. Pyrolysis. 51 (1999) 201–221. doi:10.1016/S0165-2370(99)00017-0.

[20] J. Zhou, S. Wu, T. Yu, Z. Xie, Modified pyrolytic carbon black from scrap tires and its reinforcement performance in natural rubber, Int. Conf. Comput. Distrib. Control Intell. Environ. Monit. Chang. China. (2011) 472–475. doi:10.1109/CDCIEM.2011.82.

[21] D. Bunthid, P. Prasassarakich, N. Hinchiranan, Oxidative desulfurization of tire pyrolysis naphtha in formic acid/H2O2/pyrolysis char system, J. Fuel. 89 (2010) 2617–2622. doi:10.1016/j.fuel.2010.04.026.

[22] P. Ariyadejwanich, W. Tanthapanichakoon, K. Nakagawa, S.R. Mukai, Preparation and characterization of mesoporous activated carbon from waste tires, J. Carbon. 41 (2003) 157–164. doi:10.1016/S0008-6223(02)00267-1.

[23] C. Maier, T. Calafut, Polypropylene : the definitive user's guide and databook, William Andrew, New York. (1998) 456.

[24] D. Tripathi, Practical guide to polypropylene, Rapra Technol. Ltd., United Kingdom. (2002) 104.

[25] K. Yang, Q. Yang, G. Li, Y. Sun, D. Feng, Mechanical properties and morphologies of polypropylene With different sizes of calcium carbonate particles, Polym. Compos. 16 (2006) 443–450. doi:10.1002/pc.

[26] M. Morreale, N.T. Dintcheva, F.P. La Mantia, Accelerated weathering of PP based nanocomposites : Effect of the presence of maleic anhydryde grafted polypropylene, Express Polym. Lett. J. 7 (2013) 703–715. doi:10.3144/expresspolymlett.2013.67.

[27] X. Chen, J. Yu, Z. Luo, S. Hu, Z. Zhou, S. Guo, S. Lu, Kinetics of thermo-oxidative degradation of zinc borate/microcapsulated red phosphorus with magnesium hydroxide in flame retarded polypropylene composites, J. Polym. Res. 16 (2009) 745–753. doi:10.1007/s10965-009-9281-z.

[28] Z. Demjén, B. Pukánszky, J. Nagy, Evaluation of interfacial interaction in polypropylene/surface treated CaCO3composites, J. Compos. Part A Appl. Sci. Manuf.

29 (1998) 323–329. doi:10.1016/S1359-835X(97)00032-8.

[29] H. Dalväg, C. Klason, H.-E. Strömvall, The efficiency of cellulosic Fillers in common thermoplastics. Part II. filling with processing aids and coupling agents, Int. J. Polym. Mater. Polym. Biomater. 11 (1985) 9–38. doi:10.1080/00914038508078651.

[30] N.M. Mkhize, Pyrolysis process optimisation to maximise limonene production from waste tyres, Dissertation, Stellenbosch Univ. (2018). doi:10019.1/103481.

[31] B. Singh, N. Sharma, Mechanistic implications of plastic degradation, J. Polym. Degrad. Stab. 93 (2008) 561–584. doi:10.1016/j.polymdegradstab.2007.11.008.

[32] A. Kongo Konde, I. Rosu, F. Lebon, N. Cocheteau, L. Seguin, Numerical modelling of thermomechanics couplings in frictional contact: Application to tire rolling, Proc. Tenth Int. Conf. Comput. Struct. Technol. (2010) 1–18.

[33] P.T. Williams, Pyrolysis of waste tyres: A review, J. Waste Manag. 33 (2013) 1714–1728. doi:10.1016/j.wasman.2013.05.003.

[34] B. Rodgers, W. Waddel, Tire engineering, in: M. James, E. Burak and R. Mike (Eds.), The science and technology of rubber, 4th Edition, Acad. Press. New York. (2013) 653–695.

[35] P.T. Williams, D.T. Taylor, S. Besler, D.T. Taylor, The pyrolysis of scrap automotive tyres. The influence of temperature and heating rate on product composition, J. Fuel. 69 (1990) 1474–1482. doi:10.1016/0016-2361(90)90193-T.

[36] P.T. Williams, S. Besler, Pyrolysis-thermogravimetric analysis of tyres and tyre components, J. Fuel. 74 (1995) 1277–1283. doi:10.1016/0016-2361(95)00083-H.

[37] C. Roy, A. Chaala, H. Darmstadt, B. De Caumia, H. Pakdel, J. Yang, Conversion of used tires to carbon black and oil by pyrolysis, in: K. Sadhan, I. Avraam, K. Klementina (Eds.), Rubber Recycling, CRC Press. New York. (2005) 426–467.

[38] D. Czajczyńska, T. Nannou, L. Anguilano, R. Krzyzyńska, H. Ghazal, N. Spencer, H. Jouhara, Potential of pyrolysis processes in the waste management sector, J. Therm. Sci. Eng. Prog. 123 (2017) 387–394. doi:10.1016/j.egypro.2017.07.275.

[39] J.A. Conesa, I. Martín-Gullón, R. Font, J. Jauhiainen, Complete study of the pyrolysis and gasification of scrap tires in a pilot plant reactor, J. Environ. Sci. Technol. 38 (2004) 3189–3194. doi:10.1021/es034608u.

[40] M. Ryms, K. Januszewicz, W.M. Lewandowski, E. Klugmann-Radziemska, Pyrolysis process of whole waste tires as a biomass energy recycling, J. Soc. Ecol. Chem. Eng. 20 (2013) 93–107. doi:10.2478/eces-2013-0007.

[41] A. Rowhani, T.J. Rainey, Scrap tyre management pathways and their use as a fuel - A review, Energies. 9 (2016) 1–26. doi:10.3390/en9110888.

[42] S. Karthikeyan, C. Sathiskumar, S.R. Moorthy, Effect of process parameters on tire pyrolysis: A review, J. Sci. Ind. Res. 71 (2012) 309–315. doi:123456789/13986.

[43] Y. Kar, Catalytic pyrolysis of car tire waste using expanded perlite, Waste Manag. 31 (2011) 1772–1782. doi:10.1016/j.wasman.2011.04.005.

[44] J.I. Osayi, S. Iyuke, S.E. Ogbeide, Biocrude production through pyrolysis of used tyres, J. Catal. 2014 (2014) 1–9. doi:10.1155/2014/386371.

[45] J.F. Gonzalez, M. Encinar, L. Canito, J.J. Rodrı, Pyrolysis of automobile tyre waste . Influence of operating variables and kinetics study, J. Anal. Appl. Pyrolysis. 59 (2001) 667–683. doi:10.1016/S0165-2370(00)00201-1.

[46] S. Li, Q. Yao, Y. Chi, J. Yan, K. Cen, Pilot-Scale prolysis of scrap tires in a continuous rotary kiln, J. Ind. Eng. Chem. Res. 43 (2004) 5133–5145. doi:10.1021/ie030115m.

[47] A.M. Cunliffe, P.T. Williams, Composition of oils derived from the batch pyrolysis of tyres, Anal. Appl. Pyrolysis. 44 (1998) 131–152. doi:10.1016/S0165-2370(97)00085-5.

[48] S. Galvagno, S. Casu, T. Casabianca, A. Calabrese, G. Cornacchia, Pyrolysis process for the treatment of scrap tyres: Preliminary experimental results, J. Waste Manag. 22 (2002) 917–923. doi:10.1016/S0956-053X(02)00083-1.

[49] K.L. Henry, Upgrading pyrolytic tyre char through acid-alkali demineralisation,Thesis, Stellenbosch Univ. (2015). doi:10019.1/98055.

[50] J. Pilusa, E. Muzenda, Beneficiation of pyrolitic carbon black, Int. J. Chem. Nucl. Mater. Metall. Eng. 7 (2013) 392–396.

[51] J.D. Martínez, R. Murillo, T. García, Production of carbon black from the waste tires pyrolysis, Bol. Grup. Español Carbón. 30 (2013) 10–14.

[52] R. Helleur, N. Popovic, M. Ikura, M. Stanciulescu, D. Liu, Characterization and potential applications of pyrolytic char from ablative pyrolysis of used tires, J. Anal. Appl. Pyrolysis. 58–59 (2001) 813–824. doi:10.1016/S0165-2370(00)00207-2.

[53] G. López, M. Olazar, R. Aguado, J. Bilbao, Continuous pyrolysis of waste tyres in a conical spouted bed reactor, J. Fuel. 89 (2010) 1946–1952. doi:10.1016/j.fuel.2010.03.029.

[54] J. Zhu, B. Shi, J. Zhu, L. Chen, D. Liu, J. Zhu, H. Liang, Production, characterization and properties of chloridized mesoporous activated carbon from waste tyres, J. Waste Manag. Res. 27 (2009) 553–560. doi:10.1177/0734242X08096137.

[55] A. Quek, R. Balasubramanian, Preparation and characterization of low energy post-pyrolysis oxygenated tire char, Chem. Eng. J. 170 (2011) 194–201. doi:10.1016/j.cej.2011.03.053.

[56] W. Kaminsky, C. Mennerich, Z. Zhang, Feedstock recycling of synthetic and natural rubber by pyrolysis in a fluidized bed, J. Anal. Appl. Pyrolysis. 85 (2009) 334–337. doi:10.1016/j.jaap.2008.11.012.

[57] A.M. Cunliffe, P.T. Williams, Influence of process conditions on the rate of activation of chars derived from pyrolysis of used tires, J. Energy Fuels. 13 (1999) 166–175. doi:10.1021/ef9801524.

[58] F.A. López, T.A. Centeno, F.J. Alguacil, B. Lobato, Distillation of granulated scrap tires in a pilot plant, J. Hazard. Mater. 190 (2011) 285–292.

doi:10.1016/j.jhazmat.2011.03.039.

[59] Y.R. Lin, H. Teng, Mesoporous carbons from waste tire char and their application in wastewater discoloration, J. Microporous Mesoporous Mater. 54 (2002) 167–174. doi:10.1016/S1387-1811(02)00380-3.

[60] B. Bilitewski, G. Hardle, K. Marek, Usage of carbon black and activated carbon in relation to input and technical aspects of pyrolysis process, in: G. L. Ferrero, K. Maniatis, A. Buekens, A.V. Bridgewater (Eds.), Pyrolysis and gasification, Elsievier Appl. Sci. London. (1989) 98–109.

[61] A.A. Merchant, M.A. Petricht, Pyrolysis of scrap tires and conversion of chars to activated carbon, Am. Inst. Chem. Eng. J. 39 (1993) 1370–1376. doi:10.1002/aic.690390814.

[62] S. Ogasawara, M. Kuroda, N. Wakao, Preparation of activated carbon by thermal decomposition of used automotive tires, J. Ind. Eng. Chem. Res. 26 (1987) 2552–2556. doi:10.1021/ie00072a030.

[63] W. Heschel, E. Klose, On the suitability of agricultural by-products for the manufacture of granular activated carbon, J. Fuel. 74 (1995) 1786–1791. doi:10.1016/0016-2361(95)80009-7.

[64] B. McEnaney, N. Dovaston, The development of porosity in heat-treated polymer carbons upon activation by carbon dioxide, J. Carbon. 13 (1975) 515–519. doi:10.1016/0008-6223(75)90054-8.

[65] P.H. Brunner, P. V. Roberts, The significance of heating rate on char yield and char properties in the pyrolysis of cellulose, J. Carbon. 18 (1980) 217–224. doi:10.1016/0008-6223(80)90064-0.

[66] K. Tomków, T. Siemieniewska, A. Jankowska, F. Czechowski, Multi-stage activation of brown-coal chars with oxygen, J. Fuel. 56 (1977) 266–270. doi:10.1016/0016-2361(77)90006-0.

[67] R.C. Bansal, J.-B. Donnet, F. Stoeckli, Active carbon, Marcel Dekker, Inc. New York Basal. (1988) 504.

[68] A.M. Cunliffe, P.T. Williams, Properties of chars and activated carbons derived from the pyrolysis of used tyres, J. Environ. Technol. 19 (1998) 1177–1190. doi:10.1080/09593331908616778.

[69] Y.S. Thio, A.S. Argon, R.E. Cohen, M. Weinberg, Toughening of isotactic polypropylene with CaCO3 particles, Polym. J. 43 (2002) 3661–3674. doi:10.1016/S0032-3861(02)00193-3.

[70] C. Giavarini, Active carbons from scrap tyres, J. Fuel. 64 (1985) 1331–1332. doi:10.1016/0016-2361(85)90202-9.

[71] T.G. and A.M.M. E. Aylón, A. Fernández-Colino, M. V. Navarro, R. Murillo, Waste tire pyrolysis: comparison between fixed bed reactor and moving bed reactor, J. Ind. Eng. Chem. Res. 47 (2008) 4029–4033. doi:10.1021/ie071573o.

[72] A.G. Buekens, Some observations on the recycling of plastics and rubber, J. Conserv.

Recycl. 1 (1977) 247–271. doi:10.1016/0361-3658(77)90014-5.

[73] F.A. López, T.A. Centeno, O. Rodríguez, F.J. Alguacil, T.A. Centeno, Preparation and characterization of activated carbon from the char produced in the thermolysis of granulated scrap tyres, J. Air Waste Manag. Assoc. 63 (2013) 534–544. doi:10.1080/10962247.2013.763870.

[74] M. Hofman, R. Pietrzak, Adsorbents obtained from waste tires for NO2 removal under dry conditions at room temperature, Chem. Eng. J. 170 (2011) 202–208. doi:10.1016/j.cej.2011.03.054.

[75] U. Andrea, S. Barbara, C. Emma, T. Nicola, R. Luca, F. Marco, F. Piero, Carbon from microwave assisted pyrolysis of waste tires, J. Anal. Appl. Pyrolysis. 19 (2013) 1–9. doi:10.1016/j.jaap.2013.06.006.

[76] C. Roy, K. Serge, H. Darmstadt, Physicochemical properties of carbon blacks from vacuum pyrolysis of used tires, J. Plast. Rubber Compos. Process. Appl. 23 (1995) 21–30. doi:10.4028/www.scientific.net/KEM.594-595.178.

[77] V.K. Gupta, M.R. Ganjali, A. Nayak, B. Bhushan, S. Agarwal, Enhanced heavy metals removal and recovery by mesoporous adsorbent prepared from waste rubber tire, Chem. Eng. J. 197 (2012) 330–342. doi:10.1016/j.cej.2012.04.104.

[78] X. Zhang, T. Wang, L. Ma, J. Chang, Vacuum pyrolysis of waste tires with basic additives, J. Waste Manangement. 28 (2008) 2301–2310. doi:10.1016/j.wasman.2007.10.009.

[79] I. Iraola-Arregui, P. Van Der Gryp, J.F. Görgens, A review on the demineralisation of pre- and post-pyrolysis biomass and tyre wastes, J. Waste Manag. 79 (2018) 667–688. doi:10.1016/j.wasman.2018.08.034.

[80] D. Hassim, T.Z. Zaeimoedin, Recovered carbon black (rCB) from waste tyres : Effect on mechanical properties of rubber compound, Conf. Pap. (2010) 0–11. doi:10.13140/RG.2.1.4274.6482.

[81] F. Karabork, S.T. Tipirdamaz, Influence of pyrolytic carbon black and pyrolytic oil made from used tires on the curing and (dynamic) mechanical properties of natural rubber (NR)/styrene-butadiene rubber (SBR) blends, Express Polym. Lett. 10 (2016) 72–82. doi:10.3144/expresspolymlett.2016.8.

[82] J. Zhou, Y. Yang, X. Ren, S. Stapf, Investigation of reinforcement of the modified carbon black from wasted tires by nuclear magnetic resonance, J. Zhejiang Univ. Sci. A. 7 (2006) 1440–1446. doi:10.1631/jzus.2006.A1440.

[83] X. Wen, Y. Wang, J. Gong, J. Liu, N. Tian, Y. Wang, Z. Jiang, J. Qiu, T. Tang, Thermal and flammability properties of polypropylene/carbon black nanocomposites, J. Polym. Degrad. Stab. 97 (2012) 793–801. doi:10.1016/j.polymdegradstab.2012.01.031.

[84] J. Mwila, M. Miraftab, A.R. Horrocks, Effect of carbon black on the oxidation of polyolefins-An overview, J. Polym. Degrad. Stab. 44 (1994) 351–356. doi:10.1016/0141-3910(94)90094-9.

[85] A.R. Horrocks, J. Mwila, M. Miraftab, The influence of carbon black on properties of

orientated polypropylene Part I Tensile and physical properties, J. Mater. Sci. 34 (1999) 4333–4340. doi:10.1023/A:1004687827571.

[86] J.-C.C. Huang, Carbon black filled conducting polymers and polymer blends, Adv. Polym. Technol. 21 (2002) 299–313. doi:10.1002/adv.10025.

[87] H. Teng, Y.C. Lin, L.Y. Hsu, Production of activated carbons from pyrolysis of waste tires impregnated with potassium hydroxide, J. Air Waste Manag. Assoc. 50 (2000) 1940–1946. doi:10.1080/10473289.2000.10464221.

[88] J. Shah, M.R. Jan, F. Mabood, M. Shahid, Conversion of waste tyres into carbon black and their utilization as adsorbent, J. Chinese Chem. Soc. 53 (2006) 1085–1089. doi:10.1002/jccs.200600144.

[89] G.S. Miguel, G.D. Fowler, M. Dall'Orso, C.J. Sollars, Porosity and surface characteristics of activated carbons produced from waste tyre rubber, J. Chem. Technol. Biotechnol. 77 (2002) 1–8. doi:10.1002/jctb.518.

[90] H. Darmstadt, C. Roy, S. Kaliaguine, ESCA characterization of commercial carbon black and of carbon blacks from vacuum pyrolysis of used tires, J. Carbon. 32 (1994) 1399–1406. doi:10.1016/0008-6223(94)90132-5.

[91] M. Olazar, R. Aguado, M. Arabiourrutia, G. Lopez, A. Barona, J. Bilbao, Catalyst effect on the composition of tire pyrolysis products, J. Energy Fuels. 22 (2008) 2909–2916. doi:10.1021/ef8002153.

[92] H. Hu, Y. Fang, H. Liu, R. Yu, G. Luo, W. Liu, A. Li, H. Yao, The fate of sulfur during rapid pyrolysis of scrap tires, Chemosphere. 97 (2014) 102–107. doi:10.1016/j.chemosphere.2013.10.037.

[93] S. Perry, R.H. Perry, D.W. Green, J.O. Maloney, Gasification, in: R. H. Perry, (Ed.), Perry's Chemical Engineers' Handbook, 7th Edition, McGraw-Hill, New York. (1997) 25–94.

[94] E.J. Henley, J.D. Seader, D.K. Roper, Leaching, in: Separation process principles, 3rd Edition, Wiley, New York. (2011) 708–726.

[95] E.L.K. Mui, W.H. Cheung, M. Valix, G. McKay, Mesoporous activated carbon from waste tyre rubber for dye removal from effluents, J. Microporous Mesoporous Mater. 130 (2010) 287–294. doi:10.1016/j.micromeso.2009.11.022.

[96] S. Ucar, S. Karagoz, A.R. Ozkan, J. Yanik, Evaluation of two different scrap tires as hydrocarbon source by pyrolysis, J. Fuel. 84 (2005) 1884–1892. doi:10.1016/j.fuel.2005.04.002.

[97] S. Galvagno, G. Casciaro, S. Casu, M. Martino, C. Mingazzini, A. Russo, S. Portofino, Steam gasification of tyre waste, poplar, and refuse-derived fuel: A comparative analysis, J. Waste Manag. 29 (2009) 678–689. doi:10.1016/j.wasman.2008.06.003.

[98] N. Aslam, A. Khawaja, Y. Shahid, A. Ja, Acid Base Demineralization of Pyrolytic Carbon Black Obtained From Waste Rubber, J. Austin Chem. Eng. 5 (2018) 1–3.

[99] O.H. Lin, H. Md Akil, Z.A.M. Ishak, Characterization and properties of activated nanosilica/polypropylene composites with coupling agents, J. Polym. Compos. 30

(2009) 1693–1700. doi:10.1002/pc.20744.

[100] S. Yuen, C.-C.M. Ma, C. Chiang, J. Chang, S. Huang, S. Chen, C. Chuang, C. Yang, M. Wei, Silane-modified MWCNT/PMMA composites – Preparation, electrical resistivity, thermal conductivity and thermal stability, J. Compos. Part A Appl. Sci. Manuf. 38 (2007) 2527–2535. doi:10.1016/j.compositesa.2007.07.015.

[101] D. Reger, S. Goode, D. Ball, Reactions between acids and bases, in: Chemsitry, Principles and Practice, 3rd Edition, Cengage Learn. New York. (2009).

[102] D. Dougherty, M. Fuhrmann, Y. Sanborn, R. Doty, P. Colombo, Leaching mechanisms of solidified low-level waste: The literature survey, Nucelar Waste Res. Gr. - Dep. Nucl. Energy. New York. (1985). doi:10.2172/5158484.

[103] R.N. Rothon, Particulate fillers for polymers, Rapra Technol. Ltd, United Kingdom. (2001) 162.

[104] R.N. Rothon, Particulate- filled polymer composites, 2nd Edition, Rapra Technol. Ltd, United Kingdom. (2003) 564.

[105] H.S. Katz, Particulate fillers, in: S.T. Peters (Ed.), Handbook of composite, 2nd Edition, Springer-Science Bus. Media, Engl. (1998) 242–253.

[106] M. Xanthos, Functional fillers for plastics, 2nd Edition, Wiley-VCH, New Jersey. (2004) 538.

[107] J. Hari, B. Pukanszky, Nanocomposites: Preparation, structure and properties, in: M.Kutz (Ed.), Applied plastic engineering handbook., William Andrew, Oxford. (2011) 109–142.

[108] G. Bogoeva-Gaceva, A. Janevski, E. Mader, Nucleation activity of glass fibers towards iPP evaluated by DSC and polarizing light microscopy, Polym. J. 42 (2001) 4409–4416. doi:https://doi.org/10.1016/S0032-3861(00)00659-5.

[109] Y. Wang, W.-C. Lee, Interfacial interactions in calcium carbonate–Polypropylene composites. 2: Effect of compounding on the dispersion and the impact properties of surface-modified composites, J. Polym. Compos. 25 (2004) 451–460. doi:10.1002/pc.20038.

[110] D. Eiras, L.A. Pessan, Mechanical properties of polypropylene/calcium carbonate nanocomposites, J. Mater. Res. 12 (2009) 517–522. doi:10.1590/S1516-14392009000400023.

[111] G.Z. Papageorgiou, D.S. Achilias, D.N. Bikiaris, G.P. Karayannidis, Crystallization kinetics and nucleation activity of filler in polypropylene/surface-Treated SiO2 nanocomposites, J. Thermochim. Acta. 427 (2005) 117–128. doi:10.1016/j.tca.2004.09.001.

[112] D.M. Bigg, Mechanical properties of particulate filled polymers, J. Polym. Compos. 8 (1987) 115–122. doi:10.1002/pc.750080208.

[113] G.C. Onuegbu, C.H. Obasi, F.N. Onuoha, Effect of Titanate coupling Agent on the mechanical properties of talc filled polypropylene, J. Acad. Res. Int. 5 (2014) 26–30. doi:10.1080/00914030390256864.

[114] H. Mohammadi, M. Moghbeli, Organically modified grafted mica (OMGM) nanoparticles for reinforcement of polypropylene, Iran. Polym. J. 27 (2018) 125–135. doi:10.1007/s13726-017-0593-2.

[115] A.S. Luyt, M.D. Dramićanin, Ž. Antić, V. Djoković, Morphology, mechanical and thermal properties of composites of polypropylene and nanostructured wollastonite filler, Polym. Test. 28 (2009) 348–356. doi:10.1016/j.polymertesting.2009.01.010.

[116] M.N. Akanbi, O. Ogbobe, M.U. Obidiegwu, P.C. Uzoma, G.C. Onuegbu, P.I. Anynwu, Effects of dolomite filler and compatibilizer on the mechanical properties of polypropylene, Int. Reseach J. Eng. Sci. Technol. 13 (2015) 11–16.

[117] P. Zhu, C. Chen, C. Wu, Crystallization behaviour and mechanical properties of polypropylene/modified carbon black composites, J. Polym. Compos. 30 (2009) 391–398. doi:10.1002/pc.20566.

[118] Y. Kanbur, Z. Küçükyavuz, Electrical and mechanical properties of polypropylene/carbon black composites, J. Reinf. Plast. Compos. 28 (2009) 2251–2260. doi:10.1177/0731684408092378.

[119] H. Karian, Handbook of polypropylene and polypropylene composite, 2nd Edition, Revised and expanded, Marcel Dekker, New York. (2003) 741.

[120] M. Tolinski, Additives for polyolefins : Getting the most out of Polypropylene, Polyethylene and TPO, 2nd Edition, William Andrew, New York. (2015) 234.

[121] M. Garcia, G. van Vliet, S.H. Jain, B.A. Schrauwen, A.U. Sarkissov, W.E. van Zyl, B.A. Boukamp, Polypropylene/SiO2 nanocomposites with improved mechanical properties, J. Rev. Adv. Mater. Sci. 6 (2005) 169–175. doi:2481802/619347.

[122] A.B. Bas, O. Yilmaz, A. Ibis, M. Dogu, K. Kirkkopru, F.S. Guner, Melt flow properties of graphite nanoplatelets-filled polypropylene, J. Compos. Mater. 0 (2016) 1–12. doi:10.1177/0021998316675502.

[123] L.E. Nielsen, Mechanical properties of polymers and composites, Marcel Dekker, New York. (1974) 580.

[124] W.C.J. Zuiderduin, C. Westzaan, J. Huétink, R.J. Gaymans, Toughening of polypropylene with calcium carbonate particles, Polym. J. 44 (2003) 261–275. doi:10.1016/S0032-3861(02)00769-3.

[125] Z. Demjén, B. Pukánszky, J. Nagy, Possible coupling reactions of functional silanes and polypropylene, J. Polym. 40 (1999) 1763–1773. doi:10.1016/S0032-3861(98)00396-6.

[126] J.D. Tucker, P.L. Lear, G.S. Atkinson, S. Lee, S.J. Lee, Use of polymeric compatibilizers in polypropylene / calcium carbonate composites, Korean J. Chem. Eng. 17 (2000) 506–509. doi:10.1007/BF02707157.

[127] Y. Wang, J.S. Huang, Single screw extrusion compounding of particulate filled thermoplastics: state of dispersion and its influence on impact properties, J. Appl. Polym. Sci. 60 (1996) 1779–1791. doi:10.1002/(SICI)1097-4628(19960613)60:11<1779::AID-APP1>3.0.CO;2-I.

[128] Li.Q, Wu.C, Zhu.P, Effect of Maleic-Anhydride-grafted Polypropylene as a compatibilizer on the properties /(modified carbon black) composite, J. Vinyl Addit. Technolgy. 17 (2001) 260–264. doi:10.1002/vnl.20272.

[129] F. Qiu, M. Wang, Y. Hao, S. Guo, The effect of talc orientation and transcrystallization on mechanical properties and thermal stability of the polypropylene/talc composites, J. Compos. Part A Appl. Sci. Manuf. 58 (2014) 7–15. doi:10.1016/j.compositesa.2013.11.011.

[130] K. Wang, N. Bahlouli, F. Addiego, S. Ahzi, Y. Rémond, D. Ruch, R. Muller, Effect of talc content on the degradation of re-extruded polypropylene / talc composites, Polym. Degrad. Stab. 98 (2013) 1275–1286. doi:10.1016/j.polymdegradstab.2013.04.006.

[131] O.H. Lin, H.M. Akil, Z.A. Mohd Ishak, Surface-activated nanosilica treated with silane coupling agents/polypropylene composites: Mechanical, morphological, and thermal studies, J. Polym. Compos. 32 (2011) 1568–1583. doi:10.1002/pc.21190.

[132] A.K. Nurdina, M. Mariatti, P. Samayamutthirian, Effect of filler surface treatment on mechanical properties and thermal properties of single and hybrid filler-filled PP composites, J. Appl. Polym. Sci. 120 (2011) 857–865. doi:10.1002/app.33156.

[133] S. Tan, T. Tinçer, Flammability and mechanical properties of Al(OH)3 and BaSO4 filled polypropylene, J. Appl. Polym. Sci. 118 (2010) 3034–3040. doi:10.1002/app.32729.

[134] M. Akil, N. Lily, A. Razak, O. Huilin, A. Zainal, Effect of various coupling agents on properties of alumina-filled polypropylene Composites, J. Reinf. Plast. Compos. 25 (2006) 745–759. doi:10.1177/0731684406062068.

[135] G. Guerrica-Echevarría, J.I. Eguiazábal, J. Nazábal, Influence of molding conditions and talc content on the properties of polypropylene composites, Eur. Polym. J. 34 (1998) 1213–1219. doi:10.1016/S0014-3057(97)00228-0.

[136] M.N.M. Ansari, H. Ismail, The effect of silane coupling agent on mechanical properties of feldspar filled polypropylene Composites, J. Reinf. Plast. Compos. 28 (2009) 3049–3060. doi:10.1177/0731684408092377.

[137] Z. Jiang, J. Jin, C. Xiao, X. Li, Effect of surface modification of carbon black (CB) on the morphology and crystallization of poly(ethylene terephthalate)/CB masterbatch, J. Colloids Surfaces A Physicochem. Eng. Asp. 395 (2012) 105–115. doi:10.1016/j.colsurfa.2011.12.013.

[138] C. DeArmitt, R. Rothon, Dispersants and coupling agents, in: M. Kutz (Ed.), Applied plastics engineering handbook, William Andrew, Oxford. (2011) 441–454.

[139] M.-K. Seo, J.-R. Lee, S.-J. Park, Crystallization kinetics and interfacial behaviors of polypropylene composites reinforced with multi-walled carbon nanotubes, J. Mater. Sci. Eng. 404 (2005) 79–84. doi:10.1016/j.msea.2005.05.065.

[140] Z. Demjen, B. Pukanszky, E. Foldes, J. Nagy, Interaction of silane coupling agents with CaCO3, J. Colloid Interface Sci. 190 (1997) 427–436. doi:papers://590F92D9-0B76-4B88-8729-9AF064BE5AC8/Paper/p5242.

[141] M. Peng, M. Zhou, Z. Jin, W. Kong, Z. Xu, D. Vadillo, Effect of surface modifications

of carbon black (CB) on the properties of CB/polyurethane foams, J. Mater. Sci. 45 (2010) 1065–1073. doi:10.1007/s10853-009-4043-1.

[142] X. Ding, J.J. Wang, S. Zhang, J.J. Wang, S. Li, Carbon black-filled polypropylene as a positive temperature coefficient material: effect of filler treatment and heat treatment, J. Polym. Bull. 73 (2016) 369–383. doi:10.1007/s00289-015-1492-3.

[143] C. Ai Wah, L. Yub Choong, G. Seng Neon, Effects of titanate coupling agent on rheological behaviour, dispersion characteristics and mechanical properties of talc filled polypropylene, Eur. Polym. J. 36 (2000) 789–801. doi:10.1016/S0014-3057(99)00123-8.

[144] J. z Lu, Q. Wu, H. s McNabb, Chemical coupling in wood fiber and polymer composites: a review of coupling agents and treatments, Wood Fiber Sci. 32 (2000) 88–104.

[145] M. Bengtsson, K. Oksman, Silane crosslinked wood plastic composites: Processing and properties, J. Compos. Sci. Technol. 66 (2006) 2177–2186. doi:10.1016/j.compscitech.2005.12.009.

[146] S.M.B. Nachtigall, G.S. Cerveira, S.M.L. Rosa, New polymeric-coupling agent for polypropylene/wood-flour composites, J. Polym. Test. 26 (2007) 619–628. doi:10.1016/j.polymertesting.2007.03.007.

[147] R. Bouza, A. Lasagabaster, M.J. Abad, L. Barral, Effects of vinyltrimethoxy silane on thermal properties and dynamic mechanical properties of polypropylene-wood flour composites, J. Appl. Polym. Sci. 109 (2008) 1197–1204. doi:10.1002/app.28159.

[148] V.N. Hristov, S.T. Vasileva, M. Krumova, R. Lach, G.H. Michler, Deformation mechanisms and mechanical properties of modified polypropylene/wood fiber composites, J. Polym. Compos. 25 (2004) 521–526. doi:Doi 10.1002/Pc.20045.

[149] N. Elshereksi, M. Ghazali, A. Muchtar, Aspects of Titanate coupling agents and their application in dental polymer composites: A review, J. Adv. Mater. 1134 (2016) 96–102. doi:10.4028/www.scientific.net/AMR.1134.96.

[150] S. Shokoohi, A. Arefazar, R. Khosrokhavar, Silane coupling agents in polymer-based reinforced composites: A review, J. Reinf. Plast. Compos. 27 (2008) 473–485. doi:10.1177/0731684407081391.

[151] P.G.G. Pape, Adhesion promoters: Silane coupling agents, in: M.Kutz (Ed.), Applied plastics engineering handbook, William Andrew, Oxford. (2011) 503–517.

[152] Z. Zhou, S. Wang, L. Lu, Y. Zhang, Y. Zhang, Functionalization of multi-wall carbon nanotubes with silane and its reinforcement on polypropylene composites, J. Compos. Sci. Technol. 68 (2008) 1727–1733. doi:10.1016/j.compscitech.2008.02.003.

[153] P.S. Razi, R. Portier, A. Raman, Studies on polymer-wood interface bonding: effect of coupling agents and surface modification, J. Compos. Mater. (1998) 1064–1079. doi:10.1177/002199839903301201.

[154] O. Vantsi, T. Karki, Different coupling agents in wood-polypropylene composites containing recycled mineral wool: A comparison of the effects, J. Reinf. Plast. Compos. 34 (2015) 879–895. doi:10.1177/0731684415583524.

[155] C.A.S. Hill, M.R.M. Farahani, M.D.C. Hale, The use of organo alkoxysilane coupling agents for wood preservation, J. Holzforschung. 58 (2004) 316–325. doi:10.1515/HF.2004.049.

[156] Y. Xie, C.A.S. Hill, Z. Xiao, H. Militz, C. Mai, Silane coupling agents used for natural fiber/polymer composites: A review, J. Compos. Part A Appl. Sci. Manuf. 41 (2010) 806–819. doi:10.1016/j.compositesa.2010.03.005.

[157] S.J. Monte, Neoalkoxy Titanate & Zirconate coupling agent additives in thermoplastics, J. Polym. Polym. Compos. 10 (2002) 121–172. doi:10.1177/096739110201000202.

[158] K.L. Pickering, M.G.A. Efendy, T.M. Le, A review of recent developments in natural fibre composites and their mechanical performance, J. Compos. Part A Appl. Sci. Manuf. 83 (2016) 98–112. doi:10.1016/j.compositesa.2015.08.038.

[159] P.G. Pape, Adhesion promoters: Silane coupling agents, in: M.Kutz (Ed.), Applied plastics engineering handbook, William Andrew, Oxford. (2011) 503–517.

[160] Plueddemann, Shin-Etsu Chemical Ltd., K. Weissenbach, H. Mack, F.D. Blum, Silane Coupling Agents, Shin-Etsu Chem. Ltd. (n.d.). doi:http://www.shinetsusilicone-global.com/catalog/pdf/SilaneCouplingAgents_e.pdf.

[161] I. Kemal, A. Whittle, R. Burford, T. Vodenitcharova, M. Hoffman, Toughening of unmodified polyvinylchloride through the addition of nanoparticulate calcium carbonate and titanate coupling agent, J. Appl. Polym. Sci. 127 (2013) 2339–2353. doi:10.1002/app.37774.

[162] C.Y.K. Lung, J.P. Matinlinna, Aspects of silane coupling agents and surface conditioning in dentistry: An overview, J. Dent. Mater. 28 (2012) 467–477. doi:10.1016/j.dental.2012.02.009.

[163] C. Albano, M. Ichazo, M. Herna, Analysis of thermogravimetric data of blends of polyolefins with calcium carbonate treated with Lica 12, J. Polym. Degrad. Stab. 73 (2001) 211–224. doi:10.1016/S0141-3910(01)00020-9.

[164] N.W. Elshereksi, M. Ghazali, A. Muchtar, C.H. Azhari, Review of titanate coupling agents and their application for dental composite fabrication, Dent. Mater. J. 36 (2017) 539–552. doi:10.4012/dmj.2016-014.

[165] M. Hajian, G.A. Koohmareh, A. Mostaghasi, Investigation of the effects of titanate as coupling agent and some inorganic nanoparticles as fillers on mechanical properties and morphology of soft PVC, J. Polym. Sci. (2011) 1–9. doi:10.1155/2011/238619.

[166] J.M. Felix, P. Gatenholm, The nature of adhesion in composites of modified cellulose fibers and polypropylene, J. Appl. Polym. Sci. 42 (1991) 609–620. doi:10.1002/app.1991.070420307.

[167] J. Lu, J.Z., Wu, Q, McNabb, A review of coupling agents and treatments, J. Wood Sci. Technol. 32 (2000) 88–104.

[168] K.H. Wong, D. Syed Mohammed, S.J. Pickering, R. Brooks, Effect of coupling agents on reinforcing potential of recycled carbon fibre for polypropylene composite, J. Compos. Sci. Technol. 72 (2012) 835–844. doi:10.1016/j.compscitech.2012.02.013.

[169] L. Techawinyutham, A. Frick, S. Siengchin, Polypropylene/Maleic Anhydride grafted Polypropylene (MAgPP)/coconut fiber composites, J. Adv. Mech. Eng. 8 (2016) 1–9. doi:10.1177/1687814016645446.

[170] R. Doufnoune, F. Chebira, N. Haddaoui, Effect of titanate coupling agent on the mechanical properties of calcium carbonate filled polypropylene, Int. J. Polym. Mater. 52 (2003) 967–984. doi:10.1080/714975875.

[171] B. Fisa, Fracture of Mica-Reinforced Polypropylene: Mica Concentration Effect, 6 (1985) 249–260.

[172] M. Hemmati, G.H. Rahimi, A.B. Kaganj, S. Sepehri, A.M. Rashidi, Rheological and mechanical characterization of multi-walled carbon nanotubes/polypropylene nanocomposites, J. Macromol. Sci. Part B Phys. 47 (2008) 1176–1187. doi:10.1080/00222340802403396.

[173] P. Mareri, S. Bastide, N. Binda, A. Crespy, Mechanical behaviour of polypropylene composites containing fine mineral filler: Effect of filler surface treatment, Compos. Sci. Technol. 58 (1998) 747–752. doi:10.1016/S0266-3538(97)00156-5.

[174] D. He, B. Jiang, The elastic modulus of filled polymer composites, J. Appl. Polym. Sci. 49 (1993) 617–621. doi:10.1002/app.1993.070490408.

[175] M. Chen, C. Wan, W. Shou, Y. Zhang, Y. Zhang, J. Zhang, Effects of Interfacial Adhesion on Properties of Polypropylene / Wollastonite Composites, J. Appl. Polym. Sci. 107 (2008) 1718–1723. doi:10.1002/app.

[176] D.M. Laura, H. Keskkula, J.W. Barlow, D.R. Paul, Effect of glass fiber surface chemistry on the mechanical properties of glass fiber reinforced, rubber-toughened nylon 6, J. Polym. 43 (2002) 4673–4687. doi:10.1016/S0032-3861(02)00302-6.

[177] N. Grassie, W.B.H. Leeming, Some aspects of photo, photo-thermal and thermal decomposition of polypropylene under vacuum., Eur. Polym. J. 11 (1975) 809–818. doi:10.1016/0014-3057(75)90080-4.

[178] C. Kujirai, S. Hashiya, H. Furuno, N. Terada, Photochemical crosslinking of polypropylene, J. Polym. Sci. Part A-1 Polym. Chem. 6 (1968) 589–593. doi:10.1002/pol.1968.150060314.

[179] A. Brzozowska-Stanuch, S. Rabiej, J. Fabia, J. Nowak, Changes in thermal properties of isotactic polypropylene with different additives during aging process, Polimery/Polymers. 59 (2014) 302–307. doi:10.14314/polimery.2014.302.

[180] E. Yousif, R. Haddad, Photodegradation and photostabilization of polymers, especially polystyrene: review, J. SpringerPlus. 2 (2013) 1–32. doi:10.1186/2193-1801-2-398.

[181] J. Guillet, Photochemistry of man-made polymers, McKellar, J.F Allen, S.N, Applied Science Publishers, London, 1979, J. Polym. Sci. Part C Polym. Lett. 18 (1980) 155. doi:10.1002/pol.1980.130180227.

[182] D. Chen, H. Zhang, Q. Zheng, F. Liu, K. Xu, M. Chen, Polypropylene composites filled by magnesium hydroxide coprecipitated with foreign ions, Polym. Adv. Technol. 19 (2008) 1353–1360. doi:10.1002/pat.

[183] E. Abdel-Bary, Handbook of plastic films., Rapra Technol. Ltd, UK. (2003) 404.

[184] M.G. Wyzgoski, Effect of oven aging on polypropylene, J. Appl. Polym. Sci. 26 (1981) 1689–1704. doi:10.1002/app.1981.070260524.

[185] K.T. Gillen, R. Bernstein, R.L. Clough, M. Celina, Lifetime predictions for semi-crystalline cable insulation materials : I . Mechanical properties and oxygen consumption measurements on EPR materials, Polym. Degrad. Stab. 91 (2006) 2146–2156. doi:10.1016/j.polymdegradstab.2006.01.009.

[186] H. Oswald, E. Turi, The deterioration of polypropylene by oxidative degradation, Polym. Eng. Sci. 5 (1965) 152–158. doi:10.1002/pen.760050312.

[187] X. Gao, X. Meng, H. Wang, B. Wen, Y. Ding, S. Zhang, M. Yang, Antioxidant behaviour of a nanosilica-immobilized antioxidant in polypropylene, J. Polym. Degrad. Stab. 93 (2008) 1467–1471. doi:10.1016/j.polymdegradstab.2008.05.009.

[188] H.A. Craddock, Oilfield chemistry and its environmental impact, John Wiley Sons, Ltd, United Kingdom. (2018) 746.

[189] Zeus, Thermal Degradation of Plastics, Zeus Ind. Prod. (2005) 1–8.

[190] S. Su, C.A. Wilkie, The thermal degradation of nanocomposites that contain an oligomeric ammonium cation on the clay, Polym. Degrad. Stab. 83 (2004) 347–362. doi:10.1016/S0141-3910(03)00279-9.

[191] I. Krupa, A.S. Luyt, Thermal properties of isotactic polypropylene degraded with gamma irradiation, Polym. Degrad. Stab. 72 (2001) 505–508. doi:10.1016/S0141-3910(01)00052-0.

[192] M. Nechifor, Factors Influencing the Photochemical Behavior of Multicomponent Polymeric Materials, in: D. Rosu, P.M. Visakh (Eds.), Photochemical Behavior of Multicomponent Polymeric-based Materials, Springer. 26 (2016) 21–65. doi:10.1007/978-3-319-25196-7_2.

[193] P. Gijsman, Polymer Stabilization, in: M. Kutz (Ed.), Applied plastics engineering handbook, William Andrew, Oxford. (2011) 375–399.

[194] M. Lu, X. Gao, P. Liu, H. Tang, F. Wang, Y. Ding, S. Zhang, M. Yang, Photo and thermo-oxidative aging of polypropylene filled with surface modified fumed nanosilica, J. Compos. Commun. 3 (2017) 51–58. doi:10.1016/j.coco.2017.02.004.

[195] S. Aslanzadeh, M. Haghighat Kish, A.A. Katbab, Effects of melt processing conditions on photo-oxidation of PP/PPgMA/OMMT composites, J. Polym. Degrad. Stab. 95 (2010) 1800–1809. doi:10.1016/j.polymdegradstab.2010.05.004.

[196] M.S. Rabello, J.R. White, Photodegradation of talc-filled polypropylene, J. Polym. Compos. 17 (1996) 691–704. doi:10.1002/pc.10661.

[197] J. Li, R. Yang, J. Yu, Y. Liu, Natural photo-aging degradation of polypropylene nanocomposites, J. Polym. Degrad. Stab. 93 (2008) 84–89. doi:10.1016/j.polymdegradstab.2007.10.022.

[198] P.A. Zapata, Z. Andres, F.M. Rabagliati, F. Sepúlveda, F. Catalina, T. Corrales, Study

on the photodegradation of nanocomposites based on polypropylene and TiO2 nanotubes, J. Polym. Degrad. Stab. 133 (2016) 101–107. doi:10.1016/j.polymdegradstab.2016.08.008.

[199] S. Morlat, B. Mailhot, D. Gonzalez, J.L. Gardette, Photo-oxidation of Polypropylene/Montmorillonite Nanocomposites. 1. Influence of Nanoclay and Compatibilizing Agent, J. Chem. Mater. 16 (2004) 377–383. doi:10.1021/cm031079k.

[200] S. Morlat-Therias, B. Mailhot, D. Gonzalez, J.L. Gardette, Photooxidation of polypropylene/montmorillonite nanocomposites. 2. Interactions with antioxidants, J. Chem. Mater. 17 (2005) 1072–1078. doi:10.1021/cm040172l.

[201] M. Morreale, T. Dintcheva, F. Paolo, L. Mantia, The role of filler type in the photo-oxidation behaviour of micro- and nano-filled polypropylene, J. Polym. Int. 60 (2011) 1107–1116. doi:10.1002/pi.3049.

[202] D. Vaillant, J. Lacoste, J. Lemaire, Stabilization of isotactic polypropylene. Problems bound to the interactions of stabilizers with pigments and fillers, J. Appl. Polym. Sci. 65 (1997) 609–615. doi:10.1002/(SICI)1097-4628(19970718)65:3<609::AID-APP21>3.0.CO;2-Q.

[203] H. Zhao, R.K.Y. Li, A study on the photo-degradation of zinc oxide (ZnO) filled polypropylene nanocomposites, Polym. J. 47 (2006) 3207–3217. doi:10.1016/j.polymer.2006.02.089.

[204] N.S. Allen, M. Edge, A. Ortega, G. Sandoval, C.M. Liauw, J. Verran, J. Stratton, R.B. Mcintyre, Degradation and stabilisation of polymers and coatings : nano versus pigmentary titania particles, J. Polym. Degrad. Stab. 85 (2004) 927–946. doi:10.1016/j.polymdegradstab.2003.09.024.

[205] B. Mailhot, S. Morlat, J.L. Gardette, S. Boucard, J. Duchet, J.F. Gérard, Photodegradation of polypropylene nanocomposites, J. Polym. Degrad. Stab. 82 (2003) 163–167. doi:10.1016/S0141-3910(03)00179-4.

[206] H.P. Boehm, Some aspects of the surface chemistry of carbon blacks and other carbons, J. Carbon. 32 (1994) 759–769. doi:10.1016/0008-6223(94)90031-0.

[207] J.M. Pena, N.S. Allen, M. Edge, C.M. Liauw, S.R. Hoon, B. Valange, R.I. Cherry, Analysis of radical content on carbon black pigments by electron spin resonance: Influence of functionality, thermal treatment and adsorption of acidic and basic probes, J. Polym. Degrad. Stab. 71 (2001) 153–170. doi:10.1016/S0141-3910(00)00166-X.

[208] R. Benavides, R. González-Hernandez, M.C. González-Cantú, B. Reyes-Vielma, N.C. Billingham, Accelerated degradation of highly loaded polypropylene., J. Vinyl Addit. Technol. 9 (2003) 41–49. doi:10.1002/vnl.10060.

[209] M. Atif, R. Bongiovanni, M. Giorcelli, E. Celasco, A. Tagliaferro, Modification and characterization of carbon black with mercaptopropyltrimethoxysilane, J. Appl. Surf. Sci. 286 (2013) 142–148. doi:10.1016/j.apsusc.2013.09.037.

[210] N. Chand, U.K. Dwivedi, Effect of coupling agent on abrasive wear behaviour of chopped jute fibre-reinforced polypropylene composites, J. Wear. 261 (2006) 1057–1063. doi:10.1016/j.wear.2006.01.039.

[211] Y.W. Leong, M.B.A. Bakar, Z.A.M. Ishak, A. Ariffin, Effects of filler treatments on the mechanical, flow, thermal, and morphological properties of talc and calcium carbonate filled polypropylene hybrid composites, J. Appl. Polym. Sci. 98 (2005) 413–426. doi:10.1002/app.21507.

[212] F. Xin, L. Li, The role of a silane coupling agent in carbon nanotube/polypropylene composites, J. Compos. Mater. 46 (2012) 3267–3275. doi:10.1177/0021998312437235.

[213] Combination of Organic and Inorganic Materials Silane Coupling Agents, (n.d.). https://www.shinetsusilicone-global.com/catalog/pdf/SilaneCouplingAgents_e.pdf (accessed March 14, 2019).

[214] H. Yang, J. Gong, X. Wen, J. Xue, Q. Chen, Z. Jiang, N. Tian, T. Tang, Effect of carbon black on improving thermal stability, flame retardancy and electrical conductivity of polypropylene/carbon fiber composites, J. Compos. Sci. Technol. 113 (2015) 31–37. doi:https://doi.org/10.1016/j.compscitech.2015.03.013.

[215] I. Burmistrov, N. Gorshkov, I. Ilinykh, D. Muratov, E. Kolesnikov, S. Anshin, I. Mazov, J.P. Issi, D. Kusnezov, Improvement of carbon black based polymer composite electrical conductivity with additions of MWCNT, Compos. Sci. Technol. 129 (2016) 79–85. doi:10.1016/j.compscitech.2016.03.032.

[216] N.A.M. Radzuan, M.Y. Zakaria, A.B. Sulong, J. Sahari, N.A. Mohd Radzuan, M. Yusuf Zakaria, A.B. Sulong, J. Sahari, The effect of milled carbon fibre filler on electrical conductivity in highly conductive polymer composites, J. Compos. Part B Eng. 110 (2017) 153–160. doi:10.1016/j.compositesb.2016.11.021.

[217] M. Akay, Introduction to polymer science and technology, Bookboon. (2012) 269. doi:10.1016/0032-3861(78)90106-4.

[218] Y. Liu, X. Zhang, C. Song, Y. Zhang, Y. Fang, B. Yang, X. Wang, An effective surface modification of carbon fiber for improving the interfacial adhesion of polypropylene composites, J. Mater. Des. 88 (2015) 810–819. doi:10.1016/j.matdes.2015.09.100.

[219] D.C. Mellor, A.B. Moir, G. Scott, The effect of processing conditions on the U.V. stability of polyolefins, Eur. Polym. J. 9 (1973) 219–225. doi:10.1016/0014-3057(73)90129-8.

[220] C. Vijayakumar, R. Chitra, R. Surender, G. Pitchaimari, K. Rajakumar, Development of photodegradable environment friendly polypropylene films, Plast. Polym. Technol. 2 (2013) 22–37.

[221] C. Naddeo, L. Vertuccio, G. Barra, L. Guadagno, Nano-charged polypropylene application: Realistic perspectives for enhancing durability, J. Mater. 10 (2017) 943. doi:10.3390/ma10080943.

[222] D. Montgomery, Design and analysis of experiments, 5th Edition, Wiley, New York. (2001) 684.

[223] P.H. Camargo, K.G. Satyanarayana, F. Wypych, Nanocomposites: Synthesis, structure, propertis and new application opportunities, J. Mater. Res. 12 (2009) 1–31.

doi:10.1590/S1516-14392009000100002.

[224] Z. Guangjian, W. Jincheng, Study on application behavior of pyrolysis char from waste tires in silicone rubber composites, J. e-Polymers. 16 (2016) 255–264. doi:10.1515/epoly-2015-0285.

[225] G. Lopez, M. Olazar, R. Aguado, G. Elordi, M. Amutio, M. Artetxe, Vacuum Pyrolysis of Waste Tires by Continuously Feeding into a Conical Spouted Bed Reactor, Ind. Enginering Chem. Res. 49 (2010) 8990–8997. doi:10.1021/ie1000604.

[226] Carbon black scrap,offgrade, prime, grade: N220, N330, N660, N550, mixed grade, (n.d.). http://www.sonepa.com/carbon-black.html (accessed October 16, 2018).

[227] P.T. Williams, D.T. Taylor, S. Besler, The pyrolysis of scrap automotive tyres. The influence of temperature and heating rate on product composition, J. Fuel. 69 (1990) 1474–1482. doi:10.1016/0016-2361(90)90193-T.

[228] H. Darmstadt, C. Roy, S. Kaliaguine, Characterization of pyrolytic carbon blacks from commercial tire pyrolysis plants, J. Carbon. 33 (1995) 1449–1455. doi:10.1016/0008-6223(95)00096-V.

[229] Sodium hydroxide (NaOH) reactions, (n.d.). http://www.allreactions.com/index.php/group-1a/natrium/sodium-hydroxide (accessed October 15, 2018).

[230] M. Bernardo, N. Lapa, M. Gonc, B. Mendes, F. Pinto, I. Fonseca, H. Lopes, M. Gonçalves, B. Mendes, F. Pinto, I. Fonseca, H. Lopes, Physico-chemical properties of chars obtained in the co-pyrolysis of waste mixtures, J. Hazard. Mater. 219–220 (2012) 196–202. doi:10.1016/j.jhazmat.2012.03.077.

[231] A.D. Thorn, R.A. Robinson, Fillers, in: A. K. Bhowmick, M. M. Hall, H. A. Benarey (Eds.), Rubber Products Manufacturing Technology, Marcel Dekker, New York. (1994) 68–71.

[232] L. Mattsson, C. Jungmann, P.A. Lieberzeit, C. Preininger, Modified carbon black as label in a colorimetric on-chip immunoassay for histamine, J. Sensors Actuators, B Chem. 246 (2017) 1092–1099. doi:10.1016/j.snb.2016.11.141.

[233] Y.W. Leong, M.B. Abu Bakar, Z.A. Mohd. Ishak, A. Ariffin, Filler treatment effects on the weathering of talc-, caco3- and kaolin-filled polypropylene hybrid composites, J. Compos. Interfaces. 13 (2006) 659–684. doi:10.1163/156855406779366840.

[234] S.K. Esthappan, S.K. Kuttappan, R. Joseph, Effect of titanium dioxide on the thermal ageing of polypropylene, J. Polym. Degrad. Stab. 97 (2012) 615–620. doi:10.1016/j.polymdegradstab.2012.01.006.

[235] F. Marti-Ferrer, F. Vilaplana, A. Ribes-Greus, A. Benedito-Borras, C. Sanz-Box, Flour rice husk as filler in block copolymer polypropylene: Effect of different coupling agents, J. Appl. Polym. Sci. 99 (2006) 1823–1831. doi:10.1002/app.22717.

[236] C.D. Han, T. Van Den Weghe, P. Shete, J.R. Haw, Effects of coupling agents on the rheological properties , processability, and mechanical properties of filled, Polym. Eng. Sci. 21 (1981) 196–204. doi:10.1002/pen.760210404.

[237] S.N. Maiti, K.K. Sharma, Studies on polypropylene composites filled with talc particles, J. Mater. Sci. 27 (1992) 4605–4613. doi:10.1007/bf01165994.

[238] M. Kazayawoko, J.J. Balatinecz, R.T. Woodhams, Diffuse reflectance fourier transform infrared spectra of wood fibers treated with maleated polypropylenes, J. Appl. Polym. Sci. 66 (1997) 1163–1173. doi:10.1002/(SICI)1097-4628(19971107)66:6<1163::AID-APP16>3.0.CO;2-2.

[239] Q. Li, L.M. Matuana, Effectiveness of Maleated and Acrylic Acid-functionalized polyolefin coupling agents for HDPE-wood flour composites, J. Thermoplast. Compos. Mater. 16 (2003) 551–564. doi:10.1177/089270503033340.

[240] H. Ismail, H. Osman, M. Jaafar, Hybrid-filler filled polypropylene /natural rubber composites : Effects of natural weathering on mechanical and thermal properties and morphology, J. Vinyl Addit. Technol. 14 (2008) 142–151. doi:10.1002/vnl.

[241] L. Audouin, V. Gueguen, A. Tcharkhtchi, J. Verdu, “Close loop” mechanistic schemes for hydrocarbon polymer oxidation, J. Polym. Sci. Part A Polym. Chem. 33 (1995) 921–927. doi:10.1002/pola.1995.080330605.

[242] S.J. Monte, Ken-react Reference Manual: Titanate, Zirconate and Aluminate coupling agents, Kenrich Petrochemicals, Inc. (1987).

[243] S.N. Maiti, B.H. Lopez, M.N. Ibrahim, Rheological properties of isotactic polypropylene/kaolin composites, J. Polym. - Plast. Technol. Eng. 41 (2002) 663–676. doi:10.1081/PPT-120006440.

[244] I.M. Ulfah, R. Fidyaningsih, S. Rahayu, D.A. Fitriani, D.A. Saputra, D.A. Winarto, L.A. Wisojodharmo, Influence of carbon black and silica filler on the rheological and mechanical properties of natural rubber compound, Procedia Chem. 16 (2015) 258–264. doi:10.1016/j.proche.2015.12.053.

[245] H. Qin, S. Zhang, H. Liu, S. Xie, M. Yang, D. Shen, Photo-oxidative degradation of polypropylene/montmorillonite nanocomposites, Polym. J. 46 (2005) 3149–3156. doi:10.1016/j.polymer.2005.01.087.

[246] Y.W. Leong, M.B. Abu Bakar, Z.A. Mohd Ishak, A. Ariffin, Characterization of talc/calcium carbonate filled polypropylene hybrid composites weathered in a natural environment, J. Polym. Degrad. Stab. 83 (2004) 411–422. doi:10.1016/j.polymdegradstab.2003.08.004.

CHAPTER 9: APPENDICES

Appendix A: Types of silane coupling agents

Table 9.1 presents the types of silane coupling agents and their most effective type of resin.

Table 9.1: Types of silane coupling agents (Adapted from [151]).

Functional group	Chemical name	Resin/application
Amine	Aminopropyltriethoxysilane	Acrylic, Nylon, Epoxy, Phenolics, Melamines, Urethanes, Nitrile Rubber
Diamine	Diaminopropyltrimethoxysilane	Acrylic, Nylon, Epoxy, Phenolics, Melamines, Urethanes, Nitrile Rubber
Methacrylate	3-Methacryloxypropyltrimethoxysilane	Unsaturated Polyesters, Acrylics, Polyolefin
Epoxy	3-Glycidoxypropyltrimethoxysilane	Epoxy, Urethanes, Acrylics, Polysulfides
Methyl	Methyltrimethoxysilane	Hydrophobing agent for mineral surfaces
Isobutyl	Isobutyltrimethoxysilane	Hydrophobing agent for mineral surfaces Masonry water, repellent
Phenyl	Phenyltrimethoxysilane	Hydrophobing, dispersing aid for minerals Blends with silanes/thermal stability
Octyl	Octyltriethoxysilane	Hydrophobing/dispersion of minerals in polyolefins; Masonry water repellent
Vinyl	Vinyltrimethoxysilane	Graft to polyethylene for moisture crosslinking Rubber, SBR, Polyolefin
Chloroalkyl	3-Chloropropyltrimethoxysilane	Urethanes, Epoxy, Nylon, Phenolics, Polyolefins
Chloroalkyl	3-Chloropropyltriethoxysilane	Urethanes, Epoxy, Nylon, Phenolics, Polyolefins
Vinylbenzy	Vinylbenzylaminotrimethoxysilane	Epoxies for CB's, polyolefins, all

lamino		polymer types

Appendix B: Types of titanate coupling agents

Table 9.2 presents the types of titanate coupling agents and their functional groups.

Table 9.2. Types of titanate coupling agents (adapted from [164]).

Functional group	Trade name	Chemical name
Monoalkoxy titanates	KR 7	Titanium IV bis 2-methyl-2-propenoato-O, isooctadecanoato-O 2-propanolato
	KR 9S	Titanium IV 2-propanolato, tris(dodecyl)benzenesulfanato-O
	KR 12	Titanium IV 2-propanolato, tris(dioctyl)phosphato-O
	KR 33DS	Titanium IV, tris(2-methyl)-2-propenoato-O, methoxydiglycolylato
	KR 38S	Titanium IV 2-propanolato, tris(dioctyl)pyrophosphato-O
	KR 39DS	Titanium IV, tris(2-propenoato-O), methoxydiglycolylato-O
	KR 44	Titanium IV 2-propanolato, tris(3,6-diaza)hexanolato
	KR® TTS	Titanium IV 2-propanolato, tris isooctadecanoato-O
Neoalkoxy titanates	LICA 01	Titanium IV 2,2(bis 2-propenolatomethyl)butanolato, tris neodecanoato-O
	LICA 09	Titanium IV 2,2(bis 2-propenolatomethyl)butanolato, iris(dodecyl)benzenesulfonato-O
	LICA 12	Titanium IV 2,2(bis 2-propenolatomethyl)butanolato, tris(dioctyl)phosphato-O
	LICA 38	Titanium IV 2,2(bis 2-propenolatomethyl)butanolato, tris(dioctyl)pyrophosphato-O
	LICA 44	Titanium IV 2,2(bis 2-propenolatomethyl)butanolato, tris(2-ethylenediamino)ethylato
	LICA 97	Titanium IV 2,2(bis 2-propenolatomethyl)butanolato, tris(3-amino)phenylato

Appendix C: Heating temperature ramp used for proximate analysis

Figure 9.1 A typical heating temperature ramp for the proximate analysis carried out in the study.

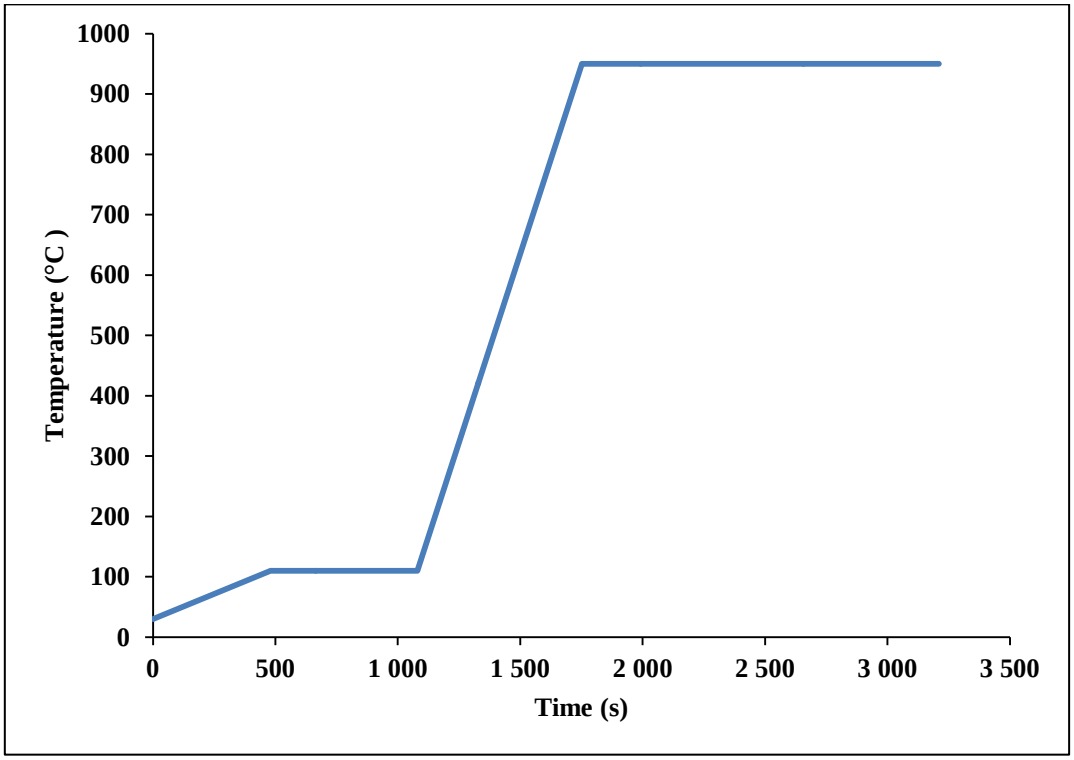

Figure 9.1: Proximate analysis heating temperature ramp.

Appendix D: PP composites formulations

As mentioned, an internal mixer was used to compound PP and untreated /treated PT-char at different PT-char loadings. The volume of the internal mixer was 69 ml and 70 % of that volume was used. **Table 9.3** presents composite formulations that were used in the study.

Table 9.3: Composites formulations for PP and UC/DC.

PP+UC/DC							
Sample	PP (%)	UC/DC (%)	PP (g)	UC/DC (g)	3-MPTS (g)	LICA 12 (g)	MAgPP (g)
Unfilled (PP)	100	-	43.7	-	-	-	-
PP+0.38-UC/DC	99.6	0.38	43.5	0.17	-	-	-
PP+0.77-UC/DC	99.2	0.77	43.3	0.34	-	-	-
PP+1.94-UC/DC	98.1	1.94	42.6	0.84	-	-	-
PP+3.91-UC/DC	96.1	3.91	41.5	1.69	-	-	-
PP+7.91-UC/DC	92.1	7.91	39.3	3.38	-	-	-
PP+UC/DC+CA							
PP+0.38-UC/DC+CA							
PP+0.38-UC/DC+3-MPTS	99.6	0.38	43.5	0.14	0.03	-	-
PP+0.38-UC/DC+LICA 12	99.6	0.38	43.5	0.16	-	0.004	-
PP+0.38-UC/DC+MAgPP	99.6	0.38	41.3	0.21	-	-	2.19
PP+0.77-UC/DC+CA							
PP+0.77-UC/DC+3-MPTS	99.2	0.770	43.3	0.27	0.06	-	-
PP+0.77-UC/DC+LICA 12	99.2	0.770	43.3	0.33	-	0.01	-
PP+0.77-UC/DC+MAgPP	99.2	0.770	41.0	0.41	-	-	2.19
PP+1.94-UC/DC+CA							
PP+1.94-UC/DC+3-MPTS	98.1	1.94	42.6	0.68	0.16	-	-
PP+1.94-UC/DC+LICA 12	98.1	1.94	42.6	0.82	-	0.02	-
PP+1.94-UC/DC+MAgPP	98.1	1.94	40.3	1.03	-	-	2.19
PP+3.91-UC/DC+CA							
PP+3.91-UC/DC+3-MPTS	96.1	3.91	41.5	1.36	0.33	-	-
PP+3.91-UC/DC+LICA 12	96.1	3.91	41.5	1.65	-	0.04	-
PP+3.91-UC/DC+MAgPP	96.1	3.91	39.0	2.05	-	-	2.19
PP+7.91-UC/DC+CA							
PP+7.91-UC/DC+3-MPTS	92.1	7.91	39.3	2.73	0.65	-	-
PP+7.91-UC/DC+LICA 12	92.1	7.91	39.3	3.29	-	0.08	-
PP+7.91-UC/DC+MAgPP	92.1	7.91	36.5	4.06	-	-	2.19

Appendix E: Full factorial design for the analysis of mechanical properties and degradation studies

A full factorial design for the analysis of mechanical properties and degradation studies was carried out to determine which factors and their interactions are significant. The design matrices are presented in **Table 9.4**, **Table 9.5** and **Table 9.6**. As mentioned, the impact strength test was carried out in all samples to examine the effectiveness of each treatment.

Table 9.4: Full factorial design ($2^1 4^1 5^1$) for analysis of impact strength.

PT-char	Coupling agent	PT-char loading (wt.%)	PT-char loading in text
PT-UC	NONE	0.38	L0
PT-UC	3-MPTS	0.38	L0
PT-UC	LICA 12	0.38	L0
PT-UC	MAgPP	0.38	L0
PT-UC	NONE	0.77	L1
PT-UC	3-MPTS	0.77	L1
PT-UC	LICA 12	0.77	L1
PT-UC	MAgPP	0.77	L1
PT-UC	NONE	1.94	L2
PT-UC	3-MPTS	1.94	L2
PT-UC	LICA 12	1.94	L2
PT-UC	MAgPP	1.94	L2
PT-UC	NONE	3.91	L3
PT-UC	3-MPTS	3.91	L3
PT-UC	LICA 12	3.91	L3
PT-UC	MAgPP	3.91	L3
PT-UC	NONE	7.91	L4
PT-UC	3-MPTS	7.91	L4
PT-UC	LICA 12	7.91	L4
PT-UC	MAgPP	7.91	L4
PT-DC	NONE	0.38	L0
PT-DC	3-MPTS	0.38	L0
PT-DC	LICA 12	0.38	L0

PT-DC	MAgPP	0.38	L0
PT-DC	NONE	0.77	L1
PT-DC	3-MPTS	0.77	L1
PT-DC	LICA 12	0.77	L1
PT-DC	MAgPP	0.77	L1
PT-DC	NONE	1.94	L2
PT-DC	3-MPTS	1.94	L2
PT-DC	LICA 12	1.94	L2
PT-DC	MAgPP	1.94	L2
PT-DC	NONE	3.91	L3
PT-DC	3-MPTS	3.91	L3
PT-DC	LICA 12	3.91	L3
PT-DC	MAgPP	3.91	L3
PT-DC	NONE	7.91	L4
PT-DC	3-MPTS	7.91	L4
PT-DC	LICA 12	7.91	L4
PT-DC	MAgPP	7.91	L4

Table 9.5: Full factorial design ($2^1 4^1 3^1$) for thermal-oxidative degradation studies.

PT-char	Coupling agent	PT-char loading (wt.%)	PT-char loading in text
PT-UC	NONE	0.38	L0
PT-UC	3-MPTS	0.38	L0
PT-UC	LICA 12	0.38	L0
PT-UC	MAgPP	0.38	L0
PT-UC	NONE	0.77	L1
PT-UC	3-MPTS	0.77	L1
PT-UC	LICA 12	0.77	L1
PT-UC	MAgPP	0.77	L1
PT-UC	NONE	1.94	L2
PT-UC	3-MPTS	1.94	L2
PT-UC	LICA 12	1.94	L2
PT-UC	MAgPP	1.94	L2
PT-DC	NONE	0.38	L0

PT-DC	3-MPTS	0.38	L0
PT-DC	LICA 12	0.38	L0
PT-DC	MAgPP	0.38	L0
PT-DC	NONE	0.77	L1
PT-DC	3-MPTS	0.77	L1
PT-DC	LICA 12	0.77	L1
PT-DC	MAgPP	0.77	L1
PT-DC	NONE	1.94	L2
PT-DC	3-MPTS	1.94	L2
PT-DC	LICA 12	1.94	L2
PT-DC	MAgPP	1.94	L2

Table 9.6: Full factorial design ($2^1 3^1 3^1$) for analysis of tensile properties and photo-oxidative degradation studies.

PT-char	Coupling agent	PT-char loading (wt.%)	PT-char loading
PP+UC	NONE	0.33	L0
PP+UC	MPTS	0.38	L0
PP+UC	LICA 12	0.38	L0
PP+UC	NONE	0.77	L1
PP+UC	MPTS	0.77	L1
PP+UC	LICA 12	0.77	L1
PP+UC	NONE	1.94	L2
PP+UC	MPTS	1.94	L2
PP+UC	LICA 12	1.94	L2
PP+DC	NONE	0.33	L0
PP+DC	MPTS	0.33	L0
PP+DC	LICA 12	0.33	L0
PP+DC	NONE	0.77	L1
PP+DC	MPTS	0.77	L1
PP+DC	LICA 12	0.77	L1
PP+DC	NONE	1.94	L2
PP+DC	MPTS	1.94	L2
PP+DC	LICA 12	1.94	L2

Appendix F: Proximate analysis

The elemental analysis was run twice to spot anomalies and the average values are indicated in **Table 9.7**.

Table 9.7: Proximate analysis results (wt.%)

	PT-UC				PT-DC			
	1st Run	2nd Run	Average	Standard deviation	1st Run	2nd Run	Average	Standard deviation
Moisture	0.70	0.20	0.45	0.35	1.50	1.40	1.45	0.07
Volatiles and Organics	7.80	7.80	7.80	0	9.70	9.50	9.60	0.14
Fixed Carbon	74.9	75.6	75.3	0.49	86.2	86.3	86.3	0.07
Ash	16.6	16.4	16.5	0.14	2.60	2.80	2.70	0.14

Appendix G: Ultimate analysis

The ultimate analysis was run twice to spot anomalies and the average values are indicated in **Table 9.8**.

Table 9.8: Ultimate analysis results (wt.%).

	PT-UC				PT-DC			
	1st Run	2nd Run	Average	Standard deviation	1st Run	2nd Run	Average	Standard deviation
N	0.28	0.28	0.28	0	0.49	0.44	0.46	0
C	77.0	76.1	76.6	0.64	90.5	91.1	90.8	0.41
H	0.68	0.67	0.68	0.01	0.71	0.70	0.71	0.01
S	2.14	2.62	2.38	0.34	0.96	0.95	0.95	0.01
Ash	16.6	16.4	16.5	0.14	2.60	2.80	2.70	0.14
O			3.61				4.36	

Appendix H: Chemical composition of the ash

Since PT-UC contains 16.5 wt.% of ash and PT-DC contains 2.70 wt.% of ash, further calculations were done to find the actual mineral content of the entire PT-char and equation 3 below was used to find their respective masses.

$$Mass_b = \frac{Mass_a \times Ash_c}{100} \quad (3)$$

Whereby,

$Mass_b$= The actual weight percent of the element within the carbon matrix (wt.%)

$Mass_a$= The weight percent of the element within the ash content (wt.%)

Ash_c= The ash content (wt.%)

Table 9.9: Chemical composition of the ash in PT-UC (wt.%).

PT-UC								
General spectra	Spec 3	Spec 10	Average	Standard deviation	Spec 3	Spec10	Average	Standard deviation
C	22.9	23.3	23.2	0.23	3.79	3.85	3.82	0.04
O	28.8	29.1	28.9	0.18	4.76	4.80	4.78	0.03
Mg	0.46	0.41	0.43	0.03	0.08	0.07	0.07	0.01
Al	1.15	1.20	1.18	0.03	0.19	0.20	0.19	0.01
Si	8.02	7.88	7.95	0.10	1.32	1.30	1.31	0.02
P	0	0	0	0				
S	0.51	0.48	0.49	0.02	0.08	0.08	0.08	0.004
Cl	0	0	0	0				
K	0.48	0.46	0.47	0.01	0.08	0.08	0.08	0.002
Ca	0.85	0.81	0.83	0.03	0.14	0.13	0.14	0.005
Fe	0.49	0.47	0.48	0.01	0.08	0.08	0.08	0.002
Co	0.34	0.33	0.33	0.01	0.06	0.05	0.06	0.001
Cu	0.41	0.54	0.47	0.09	0.07	0.09	0.08	0.02
Zn	32.0	31.9	31.9	0.10	5.28	5.26	5.27	0.02
Total			100				16.5	

Table 9.10: Chemical composition of the ash in PT-DC (wt.%).

PT-DC										
General spectra	Spec 18	Spec 29	Spec 30	Average	Standard deviation	Spec 18	Spec 29	Spec 30	Average	Standard deviation
C	33.6	28.9	27.5	29.9	3.18	0.91	0.78	0.74	0.81	0.09
O	39.8	40.7	41.3	40.6	0.75	1.08	1.09	1.11	1.09	0.02
Mg	0.10	0.16	0.25	0.17	0.07	0.003	0.004	0.007	0.005	0.002
Al	0.43	0.47	0.66	0.52	0.12	0.01	0.01	0.02	0.01	0.003
Si	2.67	1.31	2.14	2.04	0.68	0.07	0.03	0.06	0.06	0.02
P	0	0.07	0.11	0.06	0.06	0	0.002	0.003	0.002	0.002
S	7.85	10.0	9.40	9.09	1.13	0.21	0.27	0.25	0.25	0.03
Cl	0.06	0	0.02	0.03	0.03	0.002	0	0.001	0.001	0.001
K	0.4	0.57	0.61	0.56	0.06	0.013	0.02	0.02	0.01	0.002
Ca	0.27	0.26	0.42	0.32	0.09	0.007	0.007	0.01	0.009	0.002
Fe	0.25	0.13	0.39	0.26	0.13	0.007	0.004	0.01	0.007	0.004
Co	0	0	0	0	0	0.	0	0	0	0
Cu	0.41	0.35	0.36	0.37	0.03	0.01	0.01	0.01	0.01	0.001
Zn	0.31	0.42	0.49	0.41	0.09	0.01	0.01	0.01	0.01	0.002
Total				100					2.70	

Appendix I: Adsorption-isotherms of PT-UC and PT-DC

As seen from **Figure 9.2** a) and b), the adsorption isotherms of PT-UC and PT-DC shows the presence of a small knee and hysteresis loop which is associated with type IV isotherms. Generally, type IV isotherms are related to mesoporous solid [11]. Mesoporous solids contribute to low surface area and adsorption of the bigger molecule [18, 22].

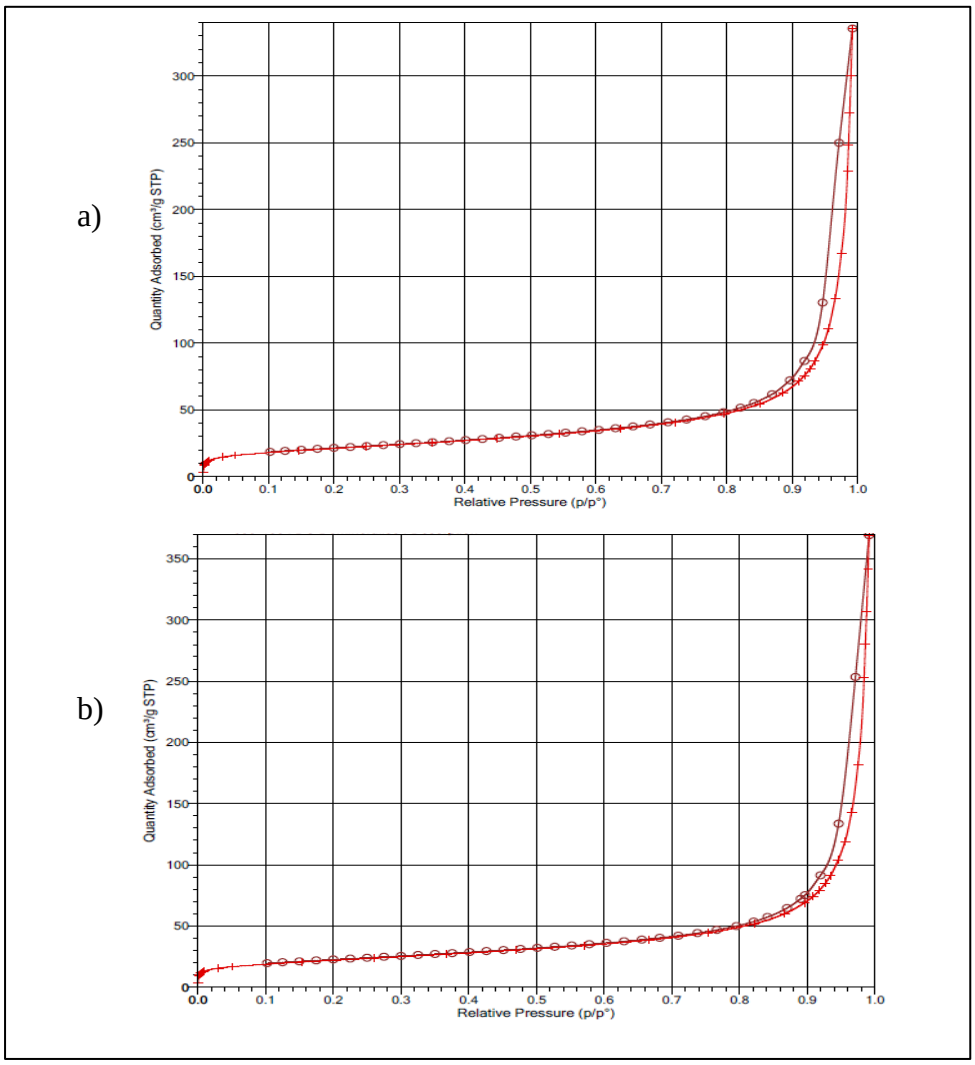

Figure 9.2: Adsorption-Desorption Isotherms of a) PT-UC and b) PT-DC.

Appendix J: FTIR spectra of coupling agents and compatibiliser

Typical spectra of 3-MPTS, LICA 12 and MAgPP are shown below in **Figure 9.3**, **Figure 9.4** and **Figure 9.5** respectively.

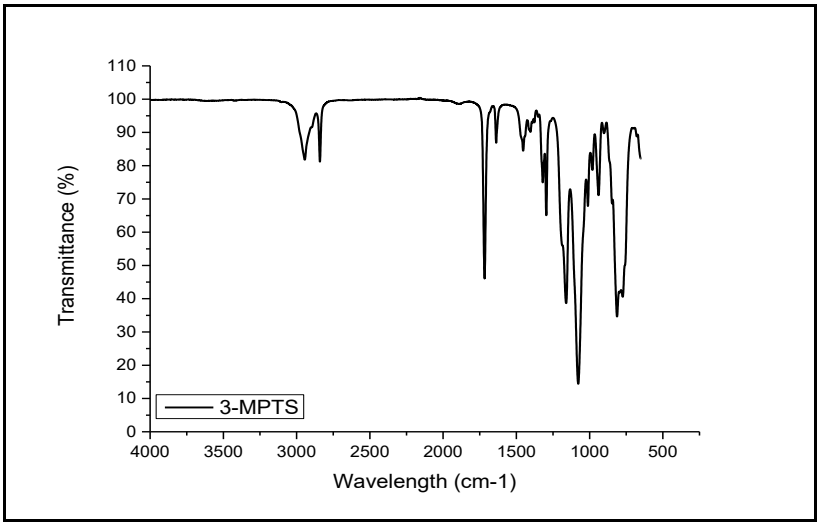

Figure 9.3: FTIR spectrum of 3-MPTS.

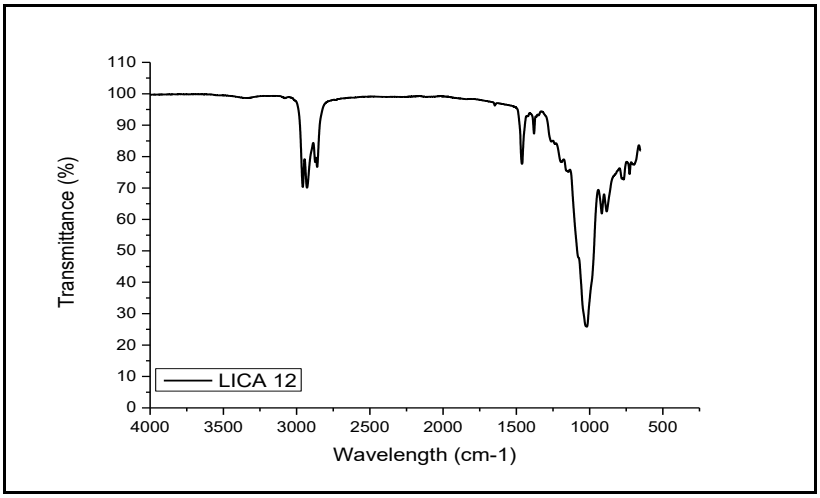

Figure 9.4: FTIR spectrum of LICA 12.

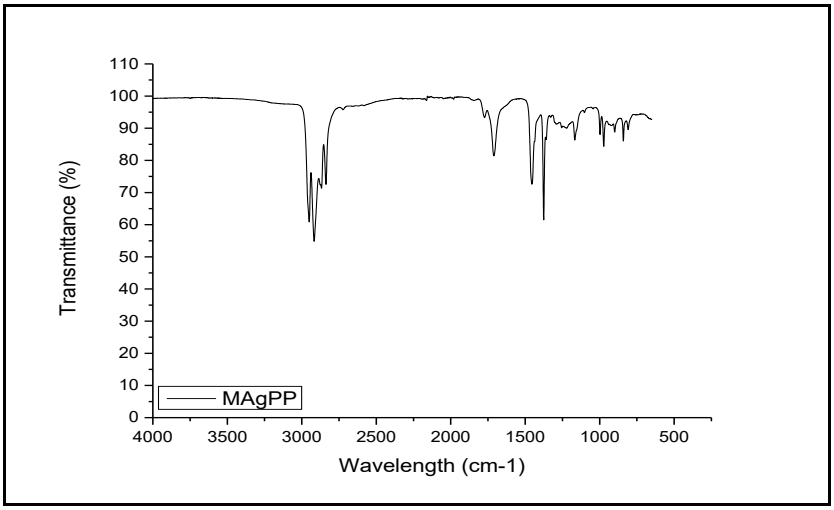

Figure 9.5: FTIR spectrum of MAgPP.

Appendix K: PP composites torque graphs

Figure 9.6 and **Figure 9.7** present temperature values at different time intervals for the pure PP and PP composites.

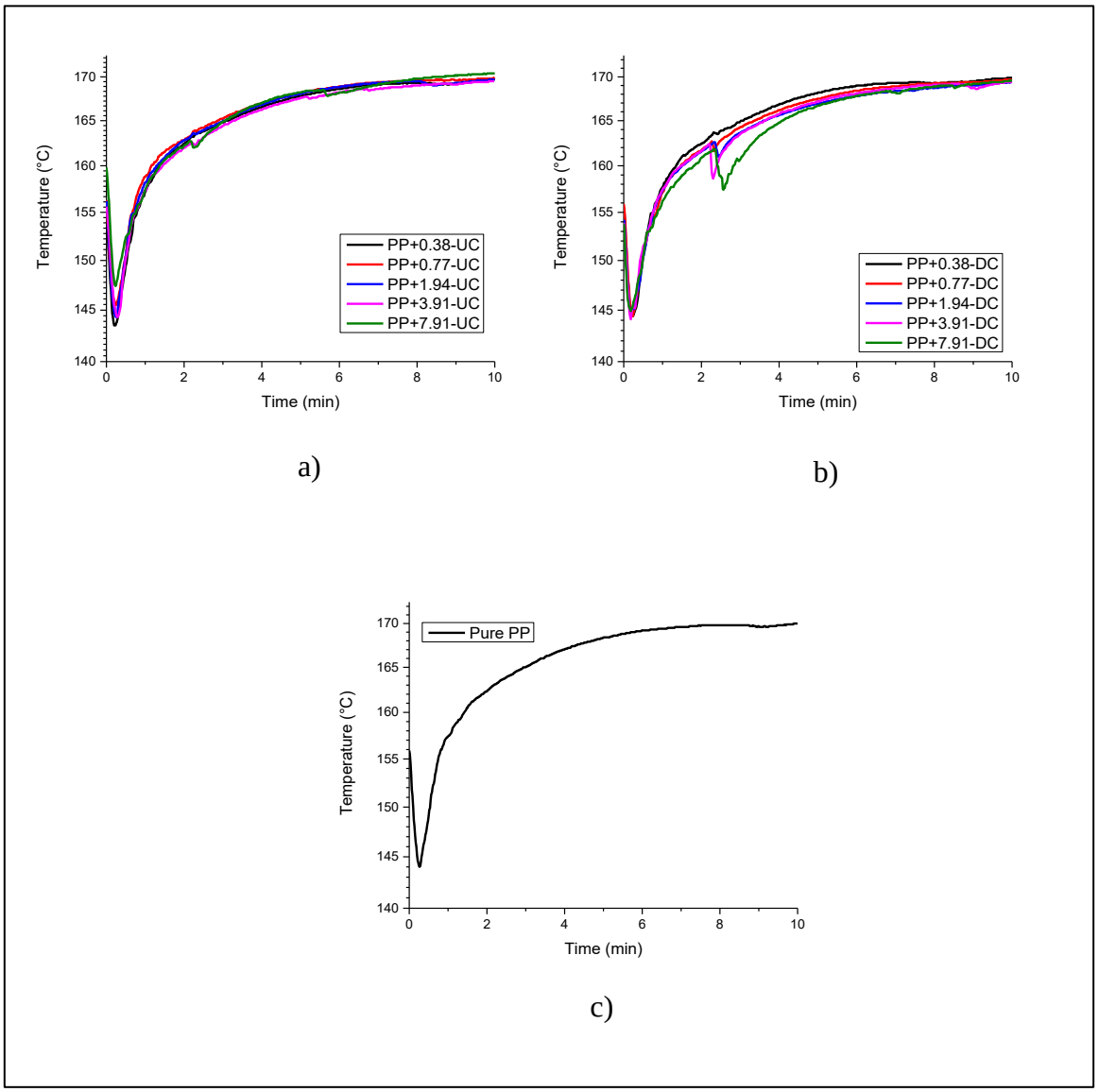

Figure 9.6: Temperature vs. time plots of pure PP and unmodified PP composites.

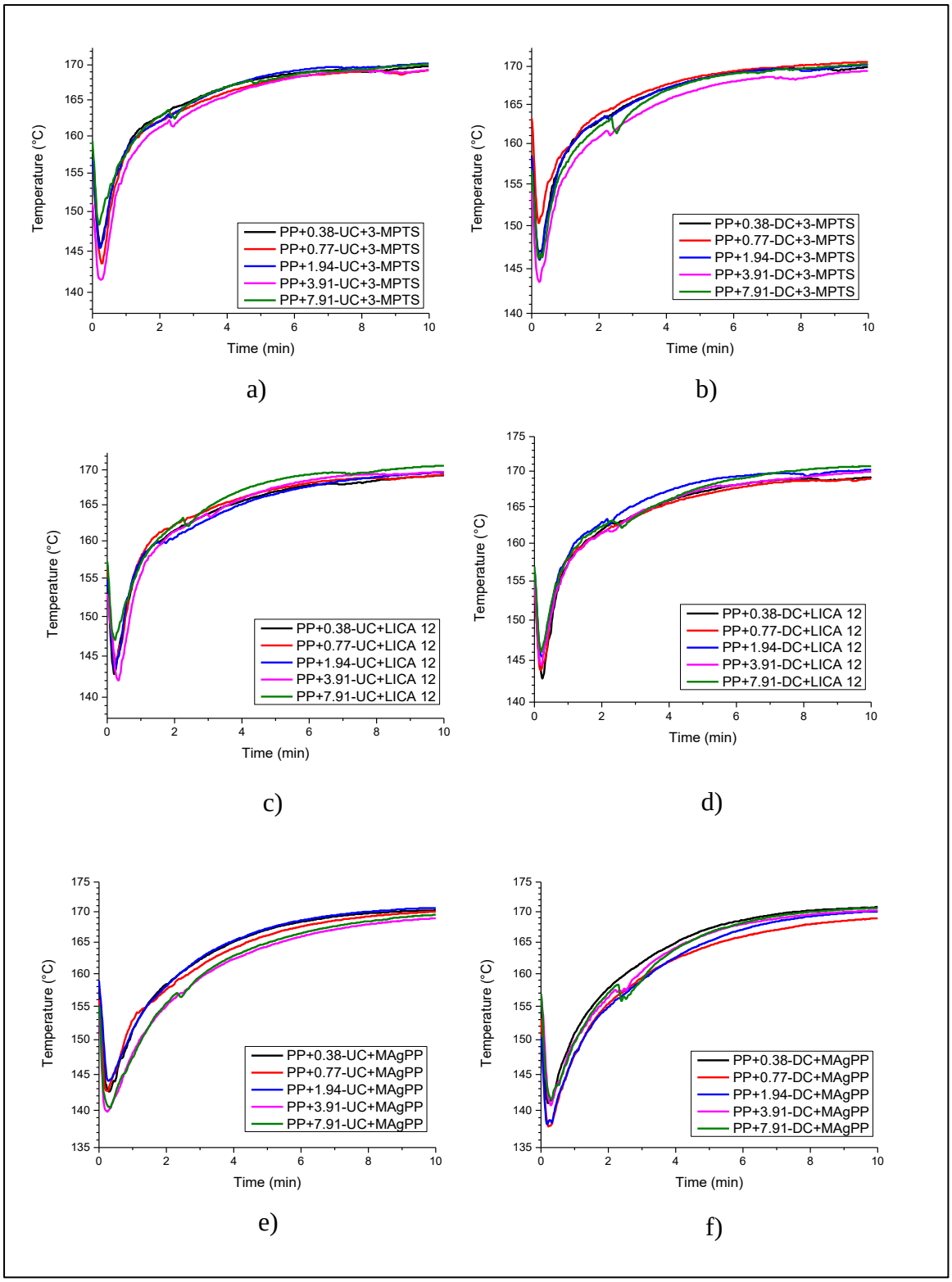

Figure 9.7: Temperature vs. time plots for modified PP composites.

Appendix L: PP composites main effects and interaction plots: Impact Strength

Table 9.11, Figure 9.8 and **Figure 9.9** present the analysis of variance along with main effects and the interaction plots for impact strengths of PP composites.

Table 9.11: Analysis of variance for the impact strength of PP composites.

	p-value
PT-char	< **0.05**
Coupling agent	< **0.05**
Loading	< **0.05**
PT-char * Coupling agent	0.112
PT-char * Loading	0.158
Coupling agent *Loading	0.730
PT-char * Coupling agent * Loading	0.440

Bold value = p-value is significant.

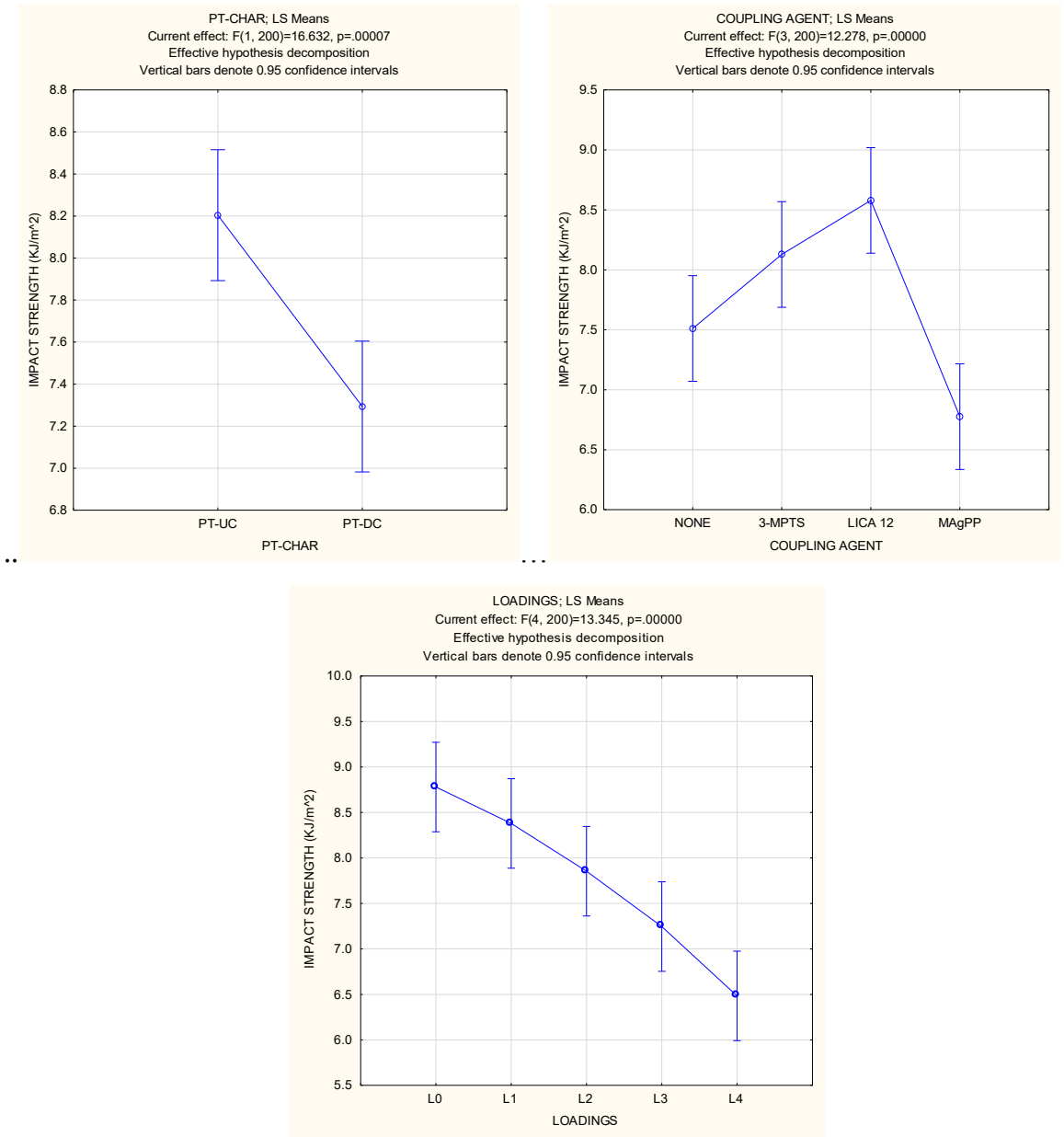

Figure 9.8: Main effects of impact strength of PP composites.

- L0=0.38 wt.%; L1=0.77 wt.%; L2=1.94 wt.%

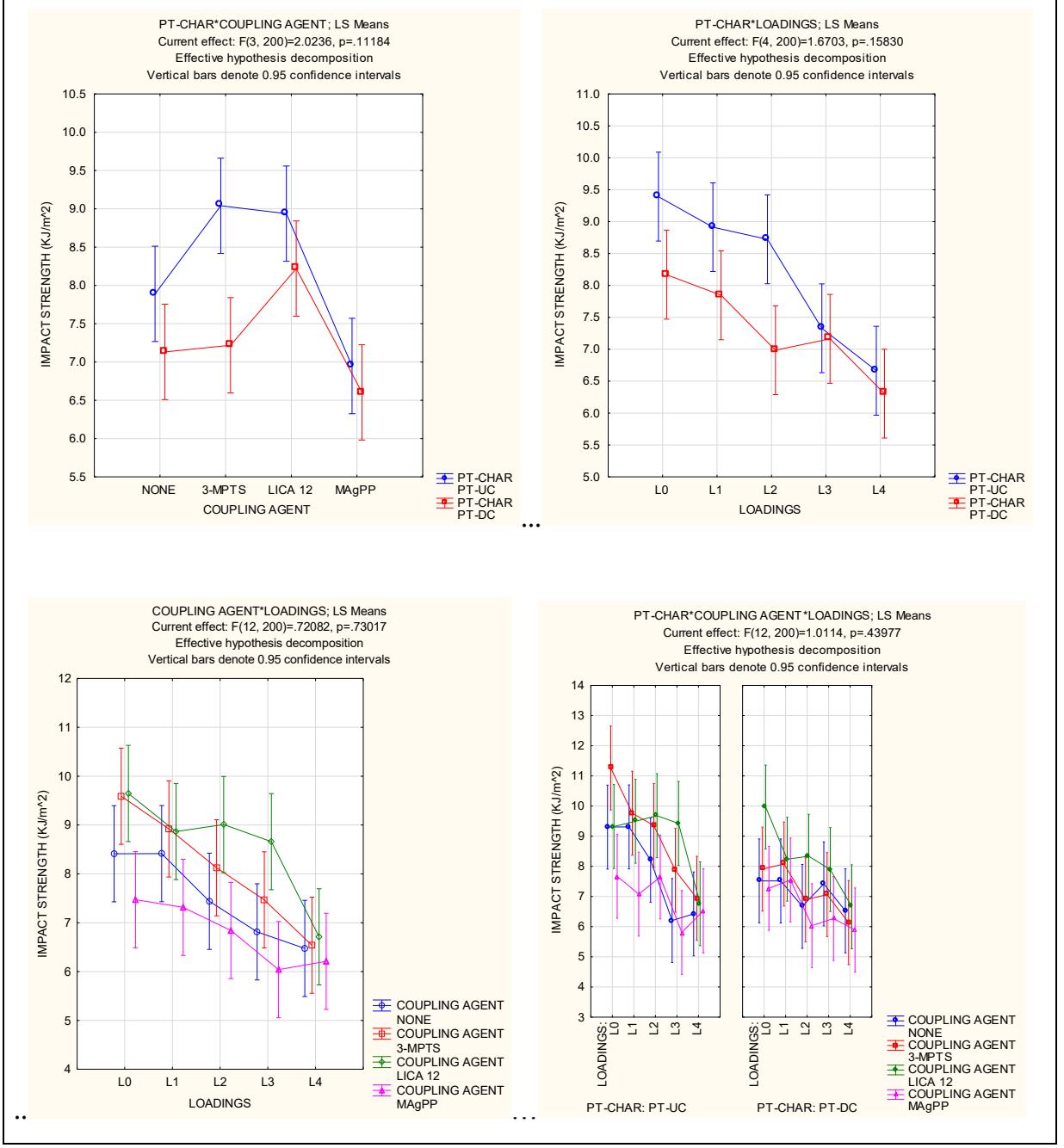

Figure 9.9: Interactions plots of impact strength of the PP composites.

- L0=0.38 wt.%; L1=0.77 wt.%; L2=1.94 wt.%

Appendix M: PP composites surface fractured images

Surface fracture images of PP composites obtained at 1.94 wt.% PT-char loading are presented in **Figure 9.10**.

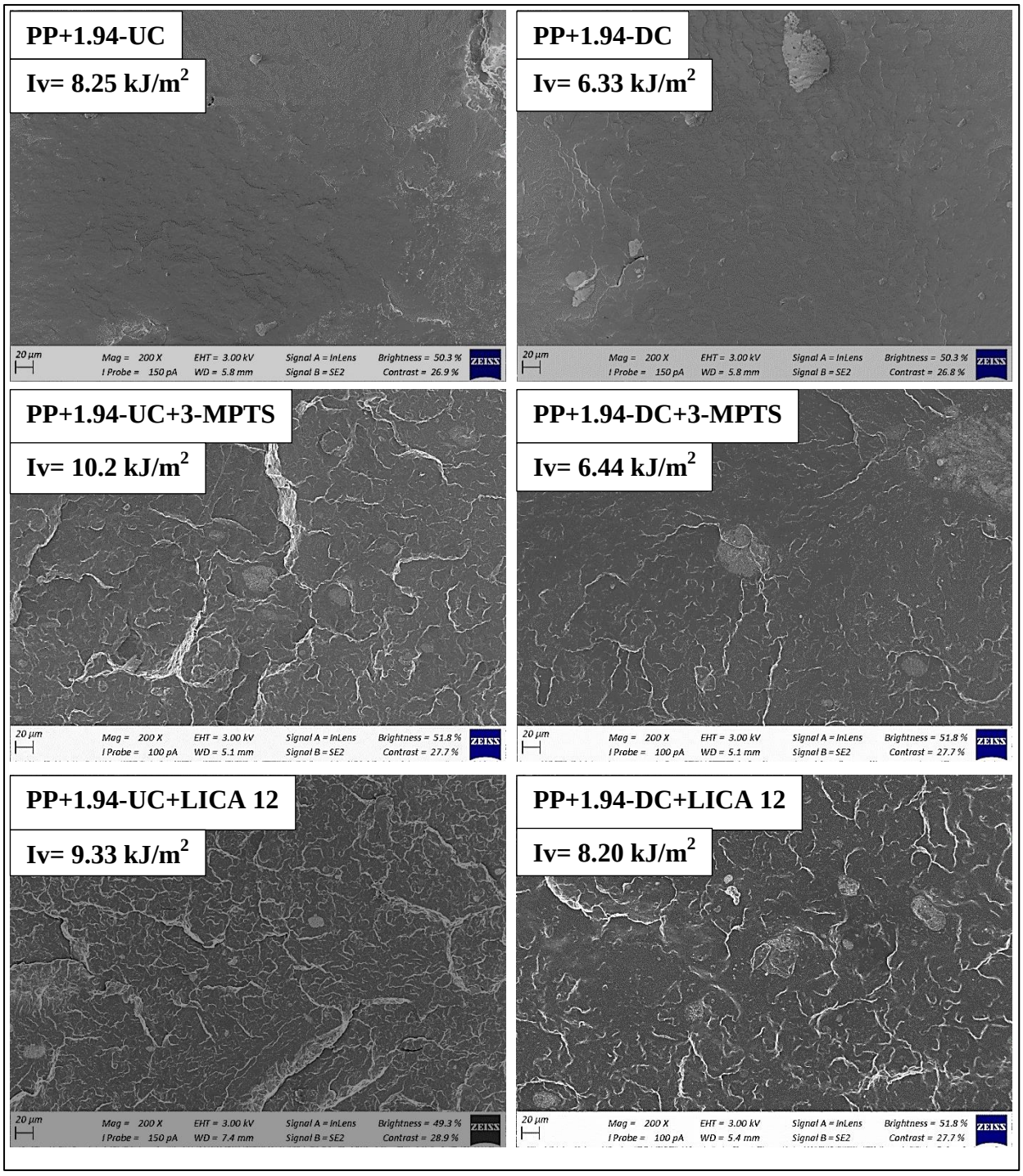

Figure 9.10: Surface fractured images of PP composites at 1.94 wt.%.

Appendix N: PP composites main effects and interactions plots: Tensile properties

Table 9.12 presents the analysis of variance for the tensile properties along with its main effects and the interaction plots for tensile properties are presented in **Figure 9.11** to **Figure 9.16**.

Table 9.12: Analysis of variance for the tensile properties of PP composites.

	Tensile strength	Young modulus	Elongation at break
	p-value		
PT-char	< **0.05**	< **0.05**	**0.003**
Coupling agent	**0.049**	< **0.05**	0.152
Loading	0.326	< **0.05**	< **0.05**
PT-char * Coupling agent	0.001	< **0.05**	**0.005**
PT-char * Loading	0.287	< **0.05**	0.227
Coupling agent * Loading	0.397	< **0.05**	0.154
PT-char * Coupling agent * Loading	**0.008**	< **0.05**	0.641

Bold value = p-value is significant.

❖ Main effects and interactions plots: Tensile Strength

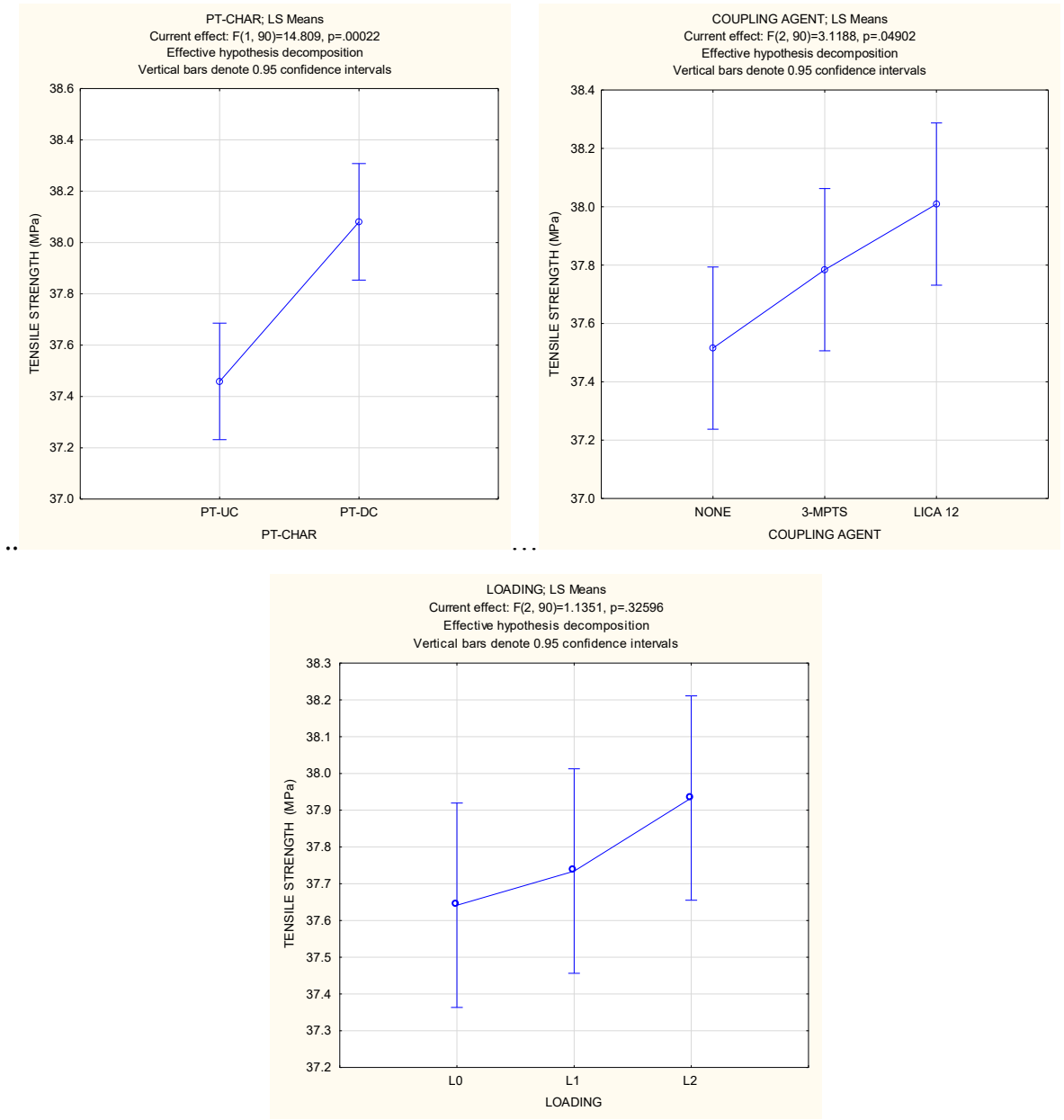

Figure 9.11: Main effect plots of tensile strength of PP composites.

- L0= 0.38 wt.%; L1= 0.77 wt.%; L2= 1.94 wt.%

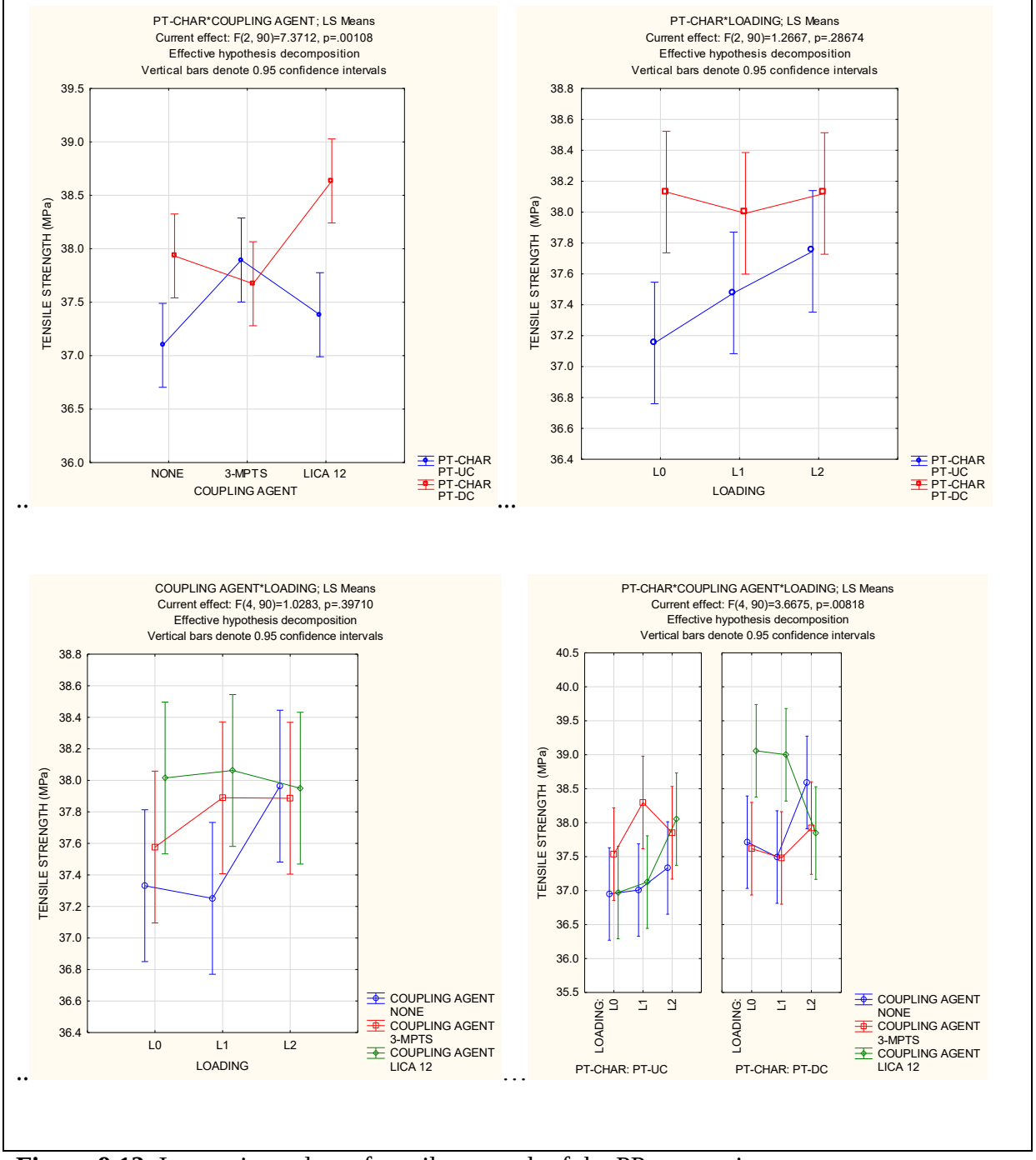

Figure 9.12: Interactions plots of tensile strength of the PP composites.

- L0= 0.38 wt.%; L1= 0.77 wt.%; L2=1.94 wt.%

❖ Main effects and interactions plots: Young Modulus

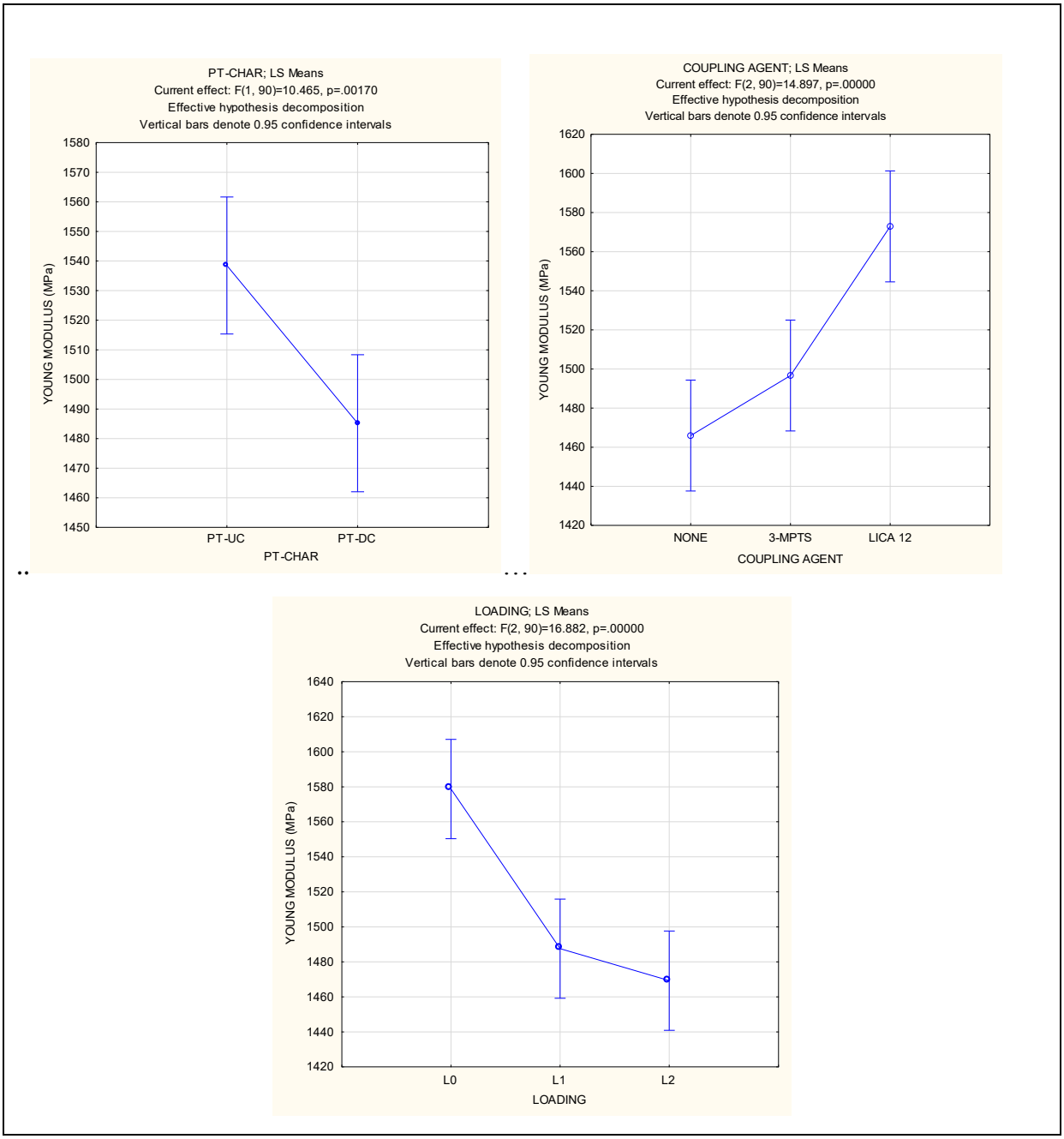

Figure 9.13: Main effects plots of young modulus of PP composites.

- L0= 0.38 wt.%; L1= 0.77 wt.%; L2=1.94 wt.%

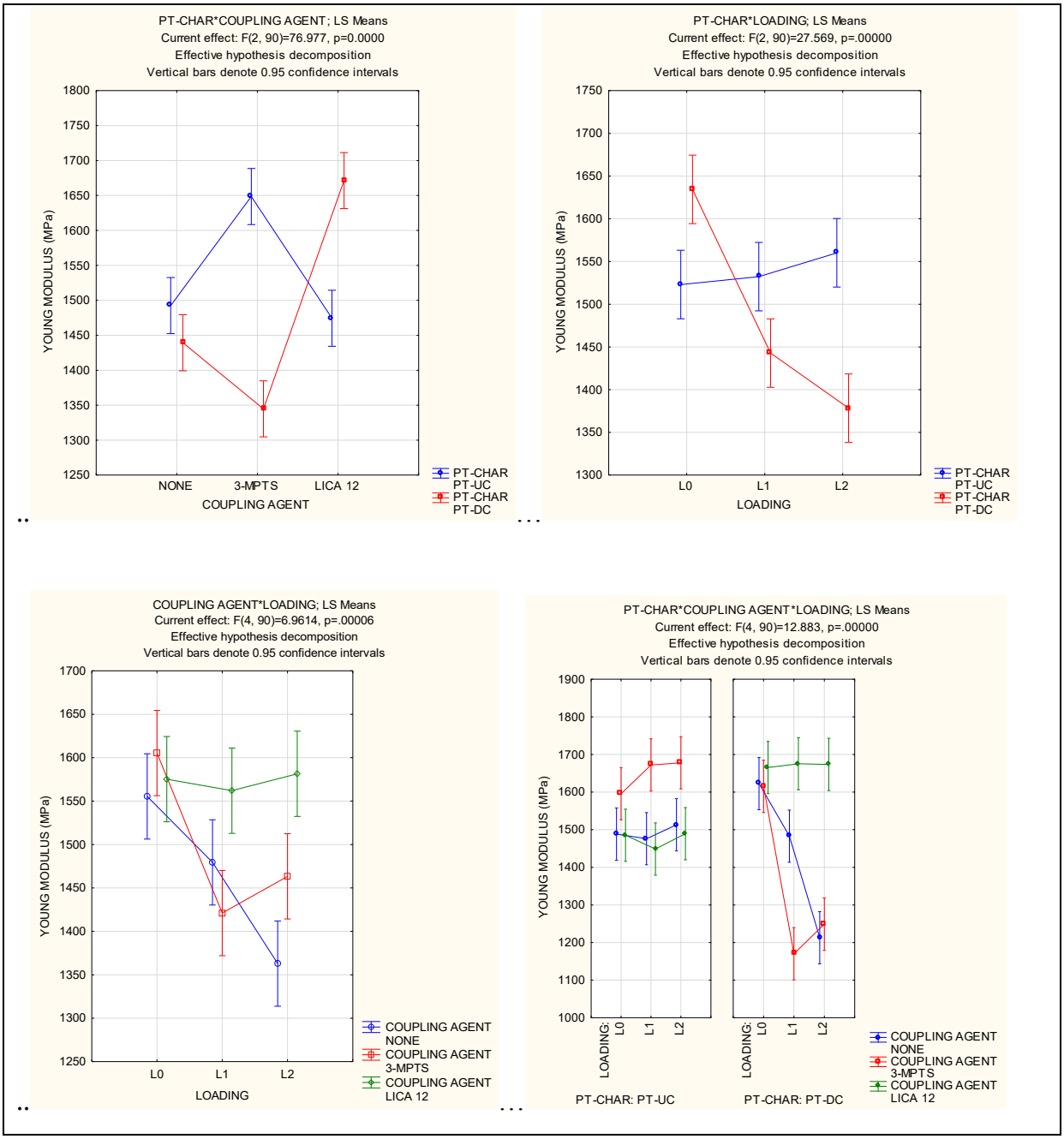

Figure 9.14: Interactions plots of young modulus of PP composites.

- L0= 0.38 wt.%; L1= 0.77 wt.%; L2= 1.94 wt.%

❖ Main effects and interactions plots: Elongation at Break

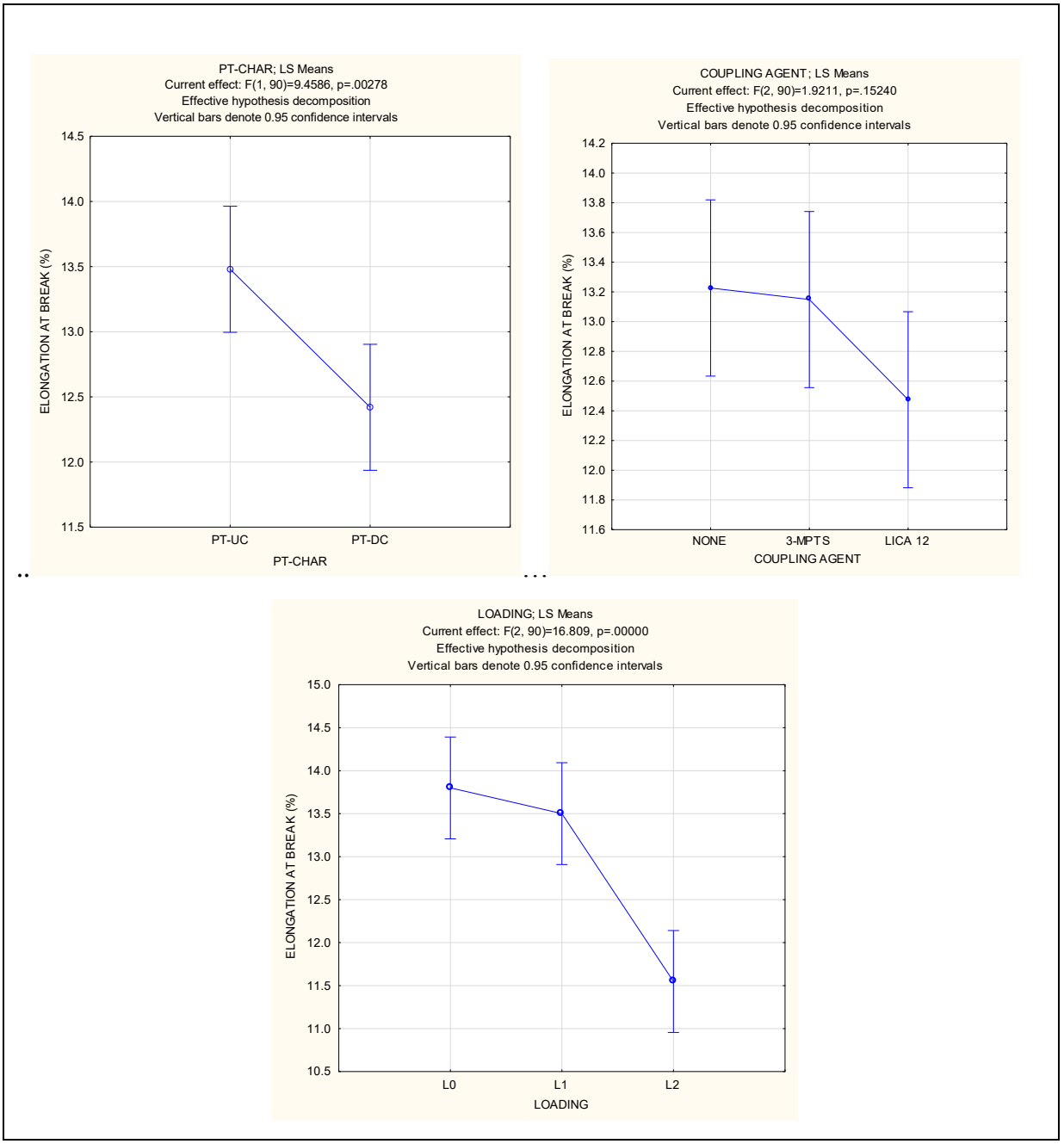

Figure 9.15: Main effects of elongation at break of PP composites.

- L0= 0.38 wt.%; L1= 0.77 wt.%; L2=1.94 wt.%

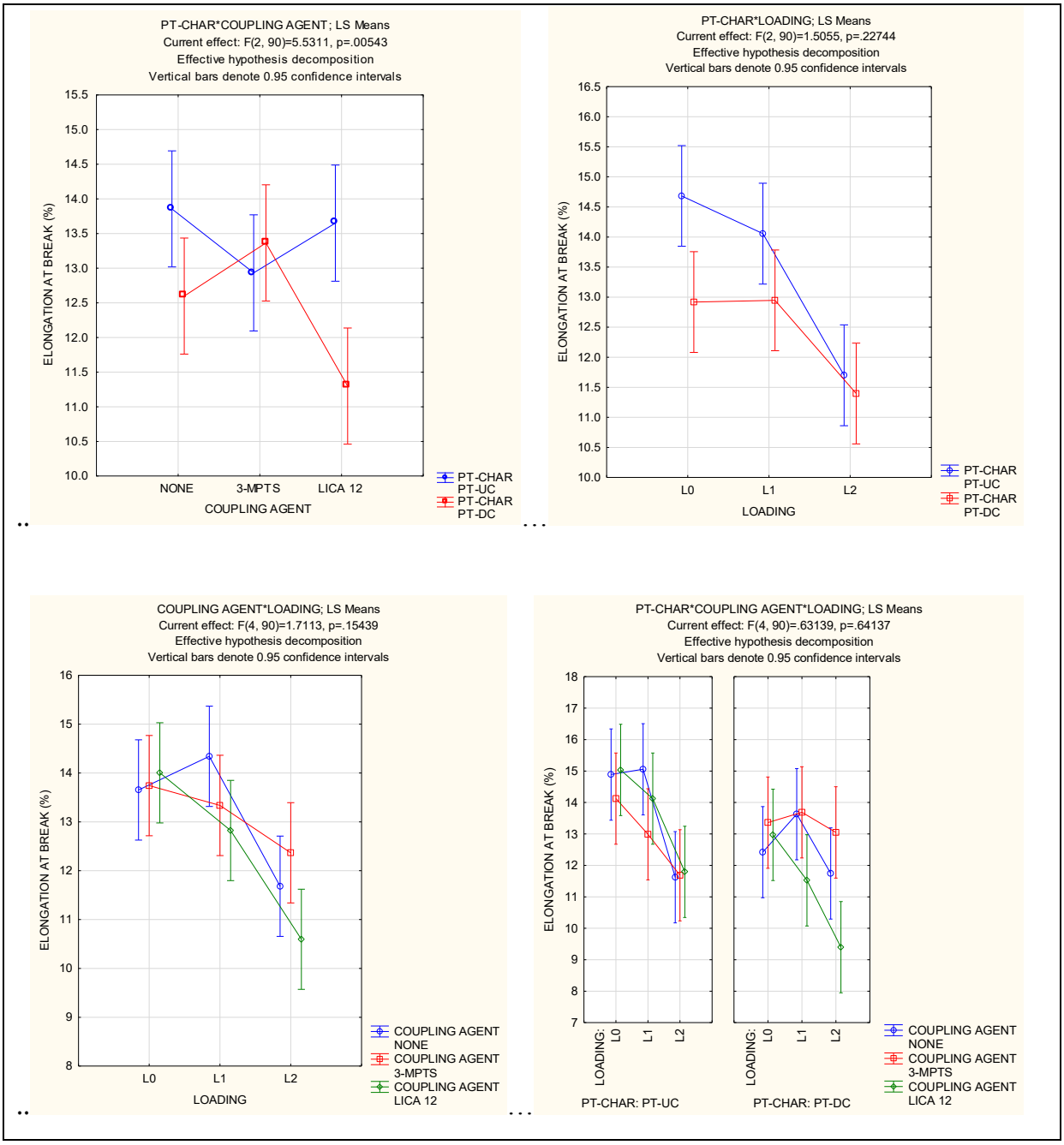

Figure 9.16: Interactions plots of elongation at break of PP composites.

- L0= 0.38 wt.%; L1= 0.77 wt.%; L2=1.94 wt.%

Appendix O: PP composites main effects and interactions plots: Degradation

Table 9.13, presents the analysis of variance for the degradation studies along with its main effects and the interaction plots are shown in **Figure 9.17** to **Figure 9.20**.

Table 9.13: Analysis of variance for degradation studies of PP composites.

	Thermal-oxidative degradation	Photo-oxidative degradation
	p-value	
PT-char	< **0.05**	0.074
Coupling agent	**0.002**	0.249
Loading	**0.025**	0.074
PT-char * Coupling agent	0.764	0.743
PT-char * Loading	0.398	0.673
Coupling agent * Loading	0.708	0.183
PT-char * Coupling agent * Loading	0.542	0.882

Bold value = p-value is significant.

❖ Main effects and interactions plots: Thermal-oxidative degradation

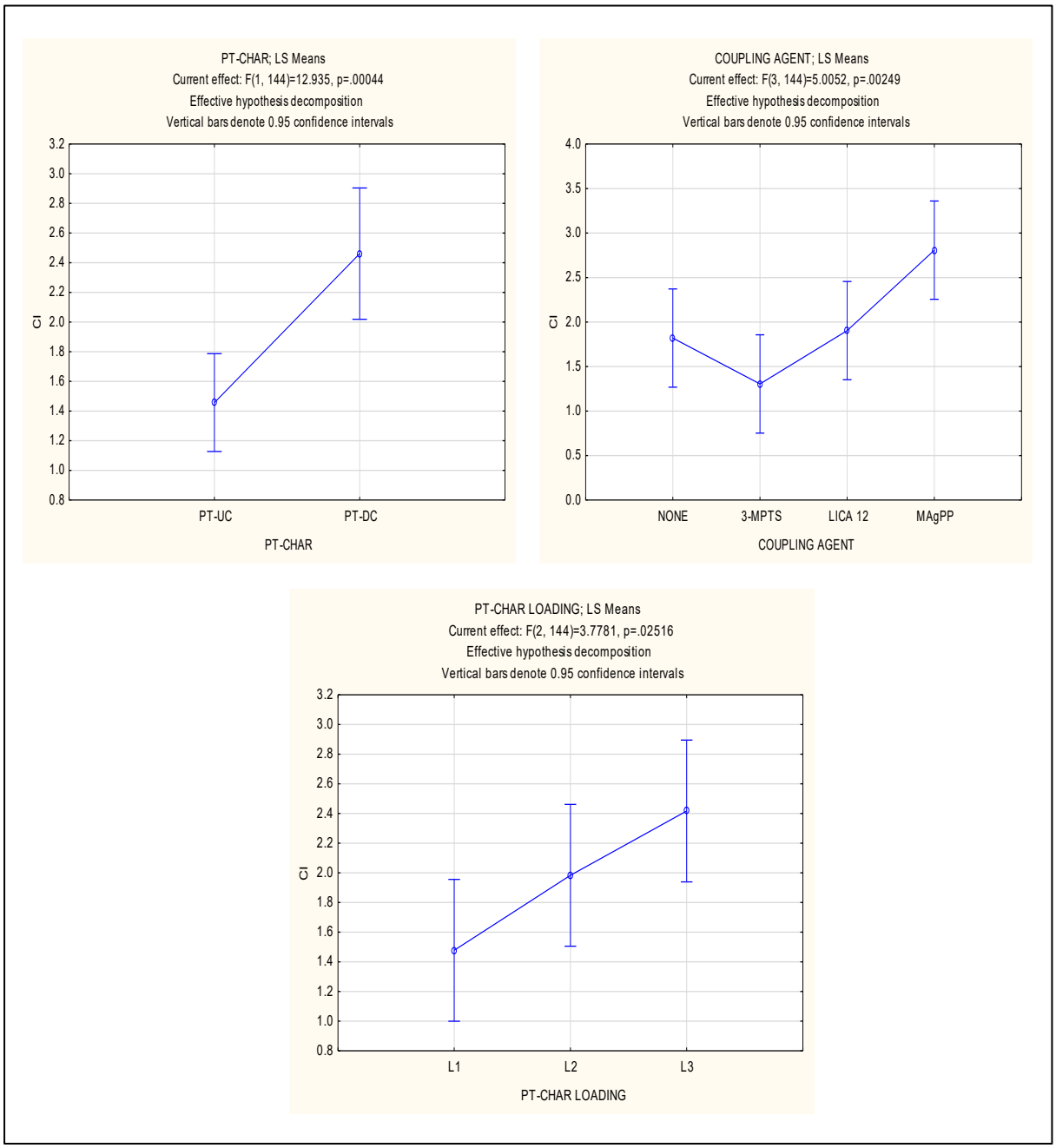

Figure 9.17: Main effects plots of thermal-oxidative degradation of PP composites

- L1= 0.38 wt.%; L2= 0.77 wt.%; L3= 1.94 wt.%

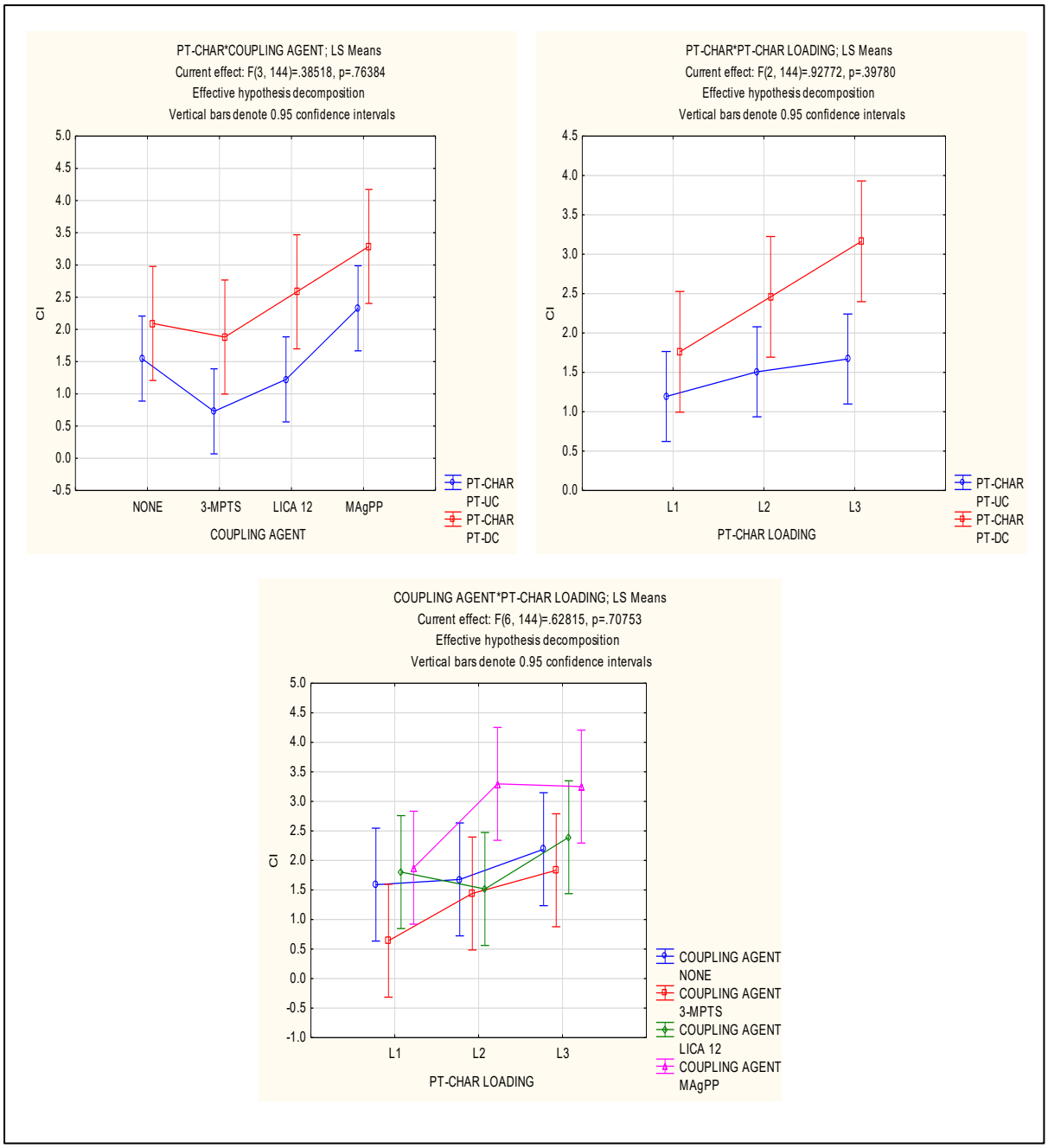

Figure 9.18: Interactions plots of thermal-oxidative degradation of PP composites

- L1= 0.38 wt.%; L2= 0.77 wt.%; L3= 1.94 wt.%

❖ Main effects and interactions plots: Photo-oxidative degradation

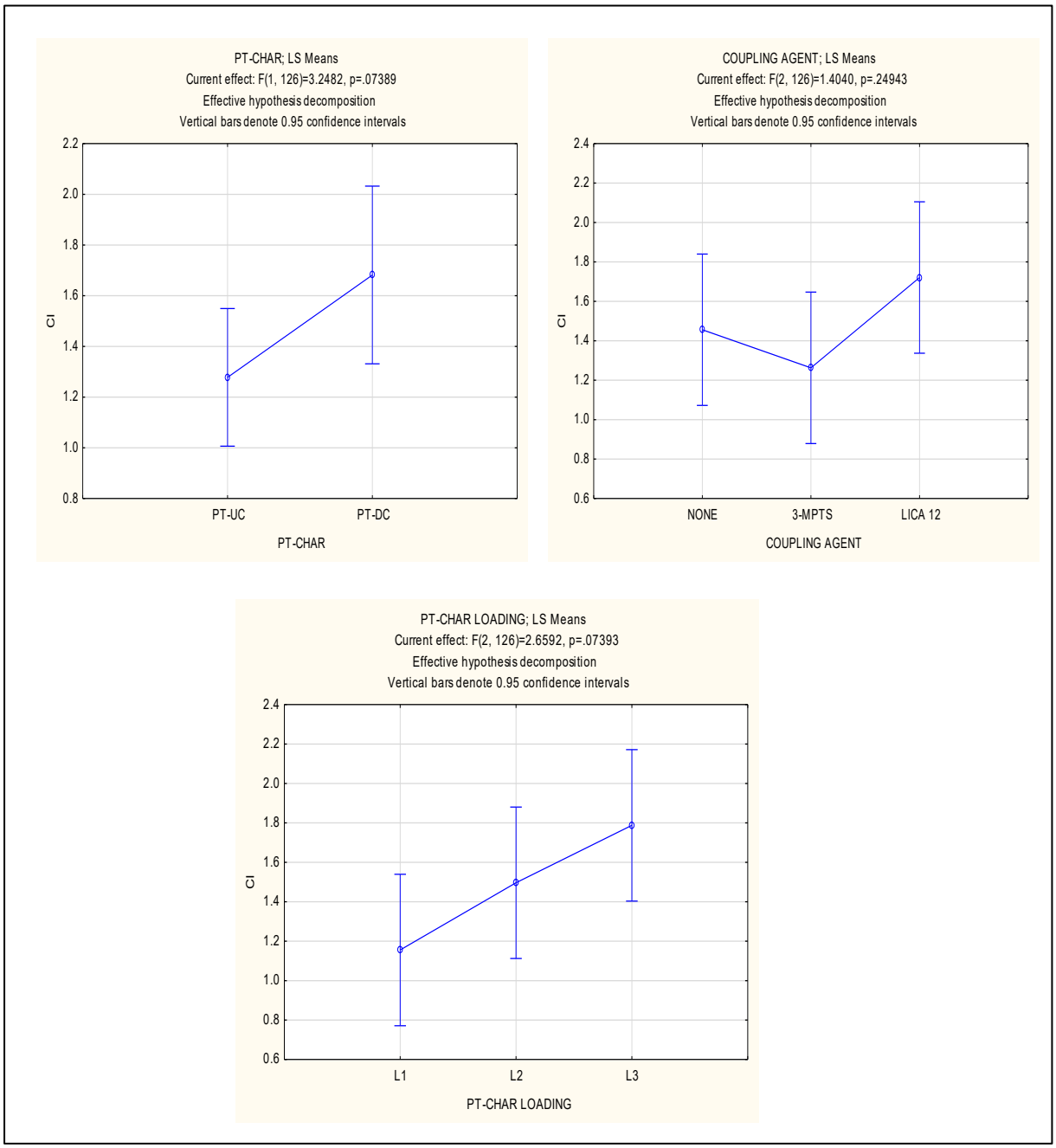

Figure 9.19: Main effects plots of photo-oxidative degradation of PP composites

- L1= 0.38 wt.%; L2= 0.77 wt.%; L3= 1.94 wt.%

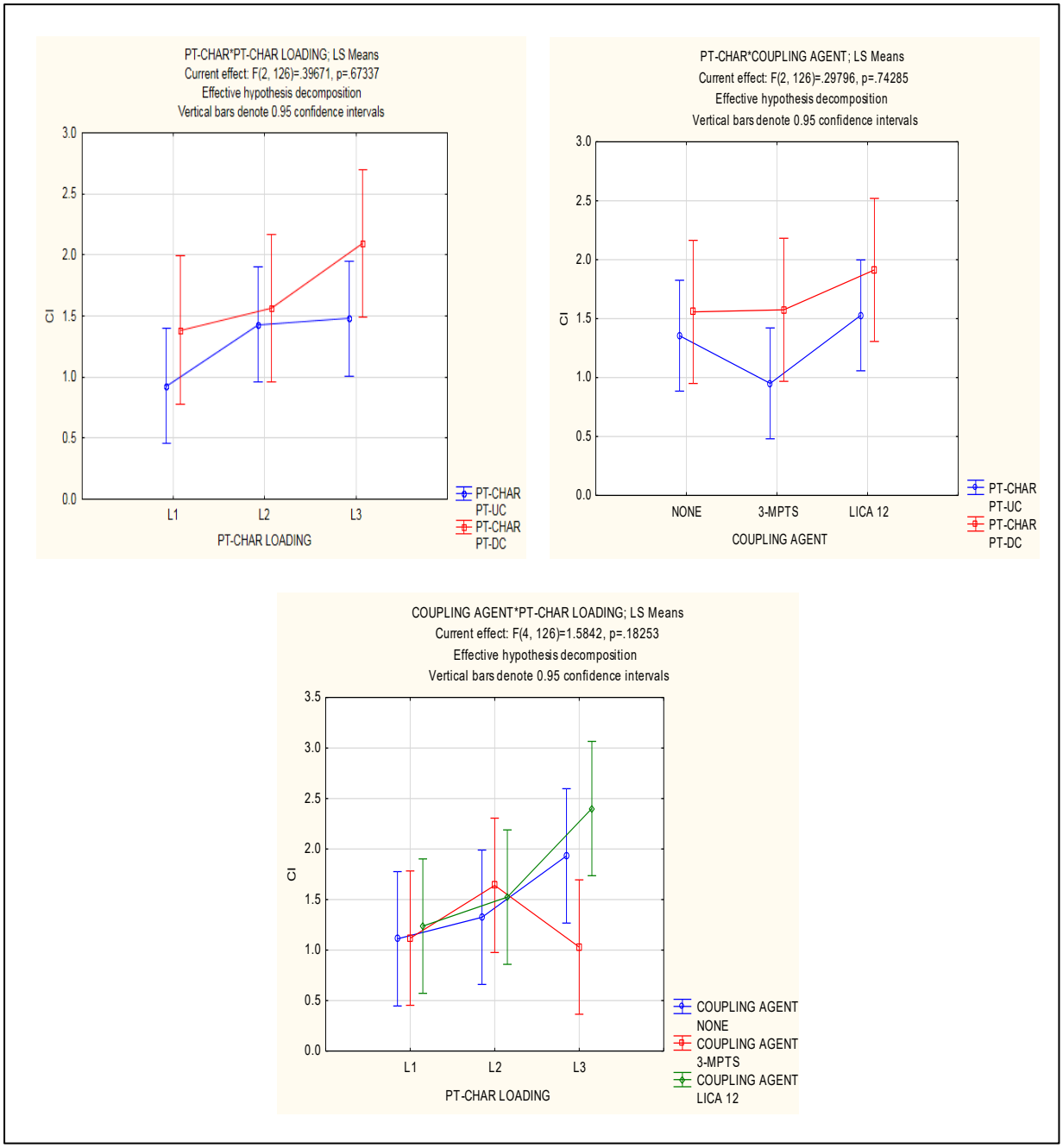

Figure 9.20: Interactions plots of photo-oxidative degradation of PP composites

- L1= 0.38 wt.%; L2= 0.77 wt.%; L3= 1.94 wt.%